NASA Technical Memorandum 86309

Simulator Study of the Stall Departure Characteristics of a Light General Aviation Airplane With and Without a Wing-Leading-Edge Modification

Donald R. Riley

MAY 1985

NASA

NASA Technical Memorandum 86309

Simulator Study of the Stall Departure Characteristics of a Light General Aviation Airplane With and Without a Wing-Leading-Edge Modification

Donald R. Riley
Langley Research Center
Hampton, Virginia

NASA
National Aeronautics
and Space Administration

Scientific and Technical
Information Branch

1985

Summary

A six-degree-of-freedom nonlinear simulation was developed for a two-place, single-engine, low-wing general aviation airplane for the stall and initial departure regions of flight. Comparison of simulation predictions with flight-test data served as model validation. Two configurations, one with and one without an outboard wing-leading-edge modification, were modeled. Comparisons of the trim characteristics and dynamic responses for straight, turning, and sideslipping flight show improved results at the higher angles of attack for the configuration with the wing-leading-edge modification. Time-history traces following elevator-ramp inputs showed improved departure characteristics for the modified configuration. Power effects were significant for both configurations.

Introduction

The NASA Langley Research Center is currently engaged in a broad research program to provide information for improving the stall departure and spin resistance of light general aviation airplanes. The program has involved wind-tunnel tests, radio-controlled-model tests, and full-scale flight tests. References 1 through 15 present some of the results obtained in the program thus far.

As part of this research effort, a six-degree-of-freedom nonlinear simulation was developed for a two-place, single-engine, low-wing general aviation airplane for the stall departure region of flight. Full-scale powered wind-tunnel test results obtained on the same type of airplane were used in establishing the math model. The objective of this particular effort was to generate a real-time simulation for analytical studies and for future piloted studies using the Langley general aviation cockpit. Such studies would supplement the results obtained from wind-tunnel and flight tests.

During the course of the stall/spin program, considerable effort was expended, both in wind-tunnel and flight tests, to examine the effects of employing an outboard-wing leading-edge modification on light aircraft stall and spin resistance. (See refs. 7, 10, and 14). As a consequence, two configurations, one with and one without the leading-edge modification, were modeled mathematically and programed for use with the simulation. Although piloted studies were not attempted in this study, a number of analytical results were obtained. The purpose of the present paper is to describe the math models developed, to discuss the validation performed, and to compare the simulation results obtained with and without the wing-leading-edge modification.

Symbols

Moment data are presented with respect to a center-of-gravity location on the fuselage centerline at 25 percent of the wing mean aerodynamic chord. The body-axis system shown in figure 1 is used for motion calculations.

a_Z	acceleration along Z body axis due to combined aerodynamic and propeller forces, ft/sec^2 (see appendix B)
b	wing span, ft
$\bar{c}_a$	aileron mean aerodynamic chord, ft
$\bar{c}_e$	elevator mean aerodynamic chord, ft
$\bar{c}_w$	wing mean aerodynamic chord, ft
$C_{D,s}$	stability-axis drag coefficient, $-F_{X,s}/\bar{q}S_w$
$C_{L,s}$	lift coefficient, $-F_{Z,s}/\bar{q}S_w$
$C_{Y,s}$	stability-axis side-force coefficient, $F_{Y,s}/\bar{q}S_w$
$C_{l,b}$	rolling-moment coefficient about X body axis, $L_b/\bar{q}S_w b$
$C_{m,b}$	pitching-moment coefficient about Y body axis, $M_b/\bar{q}S_w\bar{c}_w$
$C_{n,b}$	yawing-moment coefficient about Z body axis, $N_b/\bar{q}S_w b$
C_{H_a}	total aileron hinge-moment coefficient
$C_{H_{a_o}}$	aileron hinge-moment coefficient due to angle of attack, left and right ailerons combined
$C_{H_{a_{\delta_a}}}$	hinge-moment coefficient due to aileron deflection for a single aileron, per degree
C_{H_e}	total elevator hinge-moment coefficient
$C_{H_{e_o}}$	elevator hinge-moment coefficient due to angle of attack
$C_{H_{e_{\delta_e}}}$	hinge-moment coefficient due to elevator deflection, per degree
$C_{L,\max}$	maximum lift coefficient
$C_{L,\mathrm{trim}}$	trimmed lift coefficient

C'_P	power coefficient, $\frac{2\pi Q}{\rho n^2 D^5} = 2\pi C_Q$
C_Q	torque coefficient, $Q/\rho n^2 D^5$
C_T	thrust coefficient, $T/\bar{q}S_w$ (CT in computer-generated tables)
C'_T	propeller-thrust coefficient, $T/\rho n^2 D^4$
D	propeller diameter, ft
D_{wh}	control wheel diameter, ft
F_r	rudder pedal force, positive when right pedal depressed, lb
$F_{wh,a}$	wheel force required at rim for aileron deflection, positive clockwise, lb
$F_{wh,e}$	wheel force required for elevator deflection, pull force positive, lb
$F_{X,b}, F_{Y,b}, F_{Z,b}$	combined aerodynamic and propeller forces along X, Y, and Z body axes, respectively, lb
$F_{X,s}, F_{Y,s}, F_{Z,s}$	combined aerodynamic and propeller forces along X, Y, and Z stability axes, respectively, lb
g	gravitational constant, 32.17 ft/sec^2
G_a	aileron gearing ratio, $\frac{\delta_a}{\delta_{wh} D_{wh}} = 0.8411 \frac{\text{deg}}{\text{deg-ft}}$
G_e	elevator gearing ratio, 0.9969 rad/ft
h	altitude, ft
I_p	propeller moment of inertia about axis rotation, slug-ft^2
I_X, I_Y, I_Z	moments of inertia about body axes, slug-ft^2
I_{XZ}	body-axis product of inertia, slug-ft^2
J	propeller advance ratio, V/nD
$K_{\delta,1}, K_{\delta,2}$	constants used to adjust throttle setting (see eq. (A3))
L_b, M_b, N_b	combined aerodynamic and propeller moments about X, Y, and Z body axes, respectively, ft-lb
m	vehicle mass, slugs
MP	absolute manifold pressure, in. Hg
MPR	manifold pressure ratio
n	propeller rotational speed, rps
N	engine speed, rpm
p, q, r	rolling, pitching, and yawing angular rates about body axes, deg/sec or rad/sec
$\bar{q}$	dynamic pressure, $\frac{1}{2}\rho V^2$, lb/ft^2
Q	propeller torque, ft-lb
s	Laplace variable
S_a	surface area of single aileron, ft^2
S_e	elevator surface area, ft^2
S_w	wing area, ft^2
t	time
T	thrust measured on propeller balance, lb
u, v, w	velocity components along body axes, ft/sec
V	velocity, ft/sec
W	weight, lb
X_b, Y_b, Z_b	body axes
X_s, Y_s, Z_s	stability axes
α	angle of attack relative to airplane longitudinal axis, deg or rad (ALPHA in computer-generated tables)
β	angle of sideslip, deg (BETA in computer-generated tables)
γ	flight-path angle, deg
δ_a	total aileron deflection $(\delta_{a,R} - \delta_{a,L})$, deg
$\delta_{a,L}$	left aileron deflection, positive trailing edge down, deg
$\delta_{a,R}$	right aileron deflection, positive trailing edge down, deg
δ_e	elevator deflection, positive trailing edge down, deg

δ_f flap deflection, positive trailing edge down, deg

δ_r rudder deflection, positive trailing edge left, deg

δ_t steady-state throttle position, fraction of full throw (see appendix A)

δ_t' intermediate throttle input to thrust model (see appendix A)

$\delta_{t,c}$ commanded throttle position in cockpit, fraction of full throw

δ_{wh} control wheel deflection, deg

$\Delta C_{D,T}$ thrust increment to adjust drag model for large throttle settings at very low speeds and for the retarded setting at high speeds (see appendix B)

$\left.\begin{array}{l}\Delta C_{D,\beta}\\ \Delta C_{L,\beta}\\ \Delta C_{m,\beta}\end{array}\right\}$ increments when added to the coefficients at zero sideslip give the coefficients at the desired sideslip angle (see appendix B)

$\left.\begin{array}{l}\Delta C_{D,o}\\ \Delta C_{L,o}\\ \Delta C_{m,o}\end{array}\right\}$ power-off increments due to leading-edge modification (table IV minus table III)

ζ_d damping ratio of Dutch roll mode of motion

ζ_{ph} damping ratio of phugoid mode of motion

η propeller efficiency, $(C_T'/C_P')(V/nD)$

ρ mass density of air, slugs/ft^3

σ air density ratio

τ_e engine-response time constant, sec

τ_r roll-mode time constant

$\omega_{n,d}$ undamped natural frequency of Dutch roll mode of motion, rad/sec

$\omega_{n,ph}$ undamped natural frequency of phugoid mode of motion, rad/sec

ψ, θ, ϕ Euler angles (yaw, pitch, and roll angles, respectively), deg or rad

Subscripts:

b body axis

s stability axis

o conditions where $\delta_e = \delta_a = \delta_r = 0$ and $\beta = 0$

alt altitude

dyn dynamic

sl sea level

st static

0,1,2 constants in equations (A9) and (A12)

A dot over a quantity indicates a derivative with respect to time.

Derivatives:

$$C_{D_{\delta_e}} = \frac{\partial C_{D,s}}{\partial \delta_e} \qquad C_{L_{\delta_e}} = \frac{\partial C_{L,s}}{\partial \delta_e} \qquad C_{m_{\delta_e}} = \frac{\partial C_{m,b}}{\partial \delta_e}$$

$$C_{D_{(\delta_e)^2}} = \frac{\partial C_{D,s}}{\partial (\delta_e)^2} \qquad C_{L_{\delta_f}} = \frac{\partial C_{L,s}}{\partial \delta_f} \qquad C_{m_{\delta_f}} = \frac{\partial C_{m,b}}{\partial \delta_f}$$

$$C_{D_{\delta_f}} = \frac{\partial C_{D,s}}{\partial \delta_f} \qquad C_{L_q} = \frac{\partial C_{L,s}}{\partial \frac{q\bar{c}_w}{2V}} \qquad C_{m_q} = \frac{\partial C_{m,b}}{\partial \frac{q\bar{c}_w}{2V}}$$

$$C_{D_{(\delta_r)^3}} = \frac{\partial C_{D,s}}{\partial |(\delta_r)^3|} \qquad C_{L_{\dot{\alpha}}} = \frac{\partial C_{L,s}}{\partial \frac{\dot{\alpha}\bar{c}_w}{2V}} \qquad C_{m_{\dot{\alpha}}} = \frac{\partial C_{m,b}}{\partial \frac{\dot{\alpha}\bar{c}_w}{2V}}$$

$$C_{Y_\beta} = \frac{\partial C_{Y,s}}{\partial \beta} \qquad C_{l_\beta} = \frac{\partial C_{l,b}}{\partial \beta} \qquad C_{n_\beta} = \frac{\partial C_{n,b}}{\partial \beta}$$

$$C_{Y_{\delta_r}} = \frac{\partial C_{Y,s}}{\partial \delta_r} \qquad C_{l_{\delta_r}} = \frac{\partial C_{l,b}}{\partial \delta_r} \qquad C_{n_{\delta_r}} = \frac{\partial C_{n,b}}{\partial \delta_r}$$

$$C_{Y_{\delta_a}} = \frac{\partial C_{Y,s}}{\partial \delta_a} \qquad C_{l_{\delta_a}} = \frac{\partial C_{l,b}}{\partial \delta_a} \qquad C_{n_{\delta_a}} = \frac{\partial C_{n,b}}{\partial \delta_a}$$

$$C_{Y_p} = \frac{\partial C_{Y,s}}{\partial \frac{pb}{2V}} \qquad C_{l_p} = \frac{\partial C_{l,b}}{\partial \frac{pb}{2V}} \qquad C_{n_p} = \frac{\partial C_{n,b}}{\partial \frac{pb}{2V}}$$

$$C_{Y_r} = \frac{\partial C_{Y,s}}{\partial \frac{rb}{2V}} \qquad C_{l_r} = \frac{\partial C_{l,b}}{\partial \frac{rb}{2V}} \qquad C_{n_r} = \frac{\partial C_{n,b}}{\partial \frac{rb}{2V}}$$

$$C_{H_{a_{\delta_a}}} = \frac{\partial C_{H_a}}{\partial \delta_a} \qquad C_{H_{e_{\delta_e}}} = \frac{\partial C_{H_e}}{\partial \delta_e}$$

Background

The scope of the Langley stall/spin program includes examining concepts which improve the stall characteristics and spin resistance of light general

aviation aircraft as well as studies of the fully developed spin and recovery. One concept that has received considerable attention in all aspects of the program involved the use of an outboard-drooped-wing leading-edge modification. The range of studies involving the leading-edge modification includes wind-tunnel tests, free-flight radio-controlled-model tests, and full-scale flight tests. (See refs. 7, 10, and 14.) On the basis of these and other tests, the geometry of the particular leading-edge modification used herein was believed to be near optimum for spin resistance for this aircraft.

The fundamental concept in the use of the leading-edge modification is to control stall progression as the wing angle of attack increases and to produce a reasonably flat-top wing lift curve at the higher angles of attack. For the rectangular planform wings used on light general aviation airplanes, the stall usually begins near the root portion of the wing and proceeds both forward and outboard with increasing angle of attack. The sharp discontinuity in the modified-wing leading edge generates an effective aerodynamic fence that blocks the spanwise stall progression. In essence, the outer wing panels act like low-aspect-ratio wings (i.e., reduced lift-curve slope but higher stall angle of attack). Thus, attached flow is retained over the outboard wing panels to very high angles of attack. Not only is damping-in-roll retained but roll control is also retained since the ailerons are located near the wing tips.

Aircraft Simulated

The aircraft simulated was a two-place, low-wing vehicle with a fixed-pitch climb propeller, a 108-hp engine, and a fixed tricycle landing gear. The airplane was an extensively modified version of the Grumman American AA-1 Yankee. A photograph of the aircraft in flight is shown in figure 2. The aircraft has two booms, one at each wing tip, that support α/β vanes and velocity sensors. The right-hand seat was removed and replaced with an instrumentation pallet. A description of all flight instrumentation, including range and accuracy, is given in reference 8. In addition to the two booms, the aircraft had wheel pants and was equipped with a spin recovery parachute mounted below and to the rear of the tail assembly. The configuration shown in figure 2 is the arrangement simulated, and a three-view drawing of the aircraft is presented in figure 3. Physical characteristics are given in table I.

Since this was the first of several aircraft to undergo both flight testing and wind-tunnel testing in the Langley general aviation stall/spin program, a large number of alterations to the basic airframe were made and tested. Thus, many different configurations resulted. The wing designated number 1 and the tail designated number 4 identify the particular configuration simulated herein with configurations in other available references. In addition, the particular leading-edge treatment considered herein consisted of the outboard leading-edge droop labeled modification B in reference 14 and is illustrated in figure 4. Coordinates of the wing airfoil section with and without the droop are given in table II.

Mathematical Models

A thrust model, an aerodynamic model, and a model for control forces are required for the general aviation real-time simulation program to define a specific aircraft. Each model was developed using test data on a full-scale airplane from the Langley 30- by 60-Foot Tunnel. Although not all of the data that would have been desirable for math-model development were obtained, there were a number of advantages in using the 30- by 60-foot tunnel data. These include the following:

1. Tunnel-data were obtained for power-on settings using an identical climb prop as was used for the flight tests.
2. Additional tunnel-test data were obtained for the engine-propeller combination using a thrust-torque balance.
3. Scale effects due to differences in Reynolds number between flight and wind-tunnel tests were expected to be small. For the wind-tunnel tests, the Reynolds number was 2.5×10^6, based on the wing mean aerodynamic chord.

Thrust Model

Wind-tunnel data were obtained for both the propeller thrust and torque using a special strain-gage balance mounted between the engine shaft and the propeller. In addition, tunnel conditions of velocity V and air density ρ, propeller rotational speed n, and engine manifold pressure MP were recorded. Thus, both propeller and engine characteristics were documented. From these data the thrust model was generated. Details of the development are given in appendix A. A sketch showing the basis of the model is presented in figure 5. Airplane velocity, altitude, and throttle setting are inputs to the thrust model. The major output is thrust T. Engine speed and manifold pressure are determined separately and are used for instrument displays in the simulator. Note that for use with the equations of motion, thrust as a separate entity does not enter the equations; rather,

a thrust coefficient is calculated and is used as a parameter in establishing appropriate values for the individual entries in the aerodynamic math model.

Aerodynamic Model

The airplane is represented in the equations of motion by three force coefficients and three moment coefficients. Each of these six coefficients consists of a summation of individual aerodynamic terms and/or stability derivatives. Each individual entry contains the aerodynamic and power effects combined. The equations of motion and the expressions for the force and moment coefficients are presented in appendix B.

The expressions for the force and moment coefficients are considered to be reasonably conventional in form. The data for the various elements are contained in the program in tabular form as a function of two variables, usually angle of attack and thrust coefficient. Data were provided for an angle-of-attack range from -10° to 40° in increments of 5°, except for the range between 10° and 20° where data are provided every 2°. The power-on test data were extrapolated so that the model would cover thrust coefficients up to 0.5. Table entries are thus provided for thrust coefficients of 0 and 0.5. In addition, wind-tunnel measurements were obtained for sideslip angles up to $\pm 20^\circ$; as a result, the model is believed applicable over most of this sideslip range.

Control effectiveness data for elevator, aileron, and rudder were obtained through the angle-of-attack range only at zero sideslip. These values were used over the sideslip range without modification. The control effectiveness measurements were made on a configuration without the wing-tip booms, wheel pants, and parachute canister installed. A photograph of the airplane in this configuration is shown mounted in the Langley 30- by 60-Foot Tunnel in figure 6. It is worth noting that nearly all of the wind-tunnel testing was done with the configuration shown. (See ref. 14.)

To obtain dynamic derivatives, a number of oscillatory tests were conducted on an unpowered 1/3-scale model of the airplane in the 30- by 60-foot tunnel. Oscillation amplitude, oscillation frequency, and angle of attack were varied, and values of the p, q, and r oscillatory derivatives were obtained. In addition, some numerical values of the rate derivatives were obtained through the angle-of-attack range from flight records of the actual airplane by using the parameter extraction techniques available at the Langley Research Center. (See ref. 15.) From these two sources, single values for the derivatives at each angle of attack were established for use in the model at $C_T = 0$. Thrust effects estimated for some derivatives using the methods of reference 16 were incorporated in the model. Estimates of the $\dot{\alpha}$ derivatives were made, and tables are included for both the individual q and $\dot{\alpha}$ contributions. Because of the uncertainty of numerical values for the $\dot{\beta}$ derivatives, they were omitted in this model.

Numerical values of the various aerodynamic force and moment coefficients for the baseline (clean-wing) configuration are given in table III and for the modified configuration in table IV. A very limited number of wind-tunnel tests were conducted for the modified configuration with the wing-tip booms, wheel pants, and parachute canister attached. In some circumstances, increments due to adding the modifications were evaluated from the larger wind-tunnel data base available on the stripped version of the airplane. These increments were then added to the baseline data of table III to acquire values for table IV. Reference 14 was one of the sources from which data were used for determining these increments. For some coefficients, however, only the set of data for the clean-wing configuration was available and, of necessity, was used directly for the modified configuration. This was particularly true for some components of the lift, drag, and pitching-moment coefficients such as, for example, the flap deflection and incremental sideslip effects. Other data commonality involved contributions due to the tail assembly and elevator and rudder deflections. Since table IV presents the various coefficients in exactly the same format as table III, a comparison of the tabulated values can easily identify the common entries.

The following features of this particular model are worth noting:

1. Sideslip effects are included in the lift, drag, and pitching-moment coefficients.
2. Angle of attack and thrust effects influence nearly all individual components.
3. Rolling and yawing-moment coefficients are present at zero sideslip at the higher angles of attack.

These features promote coupling between the longitudinal and lateral vehicle motions, particularly at the larger sideslip angles and/or at angles of attack in the region of the stall and beyond.

Control-Force Model

A control loader is available in the general aviation simulator for use with the elevator and aileron controls. Measurements of elevator hinge moments were obtained during some of the full-scale wind-tunnel tests. The data were used to determine hinge-moment coefficients for use in calculating wheel forces to be generated by the simulator control loader. The equations used are given in appendix C

and values of the hinge-moment coefficients are given in table V. Although aileron hinge moments were not measured in the wind-tunnel tests, similar equations were programed for the simulator and estimates of the hinge-moment coefficients were employed. A simple spring system is used with the rudder pedals in the simulator cockpit. For completeness in comparing simulator and flight time-history results, a linear variation of rudder pedal force with rudder deflection was programed to represent simulator inputs.

Validation

Validation of the simulation requires that a comparison be made between math-model predictions and flight-test data. Although numerous flights of the aircraft pictured in figure 2 were made, most flights unfortunately were spin tests. Only a few flights were made that provide data useful for stall-departure comparisons. Note also that for spin testing, the measurement ranges of the instruments were scaled for the spin and were thus considerably larger than desired for only stall-departure testing. As a consequence, measurement accuracy was reduced. Nevertheless, a number of comparisons between simulation and flight measurements were made, most being for the baseline configuration. Comparisons were made using flight data from various speed conditions, acceleration/deceleration runs, and steady-heading sideslips, as well as dynamic-stability checks. Several time-history comparisons were also made. Figures 7 through 10 and tables VI and VII present some of these comparisons. Each of these figures and tables are discussed in detail in appendix D. An examination of the various comparisons presented indicates good overall agreement between simulation and flight-test results.

Results and Discussion

All of the information contained in the "Results and Discussion" section of this report was obtained from simulation data. Since math-model definition used tabular data, a linear interpolation scheme was employed in the simulation to provide intermediate values. The information presented herein includes (1) comparisons of the baseline and modified configurations from tabulated values, (2) trim conditions in straight, turning, and sideslipping flight, and (3) time-history departures for straight, turning, and sideslipping flight. Also included are a few dynamic-stability checks for both straight and turning flight. Only the flaps-retracted condition was examined because very limited wind-tunnel data existed for flaps deflected.

Tabulated-Data Comparisons

Differences occurring in the responses of the simulated airplane due to adding the drooped-leading-edge modification can be anticipated and/or possibly understood by examining comparisons made of the coefficients from the tabulated data. Figure 11 presents a comparison of coefficients of the configurations with and without the leading-edge modification for only those elements of the math models that differ. For those coefficients not shown, the tabular values developed for the baseline configuration are used without change for the modified configuration. It should be noted that the results given in figure 11 are for the power-off condition ($C_T = 0$). Power effects determined for the baseline configuration were applied directly to the modified configuration. Thus, power effects are identical for the two configurations.

Figure 11(a) shows the increments in the basic lift, drag, and pitching-moment coefficients due to adding the modification to the outboard wing panels of the airplane. Adding the modification causes no drag penalty in the angle-of-attack region up to about 12°; also, the lift remained nearly unchanged in this α range. However, the small amount of pitching moment obtained was probably due to the added area of the modification along the wing leading edge. At the higher angles of attack, the presence of the modification caused substantial increases in the lift coefficient with very little change in pitching moment. Some drag penalty caused by the higher lift was also experienced.

A number of changes in the vehicle lateral characteristics occurred when the leading-edge modification was added to the vehicle. Some changes occurred only at the higher angles of attack whereas some changes were evident over the complete angle-of-attack range. Adding the modification delayed the appearance of yawing and rolling-moment coefficients for the zero sideslip condition (fig. 11(b)) from just above stall until an angle of attack of 30°. The use of the modification also resulted in an increase in directional stability C_{n_β} for an angle of attack up to 25° and an increase in effective dihedral C_{l_β} over the α range (fig. 11(c)). Evidence of flow attachment over the outer-wing panels when the modification is employed can be seen in the increased aileron effectiveness $C_{l_{\delta_a}}$ (fig. 11(d)) and in the stable damping in roll C_{l_p} (fig. 11(e)) at the higher angles of attack. Undoubtedly the improvement in C_{l_p} will have a large influence on rolling and yawing motions. A larger yaw damping C_{n_r} (fig. 11(f)) occurred in the α range between 10° and 20° for the modified configuration.

Wings-Level Trim Comparisons

One feature of the real-time general aviation simulation program was the availability of a subroutine that would trim the airplane in any number of desired states. Typical examples are straight and level flight, steady climbing flight, sideslipping flight, etc. This routine uses an interactive technique involving the mathematical method of steepest descent that adjusts the control deflections and aircraft attitudes until the specified constraints of the trim maneuver are met. The routine was employed to achieve comparable trim conditions for the baseline and modified configurations. For the wings-level trim comparisons, the trim conditions specified to be met by the subroutine were $\dot{p} = \dot{q} = \dot{r} = \dot{u} = \dot{v} = \dot{w} = \dot{\psi} = \phi = 0$. Airplane weight, altitude, and speed were required program inputs. One additional input, either flight-path angle γ or throttle setting δ_t, was required. Figures 12, 13, and 14 present wings-level trim comparisons at sea level for the baseline and modified configurations for straight and level flight, throttle-closed flight, and full-throttle flight.

For straight and level flight, vehicle flight-path angle was specified zero as a trim condition. Figure 12 presents the corresponding values of angle of attack, sideslip angle, control deflections, and throttle setting necessary to trim the simulated airplane through the speed range at sea level. Values of thrust coefficient C_T and engine speed N are given for convenience. Results of the comparison show little difference between the two configurations. The modified configuration did use slightly less up-elevator through the speed range and less sideslip angle at the lower speeds. The variations of β, δ_a, and δ_r with V are due primarily to power effects. The two airspeed values from figure 12 where $\delta_t = 1.0$ represent the maximum and the minimum straight and level flight speed permitted by the simulation. For clarity, the following table itemizes values of some of the parameters:

SEA-LEVEL FULL-THROTTLE COMPARISON

Configuration	V, ft/sec	δ_t	δ_e	α, deg	N, rpm
Minimum speed					
Baseline	96.3	0.994	−7.16	14.95	2514
Modified	95.6	.999	−6.48	15.03	2518
Maximum speed					
Baseline	198.0	0.997	4.30	−1.09	3023
Modified	196.0	.997	4.66	−.75	3008

An examination of the minimum-speed table indicates that adding the modification permitted trimming at a slightly slower speed and with less up-elevator. The maximum-speed table indicates that adding the modification reduced maximum speed by 2 ft/sec. Note, however, that the simulation engine-speed value exceeds an operational limit of 2600 imposed on the flight vehicle. From the α values in this table and from the data of figure 11, it is apparent that the small difference between the baseline and modified configurations is due to the angles of attack not having reached the region where the modification is truly effective.

Comparisons of sea-level trim curves for the baseline and modified configurations are provided in figure 13 for the throttle-closed condition ($\delta_t = 0$) and in figure 14 for the full-throttle condition ($\delta_t = 1.0$). Figure 14 provides results only for the speed range less than that for straight and level flight conditions given in figure 12. Both figure 13 and figure 14 cover the angle-of-attack range where the modification is effective. The maximum up-elevator of −25° specified for the aircraft limits the lowest value of speed attainable. It is at the lower speeds where the angle of attack exceeds approximately 14° that the benefits of the leading-edge modification are apparent. With the leading-edge modification, the airplane can be trimmed at a lower speed for both throttle-closed and full-throttle conditions. Because of the large glide angles involved, some of the throttle-closed results appear of little practical use. For the full-throttle condition, however, adding the modification permits the vehicle at a given speed to operate at a lower angle of attack with essentially one-half the rate of descent of the baseline configuration. In both figures 13 and 14, large changes in the amount of aileron and rudder control deflection at the lower speeds indicate that a difficulty exists for a pilot to maintain lateral control of the airplane for small changes in speed. A comparison of the curves shows that an improved situation exists for the modified configuration at any given speed.

For completeness, trim lift curves associated with the results given in figures 12, 13, and 14 are presented in figure 15. Recall that lift coefficients as used herein include the propeller-thrust components. Also, it should be noted that in assessing the results of figures 12, 13, and 14 the trim conditions indicated here represent a solution set for the equations of motion under static conditions and in no way indicate the response of the airplane in real time if slightly disturbed from these conditions.

Departures From Level Flight

Time histories of 20- to 30-sec duration that permit comparison of the responses of the simulated airplane with and without the leading-edge modification

are given in figures 16 through 18. In all three figures, straight and level trim flight exists for the first 2 sec. Control inputs are then introduced that are different for the three figures. The throttle chops shown in figures 16 and 18 occurred in 2 sec. The elevator ramp shown in figures 16 and 17 had a rate of −1 deg/sec and was applied for 8 sec. Aileron and rudder ramps were also of 8-sec duration and were used to neutralize the controls from their trim values after power was removed. The elevator and aileron control deflections shown in figure 18 were driven by feedback laws using altitude and roll angle, respectively, to roughly approximate a pilot's attempt to maintain altitude with wings level.

An examination of figures 16(a) and 16(b) indicates that for the baseline configuration (fig. 16(a)) the airplane departs by rolling and yawing to the left (see ϕ and ψ traces); for the modified configuration (fig. 16(b)) this type of departure did not occur. Also, the roll rate and sideslip traces indicate the existence of an unstable wing rock for the baseline configuration for the last 20 sec of the record. For the modified configuration the traces indicate the possible beginning of a wing rock at the end of the record. The results given in figure 16 are for the power-off condition; figure 17 presents similar time-history comparisons for the power-on condition. For the records of figure 17, all controls were held fixed at the trim value except for the elevator. An elevator-ramp input identical to that of figure 16 was employed. An examination of the time-history traces of figure 17 indicates that the modified configuration departs into a smooth spiraling turn but the baseline configuration does not. Even so, one obvious benefit of adding the leading-edge modification in this particular situation was the elimination of the severe wing rock shown by figure 17(a).

A common flight-test technique employed for stall departure studies is for the pilot to retard the throttle from a straight and level flight condition trimmed at just below stall and then to apply elevator control smoothly and gradually in an attempt to hold constant altitude. In order to introduce the elevator displacement gradually in the simulation while at the same time holding the wings level, two closed-loop control laws were implemented. The equations used were

$$\delta_e = K_1(K_2\dot{h} + h') + \delta_{e,i}$$
$$\delta_a = K_3(K_4\dot{\phi} + \phi') + \delta_{a,i}$$

where the prime designates differences from the initial trim value and the subscript i represents the initial trim value. Several sets of gain values K_1, K_2, K_3, and K_4 were tried with results similar to those shown in figure 18. Note that the rudder input was the same as used in figure 16. An examination of figures 18(a) and 18(b) shows that more aileron activity was used for the baseline configuration. Thus the baseline configuration would be more difficult for a pilot to control laterally. Evidence of a wing-rock condition appears in the roll rate and sideslip traces for both configurations although it appeared to start at a lower value of α and to be more severe for the baseline configuration. As shown by figures 18(a) and 18(b), elevator deflection reached the limit of −25° and then was held constant at this value. Even so, the angle of attack continued to increase up to a value of 40°, which is the tabulated-data limit. Time-history motions are, of course, invalid once the data limits have been exceeded. Note that the increase in angle of attack with increasing time for both configurations occurred because the rate of descent was increasing while the pitch attitude remained constant in a nearly horizontal position.

The time-history comparisons given in figures 16 through 18 indicate a beneficial effect on the vehicle motions of adding the outboard leading-edge modification. Similar benefits were noted at other speeds, altitudes, and control inputs.

Trim In Turning Flight

Trim conditions associated with turning flight were obtained after inserting appropriate expressions into the simulation trim routine that specify the desired maneuver constraints. For example, one constraint for circular flight at constant altitude is that the body angular rates p, q, and r must combine vectorially so that the resultant angular velocity is vertical. The same condition also applies for climbing or descending flight along a helical flight path. (See ref. 17 for other constraints.) Sketches of typical results of turning flight obtained from the simulation are shown in figure 19. Roll angle for circular flight at constant altitude is shown in figure 19(a) as a function of airplane velocity. The solid curve corresponds to the simulation results for the full-throttle condition. At the higher velocities, the engine speed predicted by the simulation exceeds the operational limit of 2600 permitted for the aircraft. Also shown in figure 19 is the reduced throttle curve where the simulation engine speed is limited to that of the aircraft. The boundaries shown are for a given altitude and the envelope shrinks as altitude increases. Regions within and outside the boundary represent climbing and descending flight, respectively, along a helical flight path as illustrated in figures 19(b) and 19(c).

A comparison of trim results for full-throttle turning flight for configurations with and without the leading-edge modification is given in figure 20. A low

value of velocity was selected so that conditions are similar to those depicted by section A-A in figure 19. An examination of the information from figure 20 indicates that almost the same results were obtained for the baseline configuration as for the modified configuration, with roll angles having magnitudes less than 20°. As expected, a small difference in elevator deflection was obtained between the two configurations. For roll angles having magnitudes greater than 20°, however, differences due to the presence of the leading-edge modification are apparent. One significant benefit is that at a given roll angle adding the leading-edge modification reduces the rate of descent by a factor of one-half. Also, the modified configuration operated at a lower angle of attack and, consequently, required less elevator control.

For the power-off condition, some trim results were obtained with and without the leading-edge modification for the airplane in a descending helical flight path. Figure 21 presents a comparison of the maximum bank angle for which the airplane can be trimmed for the lower portion of the speed range. For the baseline configuration the maximum bank angle for which the airplane could be trimmed is limited by the maximum lift coefficient of the configuration. (For convenience, the curve of $C_{L,\mathrm{trim}}$ versus α shown in figure 21 was obtained for wings-level trim. Note, however, that the curve is applicable for this situation since the dynamic term $C_{L,\mathrm{dyn}}$ is small.) With the leading-edge modification, the airplane can be trimmed to a larger bank angle at a given speed than with the baseline configuration, can bank at a speed slower than the airplane can attain in the baseline configuration, and is limited in both maneuvers by the maximum up-elevator deflection available.

The trim results of figures 20 and 21 determined by the simulation are applicable only for static conditions. Note that the trim routine simply searches for numerical values for a set of unknown variables that satisfy the equations of motion and the constraint equations. To assure adequate dynamic response, additional analyses and/or time histories of the turning maneuvers are required.

Time Histories for Turning Flight

To illustrate the effect of the leading-edge modification on the dynamic response of the vehicle in a turn, time histories of the resulting motion were obtained for configurations with and without the modification with identical slow ramp inputs applied to the elevator. The same initial conditions of speed, altitude, and roll angle were used for both configurations. Initially, the vehicle was trimmed in a turn with a roll angle of 25°. An elevator ramp of 0.5 deg/sec was inserted into each run at $t = 2$ sec and was applied for 16 sec. All other control deflections were held fixed at their trim values. Figures 22 and 23 present the time histories for the power-off and power-on conditions, respectively, for the baseline configuration. Figures 24 and 25 present comparable time histories for the power-off and power-on conditions for the modified configuration.

A comparison of the various time-history traces shows that with power off the baseline configuration (fig. 22) rolled over the top (roll left from a right turn) and appeared to develop an unstable wing rock. The modified configuration (fig. 24) did not roll over the top but continued to turn in the same direction. After a heading change of about 180°, a wing rock also developed. Similar qualitative results for the two configurations were obtained during power-off flight tests when ramp-type elevator inputs were applied during turning flight while the other controls were held fixed. (See ref. 10.) With power on, the baseline configuration (fig. 23) rolled into a steep spiral of increasing tightness. Although a large angular rate developed, the motion was not a spin because the angle of attack was in the region of maximum lift and was decreasing with time. With the leading-edge modification (fig. 25), the vehicle also developed a steep spiral, but with less rate of descent and less total angular velocity than that obtained for the baseline configuration. No evidence of wing rock appeared in either power-on time history. The comparisons permitted by the time histories of figures 22 through 25 indicate that power effects were important and that the use of the leading-edge modification provided a beneficial effect both with power on and power off.

As a consequence of the results shown on figures 23 through 25, additional time histories for the baseline and modified configurations were taken with the same control inputs for turns both to the right ($\phi = +25°$) and to the left ($\phi = -25°$) for a range of steady-state throttle δ_t settings from 0 to 1.0. The time histories have been omitted here; however, the results summarized in figure 26 show sketches of the initial directional departure and the existence of wing rock. An examination of the different situations depicted shows that there is a large effect of power, turn direction, and whether the wing leading-edge modification is on or off. Note that a departure by rolling over the top can occur for both baseline and modified configurations but for different turn directions and throttle settings. Likewise, wing-rock conditions can occur when the throttle is fully deflected ($\delta_t = 1.0$). A qualitative analysis of the different situations indicates that the initial departure can be traced to the presence of asymmetrical forces and moments that exist at zero sideslip. Specifically, it is the change in $C_{Y,o}$, $C_{n,o}$, and $C_{l,o}$ with increasing angle of attack

from the trim value as a result of the elevator-ramp input that generates the disturbing forces and moments on the vehicle.

Trim in Sideslips

Comparisons of trim values for the baseline and modified configurations for various sideslip angles were obtained for several speeds, altitudes, and throttle settings. Figure 27 presents the results for the throttle-closed condition for $V = 120$ ft/sec since this flight condition was considered to be of interest. The angle of attack was around 9.5°, which is about 4° below that for trimmed $C_{L,\max}$ of the baseline configuration. (See fig. 15.) The results of figure 27 show that to achieve a given sideslip angle the modified configuration required a larger roll angle, more rudder deflection, and more aileron deflection than required by the baseline configuration. The increase in directional stability and effective dihedral when the modification is added to the wing leading edge (fig. 11(c)) is primarily responsible for the differences shown in the trim values.

Departures from a Sideslip Condition

Departures from various trim conditions in sideslip for both the baseline and modified configurations were performed that involved only an elevator-ramp input while holding the throttle setting, aileron deflection, and rudder deflection at their trim values. Elevator ramps were varied by changing the size of the incremental elevator deflection or the time interval involved. Typical time-history results for the baseline and the modified configurations are presented in figures 28(a) and 28(b), respectively. For both time histories, the airplane was at an altitude of 5000 ft with a velocity of 120 ft/sec and was trimmed at a sideslip angle of $+10°$ with the throttle closed. Elevator ramps consisted of incremental elevator deflections of $-12°$ applied linearly over a time interval of 26 sec. Trim conditions were held for the first 2 sec of each time history, and then the elevator ramp was initiated. An examination of figure 28(a) shows that the baseline configuration eventually entered a left spin. The spin was very steep with an angle of attack of about 25°, a pitch attitude of about $-65°$, and a spin rate of approximately 180 deg/sec. Comparisons with flight-test data could not be made because a match of control positions between the simulation and flight-test results could not be found. Note, however, that a good comparison would not be expected since the model was devised only for small angular rates and not those approaching steady spin values. For the modified configuration, figure 28(b) shows that the vehicle entered a slow descending left turn. A comparison of figures 28(a) and 28(b) indicates that in this situation a sizable beneficial effect was obtained by adding the wing-leading-edge modification. Additional time histories were also obtained for different sideslip angles and different elevator-ramp inputs. A brief summary of these results for the power-off condition is presented in table VIII. Both initial sideslip angle and the size of the elevator input were varied. The time interval of 26 sec for the ramp input was held constant. An examination of the results shows that the time histories of the modified configuration always involved a descending turn whereas mostly spins developed for the baseline configuration. The unsymmetrical result obtained for the baseline configuration about zero sideslip can be attributed to the presence of the aerodynamic yawing and rolling moments that exist at zero sideslip for the angle-of-attack range above stall. It appears that for most of the combinations tested, adding the leading-edge modification improved the airplane departure characteristics in sideslip.

Dynamic-Stability Comparisons

A brief examination of dynamic stability, both longitudinal and lateral, was made using the math model herein in conjunction with the linear-analysis computer program described in reference 18. The analysis assumes small perturbations and linearized aerodynamics about the trim point. Eigenvalues of the longitudinal short period and phugoid modes of motion were obtained along with those of the roll, spiral, and Dutch roll lateral modes of motion. Both straight and turning flight were examined, and some sample results are given in figures 29 and 30, respectively, for the vehicle both with and without the leading-edge modification operating at an altitude of 5000 ft.

Figure 29 presents straight flight comparisons for the damping ratio and undamped natural frequency of the Dutch roll mode and for the roll-mode time constant. These parameters showed the largest effect of adding the leading-edge modification over the speed range. The other stability parameters showed differences between the data for the baseline and modified configurations that were small or of little consequence as regards vehicle handling qualities. The results of figure 29 show that adding the leading-edge modification improved the vehicle roll response at the slower speeds. For the Dutch roll mode, however, the modified configuration appears to be a little more sensitive (higher frequency and reduced damping). Also, an examination of the damping-ratio values shows that the Dutch roll mode becomes unstable at an angle of attack of about 13°. This situation occurs for configurations with and without

the leading-edge modification with either full power or idle power. Thus, it appears that the wing-rock experiences mentioned previously can be traced to a stick-fixed unstable Dutch roll mode.

Figure 30 presents some turning-flight comparisons for the Dutch roll mode, the roll-mode time constant, and the longitudinal phugoid mode. The airplane was trimmed in a turn at an altitude of 5000 ft with a velocity of 120 ft/sec and with a roll angle of 25°, both left ($\phi = -25°$) and right ($\phi = +25°$) turns being made. Turns were made with various steady-state throttle settings from closed ($\delta_t = 0$) to full ($\delta_t = 1.0$). Thus, the trim conditions ranged from a spiral of decreasing altitude for throttle closed to climbing flight at full throttle. The results in figure 30 are plotted against throttle setting for convenience and permit directly comparable curves for the baseline and modified configurations. The results show that adding the leading-edge modification improves the roll response. Adding the modification also increased the Dutch roll undamped natural frequency but reduced the damping ratio, particularly at the larger throttle settings. The influence of the leading-edge modification on Dutch roll damping ratio, however, was considerably less than that due to power. As noted for figure 29, the effect of the leading-edge modification on all of the modes of motion was largest for the rolling mode and Dutch roll mode. Although the effect of the leading-edge modification on the phugoid mode was small, some difference was noted in the phugoid damping ratio due to turning left and turning right. In fact, for a left turn at full throttle, the phugoid mode was slightly unstable. These results are, of course, for controls held fixed. In addition, the angles of attack involved were all less than that for $C_{L,\max}$ for the baseline configuration. Thus the changes resulting from the presence of the modification were due to differences in the lateral aerodynamic characteristics since it is in the region beyond maximum lift where large benefits occur to the longitudinal characteristics as well as the lateral characteristics when the leading-edge modification is added.

Initial Stall-Departure Assessment

With throttle retarded, the vehicle with the clean wing exhibited the typical stall-departure characteristics of light general aviation airplanes that consist of rolling-off and yawing at the stall and at higher angles of attack. With the leading-edge modification the vehicle in a comparable situation had departures that occurred mainly in the plane of symmetry. These departures involved primarily the longitudinal modes of motion. Thus, the stall for the modified configuration was more docile and the airplane entered a mush type of maneuver. In addition, the modified configuration requires smaller control deflections for trim at a given speed, can be trimmed at a slower speed, and involves lower rates of descent. When power was applied, both the baseline and modified configurations at the higher angles of attack have departures involving rolling and yawing types of lateral motions. These maneuvers can be traced to the presence of asymmetrical moments at zero sideslip due to the application of power. Asymmetrical moments at zero sideslip are also involved in the departures for turning and sideslipping flight. In general, the modified configuration showed some form of improved response whether in straight, turning, or sideslipping flight with various power settings when compared with responses for the baseline configuration.

Concluding Remarks

A six-degree-of-freedom nonlinear simulation was developed for a two-place, single-engine, low-wing general aviation airplane for the stall and initial departure region of flight for analytical studies and for future piloted studies using the Langley general aviation cockpit. The math model was developed using data obtained in the Langley 30- by 60-Foot Tunnel on a full-scale airplane of the same type. Model features included power effects and aerodynamic coupling linking the longitudinal and lateral modes of motion, including the presence of yawing and rolling moments at zero sideslip for the power-off condition at the higher angles of attack. Comparisons of simulation predictions with flight-test data served to validate the model.

Two configurations, one with and one without the leading-edge modification on the outboard wing panels, were programed for use with the simulation. Comparisons of the aerodynamic coefficients as well as the trim characteristics for straight, turning, and sideslipping flight show improved results at the higher angles of attack for the configuration with the leading-edge modification. Such improvements show the airplane with the modification can be trimmed with wings level at a slower speed or at the same speed as the clean-wing configuration, but with less control deflection and less rate of descent. Also, time-history traces for straight, turning, and sideslipping flight show improved departure responses at the higher angles of attack for the configuration with the leading-edge modification. Power effects were found to be significant for both configurations.

NASA Langley Research Center
Hampton, VA 23665
February 5, 1985

Appendix A—Thrust Model

The thrust model for the simulation was developed using wind-tunnel measurements made in the Langley 30- by 60-Foot Tunnel on an airplane of the same type as used in the flight program. For a series of wind-tunnel tests, a thrust-torque balance was installed between the engine shaft and the propeller, and the engine cowling was lengthened near the fire wall to retain the relationship between the cowling and the propeller. The propeller had two blades and was of the fixed-pitch type. In addition, the propeller was a climb prop identical to that used for the flight-test program. Measurements were obtained for a range of tunnel airspeeds, engine speeds, and airplane attitude angles. From the measurements taken, standard curves of propeller-thrust coefficient C_T', power coefficient C_P', and propeller efficiency η as a function of advance ratio J were developed. (See fig. A1.) These curves are, of course, for propeller-installed conditions. Also, using the torque balance measurements and engine speed, a plot of available brake horsepower $(\mathrm{BHP})_a$ as a function of manifold pressure MP at sea level was constructed. (See fig. A2.) Note that the straight lines for constant engine speed all intersect at a common point at zero manifold pressure. (See ref. 19.) Thus, $(\mathrm{BHP})_a$ can be expressed analytically as

$$(\mathrm{BHP})_a = K_{\mathrm{MP}}\mathrm{MP} + C_{\mathrm{MP}} \tag{A1}$$

where for the engine tested $C_{\mathrm{MP}} = -27$ and the measured slope K_{MP} is a function of engine speed. (See fig. A2.)

For simulator use, a relationship between manifold pressure and throttle position is required. An intermediate throttle variable δ_t' is defined such that $\delta_t' = 0$ when $\mathrm{MP} = 0$ and $\delta_t' = 1$ for full throttle deflection. The expression developed is

$$\mathrm{MP} = 29.92\left(1 - \frac{1.42}{29.92}\frac{N}{2600}\right)\delta_t' \tag{A2}$$

The term in parentheses accounts for the drop in manifold pressure due to engine speed that occurs for a full throttle setting. Note that in a practical situation it is not possible to close the throttle in the cockpit and reduce manifold pressure to zero. Therefore, use is made of the equation

$$\delta_t' = K_{\delta,1}\delta_t + K_{\delta,2} \tag{A3}$$

where δ_t represents the steady-state throttle setting. Thus, this equation is used to adjust the engine idle conditions. Practical limits exist for the choices for the constants $K_{\delta,1}$ and $K_{\delta,2}$ in addition to the constraint that $K_{\delta,1} + K_{\delta,2} = 1$. Values of 0.65 and 0.35 are used for $K_{\delta,1}$ and $K_{\delta,2}$, respectively. The value of $K_{\delta,2}$ is believed near the minimum usable value. Engine dynamic response to a throttle movement is included in the simulation by incorporating a first-order lag following the throttle handle movement in the cockpit thusly

$$\delta_t = \frac{1}{\tau_e s + 1}\,\delta_{t,c} \tag{A4}$$

Recall that the brake horsepower required to turn the prop at sea level can be written functionally as

$$(\mathrm{BHP})_r = f(N, V) \tag{A5}$$

Note that the two horsepower conditions (i.e., brake horsepower available $(\mathrm{BHP})_a$ and brake horsepower required $(\mathrm{BHP})_r$) must match. Thus,

$$(\mathrm{BHP})_a = (\mathrm{BHP})_r \tag{A6}$$

Now, since

$$(\mathrm{BHP})_r = \frac{\mathrm{Power}}{550} = \frac{C_P'\rho n^3 D^5}{550} \tag{A7}$$

the value of C_P' can be calculated and used with the curves of figure A1 to obtain the corresponding values of J and C_T'. Finally, from expressions containing J and C_T', namely,

$$J = \frac{V}{nD} \tag{A8a}$$

$$T = C_T'\rho n^2 D^4 \tag{A8b}$$

values of thrust T and velocity V can be calculated. The particular calculating scheme employed was to choose values of δ_t' and N, determine $(\mathrm{BHP})_a$, and, then, using the equations calculate C_P' and finally T and V. From plots of T versus V for a given value of δ_t', a final form for the thrust model at sea level over the stall-departure velocity range was selected as

$$T_{sl} = T_0 + T_1 V \tag{A9}$$

where T_0 and T_1 are functions of δ_t' and are given in the following table:

δ_t'	T_0	T_1
0	−237	+0.100
.2	−100	−.060
.4	40	−.280
.6	182	−.510
.8	314	−.675
1.0	452	−.820

Thrust at altitude is obtained from

$$T = T_{sl}\sigma \tag{A10}$$

As indicated previously and sketched in figure 5, the three inputs to the thrust model are altitude, speed, and throttle setting. Finally, for use with the aerodynamic model, the following coefficient was obtained:

$$C_T = \frac{T}{\bar{q}S_w} \tag{A11}$$

A linear model was chosen for the sea-level thrust and speed relationship (eq. (A9)) as being particularly appropriate for the velocities greater than about 60 ft/sec. At lower speeds and large throttle settings, the linear model appears to underestimate the thrust that can be developed. A plot of C_T versus V for different throttle settings δ_t' for the velocity range of interest is given in figure A3.

Engine speed is used in the simulation for the calculation of the propeller gyroscopic terms in the equations of motion and for the tachometer instrument display in the cockpit. From information previously obtained in the thrust development, the following quadratic expression was used to fit the data and programed in the simulation:

$$N = N_0 + N_1 V + N_2 V^2 \tag{A12}$$

where the constants are given in the following table:

δ_t'	N_0, rpm	N_1, rpm	N_2, rpm
0	−2350	17.25	0
.2	−500	11.00	.0040
.4	700	3.70	.0200
.6	1620	−1.65	.0315
.8	2100	−2.35	.0300
1.0	2520	−2.55	.0255

For use with the engine instrument display in the simulator cockpit, engine manifold pressure was calculated with the use of equation (A2) and the altitude correction of reference 19 as follows:

$$\mathrm{MP} = \delta_t' \left(29.92 - \frac{1.42}{2600}\mathrm{N}\right)\left(\frac{\sigma - 0.117}{0.883}\right) \tag{A13}$$

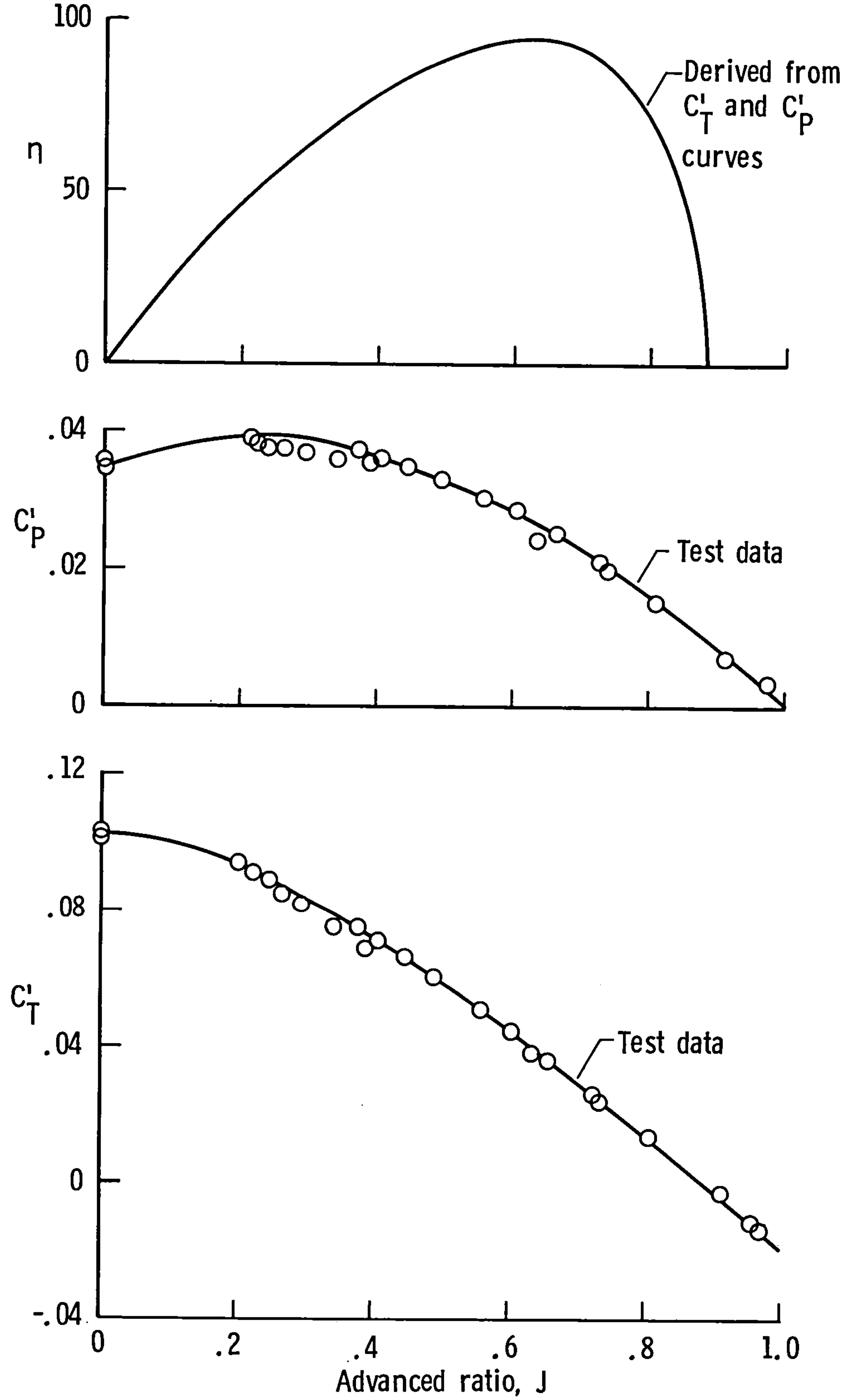

Figure A1. Thrust coefficient, power coefficient, and installed-propeller efficiency for the two-bladed climb propeller obtained from tests on airplane in Langley 30- by 60-Foot Tunnel.

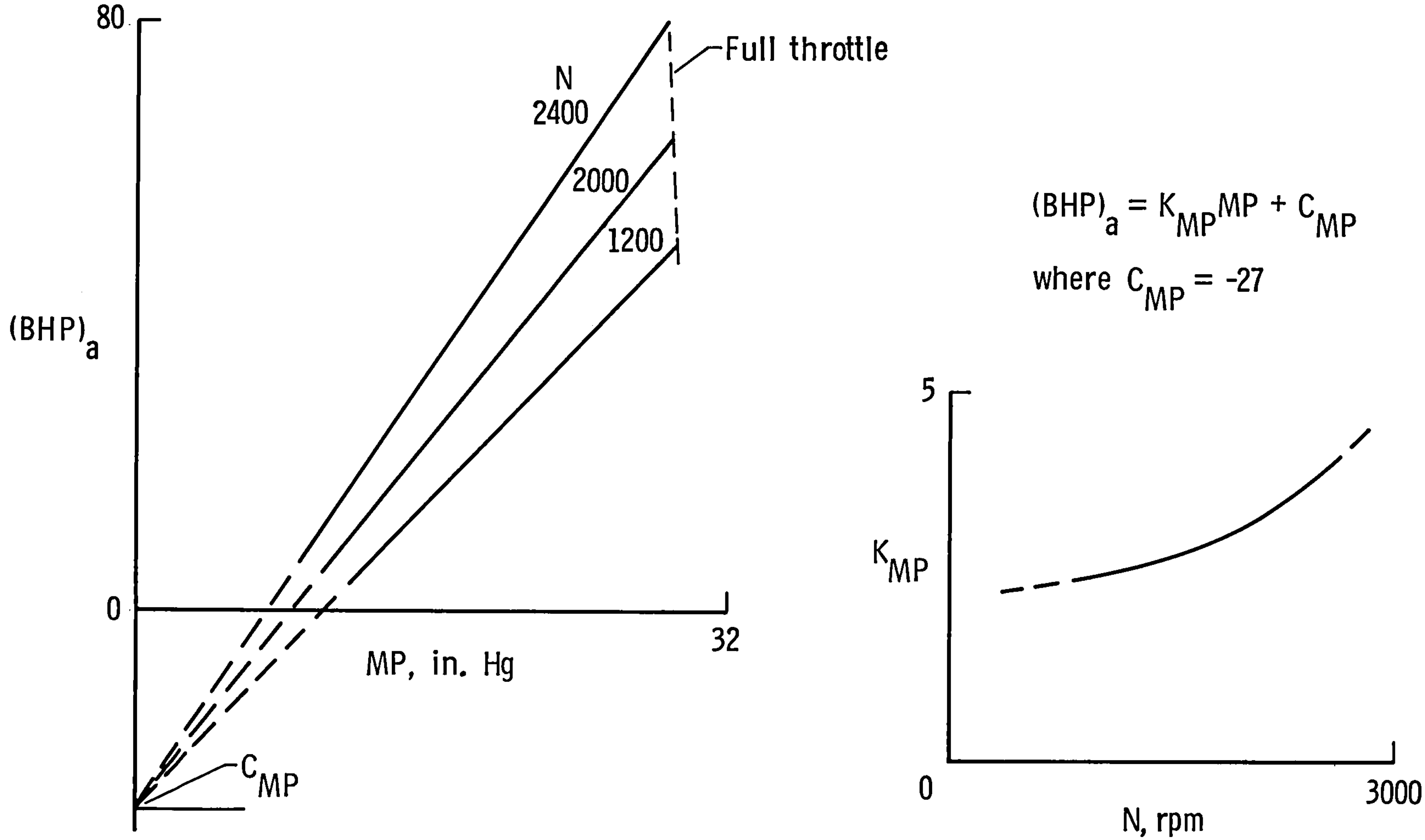

Figure A2. Sketch of a typical variation of available brake horsepower $(BHP)_a$ with manifold pressure MP at sea level for a normally aspirated aircraft engine.

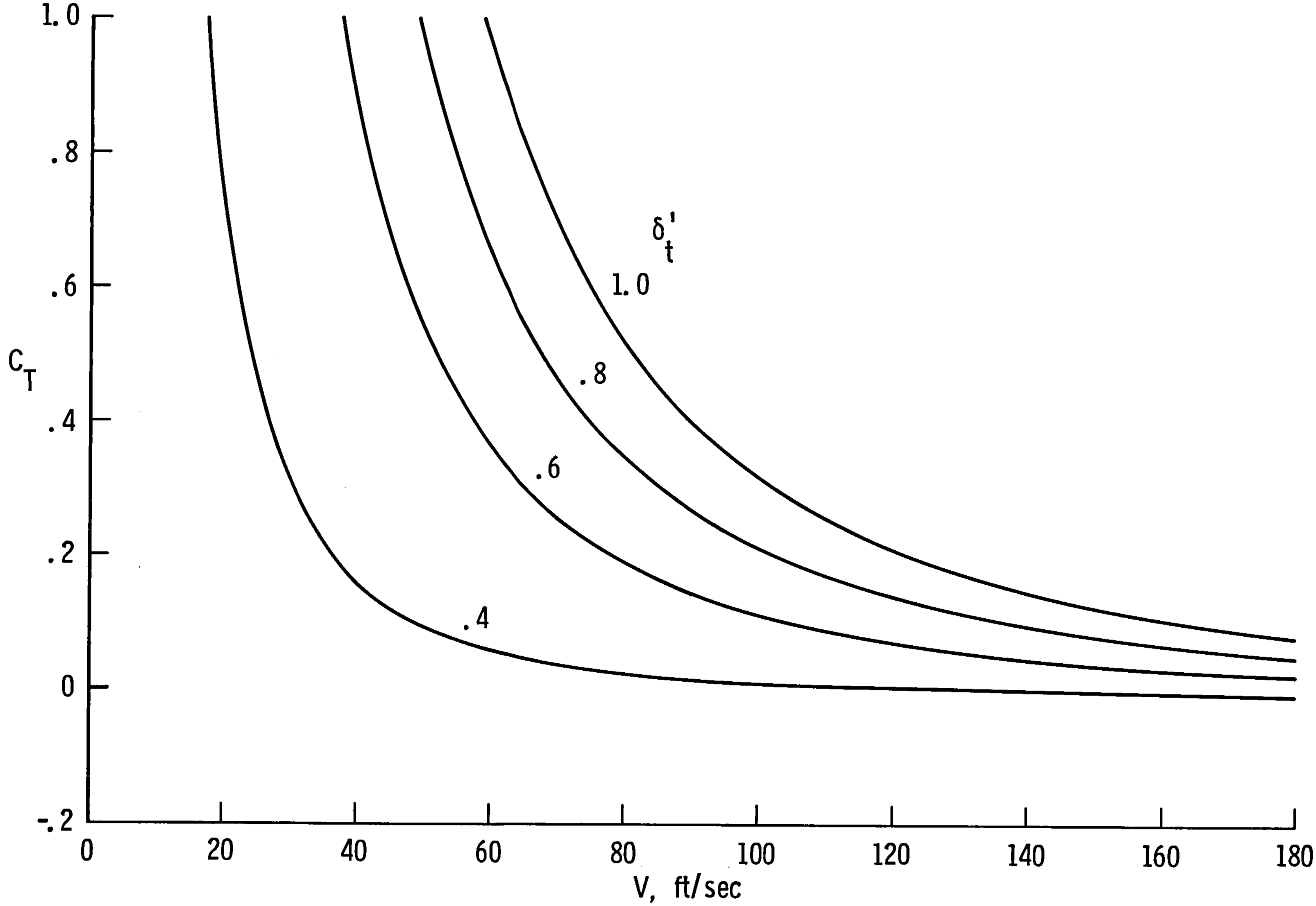

Figure A3. Variation of thrust coefficient C_T with velocity for various throttle settings δ_t'.

Appendix B—Equations of Motion and Aerodynamic Math Model

The equations used to describe the motions of the airplane for the general aviation simulation were nonlinear, six-degree-of-freedom, rigid-body equations referenced to the body-fixed system of axes shown in figure 1.

The equations are as follows:

Forces:

$$\dot{u} = rv - qw - g\sin\theta + \frac{F_{X,b}}{m}$$
$$\dot{v} = pw - ru + g\cos\theta\sin\phi + \frac{F_{Y,b}}{m}$$
$$\dot{w} = qu - pv + g\cos\theta\cos\phi + \frac{F_{Z,b}}{m}$$

Moments:

$$\dot{p} = \frac{I_Y - I_Z}{I_X}qr + \frac{I_{XZ}}{I_X}(\dot{r} + pq) + \frac{L_b}{I_X}$$
$$\dot{q} = \frac{I_Z - I_X}{I_Y}pr + \frac{I_{XZ}}{I_Y}(r^2 - p^2) + \frac{M_b}{I_Y} - \frac{I_p}{I_Y}2\pi nr$$
$$\dot{r} = \frac{I_X - I_Y}{I_Z}pq + \frac{I_{XZ}}{I_Z}(\dot{p} - qr) + \frac{N_b}{I_Z} + \frac{I_p}{I_Z}2\pi nq$$

The force and moment terms $F_{X,b}$, $F_{Y,b}$, $F_{Z,b}$, L_b, M_b, and N_b are a combination of aerodynamic and thrust effects. The terms in the $\dot{q}$ and $\dot{r}$ equations containing I_p are propeller gyroscopic terms. Although these terms are small, they are included for completeness. Euler angles were computed by using quaternions to allow continuity of large attitude motions. Auxiliary equations include the following:

$$\alpha = \tan^{-1}\frac{w}{u}$$

$$\beta = \sin^{-1}\frac{v}{V}$$

$$V = \sqrt{u^2 + v^2 + w^2}$$

$$a_Z = -qu + pv - g\cos\theta\cos\phi + \dot{w}$$

In calculating the external forces, use was made of wind-tunnel measurements obtained in the stability-axis system. The transformation

$$\begin{bmatrix} F_{X,b} \\ F_{Y,b} \\ F_{Z,b} \end{bmatrix} = \begin{bmatrix} \cos\alpha & 0 & -\sin\alpha \\ 0 & 1 & 0 \\ \sin\alpha & 0 & \cos\alpha \end{bmatrix} \begin{bmatrix} F_{X,s} \\ F_{Y,s} \\ F_{Z,s} \end{bmatrix}$$

provides the forces for the equations of motion. The subscript s signifies the stability-axis system. In addition, coefficients, rather than forces and moments, were employed by using the following equations:

$$F_{X,s} = -C_{D,s}\bar{q}S_w$$
$$F_{Y,s} = C_{Y,s}\bar{q}S_w$$
$$F_{Z,s} = -C_{L,s}\bar{q}S_w$$
$$L_b = C_{l,b}\bar{q}S_w b$$
$$M_b = C_{m,b}\bar{q}S_w\bar{c}_w$$
$$N_b = C_{n,b}\bar{q}S_w b$$

Finally, each of the six aerodynamic coefficients for calculation purposes was divided into two parts as follows:

$$C_{D,s} = C_{D,\mathrm{st}} + C_{D,\mathrm{dyn}}$$
$$C_{Y,s} = C_{Y,\mathrm{st}} + C_{D,\mathrm{dyn}}$$
$$C_{L,s} = C_{L,\mathrm{st}} + C_{L,\mathrm{dyn}}$$
$$C_{l,b} = C_{l,\mathrm{st}} + C_{l,\mathrm{dyn}}$$
$$C_{m,b} = C_{m,\mathrm{st}} + C_{m,\mathrm{dyn}}$$
$$C_{n,b} = C_{n,\mathrm{st}} + C_{n,\mathrm{dyn}}$$

where the subscript st refers to static and dyn refers to dynamic. The static and dynamic designations are used in most of the other airplane math models programed for the general aviation simulator; the scheme is retained here for consistency and convenience.

Each of the static and dynamic terms consists of the summation of several individual elements. The math model uses tables of aerodynamic coefficients and stability derivatives as functions of two variables, usually angle of attack α and thrust coefficient C_T. A linear interpolation between values is utilized during program execution. Note that in this model there are no thrust terms directly input into the equations. Thrust effects are contained in the basic aerodynamic terms and are input through the tables using the parameter C_T.

The various elements comprising each of the static and dynamic terms are presented on pages 19 and 20. In the expression for each of the six static coefficients there exists a coefficient with the subscript o. For these terms the sideslip angle β is zero, as are all control surface deflections; that is:

$$\beta = \delta_e = \delta_a = \delta_r = 0$$

Note that in the summation of terms in the static coefficients for lift, drag, and pitching moment there are incremental terms used to adjust the values for the effect of sideslip. The incremental corrections were obtained simply by substracting the power-off values at zero sideslip from those at sideslip for the airplane configuration with zero control and flap de-

flection. These values are tabulated as a function of α for $\beta = \pm 10°$ and $\beta = \pm 20°$. Although not tabulated, these particular tables have a zero value at $\beta = 0$ and require a linear interpolation on β. The incremental scheme was employed since most of the wind-tunnel data for the other terms, such as the contributions due to elevator deflection and flap deflection, were obtained only at zero sideslip. Thus, the sideslip effect which couples the lateral motion with the longitudinal equations is only approximate. Nevertheless, although inexact, this scheme is believed to provide a large part of the total coupling effect.

Note that the coefficient $C_{D,s}$, referred to herein as the drag coefficient along the stability axis, was used for convenience in fitting this math model into the existing general aviation simulation program. Also in the program, the data tables were constructed for two C_T values of 0 and 0.5. Prior to table look up, the thrust coefficient was limited so as to remain within these bounds. Such limits were acceptable for stall departure motions. For those rare occasions when the calculated C_T values fell outside the bounded region, a correction was included in the drag coefficient since it was the principal coefficient affected.

Longitudinal characteristics:

$$C_{L,\mathrm{st}} = C_{L,o} + C_{L_{\delta_e}}\delta_e + C_{L_{\delta_f}}\delta_f + \Delta C_{L,\beta}$$

$$C_{L,\mathrm{dyn}} = C_{l_q}\frac{q\bar{c}_w}{2V} + C_{L_{\dot\alpha}}\frac{\dot\alpha\bar{c}_w}{2V}$$

Coefficient	Function of—
$C_{L,o}$	α, C_T
$C_{L_{\delta_e}}$	α, C_T
$C_{L_{\delta_f}}$	α, C_T
$\Delta C_{L,\beta}$	α, β
C_{L_q}	α, C_T
$C_{L_{\dot\alpha}}$	α, C_T

$$C_{m,\mathrm{st}} = C_{m,o} + C_{m_{\delta_e}}\delta_e + C_{m_{\delta_f}}\delta_f + \Delta C_{m,\beta}$$

$$C_{m,\mathrm{dyn}} = C_{m_q}\frac{q\bar{c}_w}{2V} + C_{m_{\dot\alpha}}\frac{\dot\alpha\bar{c}_w}{2V}$$

Coefficient	Function of—
$C_{m,o}$	α, C_T
$C_{m_{\delta_e}}$	α, C_T
$C_{m_{\delta_f}}$	α, C_T
$\Delta C_{m,\beta}$	α, β
C_{m_q}	α, C_T
$C_{m_{\dot\alpha}}$	α, C_T

$$\begin{aligned} C_{D,\mathrm{st}} &= C_{D,o} + C_{D_{\delta_e}}\delta_e + C_{D_{(\delta_e)^2}}(\delta_e)^2 + C_{D_{\delta_f}}\delta_f \\ &\quad + C_{D_{(\delta_r)^3}}|(\delta_r)^3| + \Delta C_{D,\beta} + \Delta C_{D,T} \\ C_{D,\mathrm{dyn}} &= 0 \end{aligned}$$

Coefficient	Function of—
$C_{D,o}$	α, C_T
$C_{D_{\delta_e}}$	α, C_T
$C_{D_{(\delta_e)^2}}$	α, C_T
$C_{D_{\delta_f}}$	α, C_T
$C_{D_{\delta_r}}$	α, C_T
$\Delta C_{D,\beta}$	α, β
$\Delta C_{D,T}$	C_T

where $\Delta C_{D,T} = 0$ for $0 \leq C_T \leq 0.5$, $\Delta C_{D,T} = -0.80(C_T - 0.5)\cos\alpha$ for $C_T > 0.5$, and $\Delta C_{D,T} = -0.80 C_T \cos\alpha$ for $C_T < 0$.

Lateral characteristics:

$$C_{Y,\text{st}} = C_{Y,o} + C_{Y_\beta}\beta + C_{Y_{\delta_r}}\delta_r + C_{Y_{\delta_a}}\delta_a$$

$$C_{Y,\text{dyn}} = C_{Y_p}\frac{pb}{2V} + C_{Y_r}\frac{rb}{2V}$$

Coefficient	Function of—
$C_{Y,o}$	α, C_T
C_{Y_β}	α, C_T
$C_{Y_{\delta_r}}$	α, C_T
$C_{Y_{\delta_a}}$	α
C_{Y_p}	α, C_T
C_{Y_r}	α, C_T

$$C_{n,\text{st}} = C_{n,o} + C_{n_\beta}\beta + C_{n_{\delta_r}}\delta_r + C_{n_{\delta_a}}\delta_a$$

$$C_{n,\text{dyn}} = C_{n_p}\frac{pb}{2V} + C_{n_r}\frac{rb}{2V}$$

Coefficient	Function of—
$C_{n,o}$	α, C_T
C_{n_β}	α, C_T
$C_{n_{\delta_r}}$	α, C_T
$C_{n_{\delta_a}}$	α
C_{n_p}	α, C_T
C_{n_r}	α, C_T

$$C_{l,\text{st}} = C_{l,o} + C_{l_\beta}\beta + C_{l_{\delta_r}}\delta_r + C_{l_{\delta_a}}\delta_a$$

$$C_{l,\text{dyn}} = C_{l_p}\frac{pb}{2V} + C_{l_r}\frac{rb}{2V}$$

Coefficient	Function of—
$C_{l,o}$	α, C_T
C_{l_β}	α, C_T
$C_{l_{\delta_r}}$	α, C_T
$C_{l_{\delta_a}}$	α
C_{l_p}	α, C_T
C_{l_r}	α, C_T

Appendix C—Control Forces

The wheel forces used with the control loader in the simulator were calculated as follows:

For the elevator control,

$$F_{wh,e} = G_e C_{H_e} \bar{q} S_e \bar{c}_e$$

$$C_{H_e} = C_{H_{e_o}} + C_{H_{e_{\delta_e}}} \delta_e$$

Coefficient	Function of—
$C_{H_{e_o}}$	α, C_T
$C_{H_{e_{\delta_e}}}$	α, C_T

For the aileron control,

$$F_{wh,a} = G_a C_{H_a} \bar{q} S_a \bar{c}_a$$

$$C_{H_a} = C_{H_{a_o}} + C_{H_{a_{\delta_a}}} \delta_a$$

Coefficient	Function of—
$C_{H_{a_o}}$	α
$C_{H_{a_{\delta_a}}}$	α

Data for the elevator hinge-moment derivatives are given in table V. These values were determined from wind-tunnel measurements made at zero sideslip angle on the airplane without the booms, wheel pants, or parachute canister. (See fig. 6.) The values are believed usable for both the baseline and the modified configurations. Data for the aileron controls were not obtained during the wind-tunnel tests. Even so, the program was constructed to accept aileron hinge-moment coefficients through the angle-of-attack range for future use. An estimate of the aileron hinge-moment coefficients was made for the wing at a low angle of attack, and these values were then used throughout the angle-of-attack range. The values used were $C_{H_{a_o}} = 0$ and $C_{H_{a_{\delta_a}}} = -0.0137$.

In the general aviation simulator, springs are used with the rudder pedals to supply pedal forces. With a spring system, rudder deflection is proportional to pedal deflection. The equation

$$F_r = -2.74\delta_r$$

was used to provide a rudder pedal force to compare with that on the flight time histories.

Appendix D—Comparison of Simulation and Flight-Test Results

A number of comparisons of simulation and flight-test results were made for simulation validation. Included among the comparisons were those given in tables VI and VII and shown in figures 7 through 10. An explanation of each comparison is presented in this appendix, along with some comments on other comparisons attempted.

Table VI provides comparisons for two separate speed conditions. For the maximum-speed condition the flight values were obtained from a data record 30 sec in length. The flight instrumentation recorded some data at 40 times a second (the FM system) and some at 20 times a second (the PAM system). The values shown are the mean values of the total number of data points. The throttle setting for the aircraft was not recorded. The aircraft data for the high-speed condition were obtained using a 5-sec run length where all flight variables remained nearly constant. The comparisons shown for the two separate speed conditions are reasonably good. It should be realized, of course, that the weight, altitude, and velocity match because these are the required inputs to the math model.

Figure 7 shows some results obtained from the constant-altitude constant-speed flight tests compared with model predictions for trimmed straight and level flight. During the flight testing, the pilot attempted to provide constant speed conditions in segments of 5- to 10-sec duration as he progressed through a series of speed settings during the test run. The flight data for comparison were selected from these constant-speed portions of the records. Figure 7(a) shows elevator deflection δ_e as a function of trimmed lift coefficient $C_{L,\mathrm{trim}}$, figure 7(b) gives elevator deflection δ_e as a function of true airspeed, and figure 7(c) gives trimmed lift coefficient as a function of angle of attack. Note that for the trimmed math model the linear and angular accelerations are all zero. For the flight data, however, not all accelerations are necessarily zero. The comparisons shown by figures 7(a) and 7(b) are considered to be in good agreement. For figure 7(c) however, the comparisons are not as good. It is apparent that some discrepancy exists between the flight angle-of-attack measurements and the simulation predictions. Note that upwash corrections (see ref. 11) were included in the flight angle-of-attack values shown. Even with this correction included, there still remains an average discrepancy of about 2° over the angle-of-attack range presented.

Figure 8 presents steady-heading-sideslip comparisons between flight-test data and simulation for the power-on condition. Flight data were selected for time segments where the controls remained nearly constant. For each of the data points shown on figure 8, time segments were between 5- and 8-sec duration. Average values over these time segments were determined for each of the different parameters of interest. Variations of the primary variables ϕ, δ_r, and δ_a with sideslip are given in figures 8(a), 8(b), and 8(c), respectively. Agreement exists between flight and simulation results over a β range of $\pm 10°$ except for a difference in slope that exists in the aileron results.

Dynamic stability comparisons are given in table VII. Note that a comparison was not possible for the baseline configuration because flight data were only available for the aircraft with the outboard leading-edge modification. Nevertheless, entries for both configurations are presented in the table in order to permit a comparison of simulation predictions for the two configurations. The periods and damping ratios for the flight data were evaluated from time-history records of the oscillatory response of the aircraft to a control input. The corresponding simulation predictions were obtained using the linear analysis program of reference 18. The comparisons in table VII show good agreement between the values for the phugoid mode damping ratio and for the Dutch roll mode damping ratio. Some difference, however, exists in the flight and predicted values for the Dutch roll period. An effort was made to find values for the longitudinal short-period mode from the flight records for the aircraft, but with little success. The linear analysis predictions are included for completeness. Finally, in the case of the Dutch roll, it should be noted that the velocity and engine speed (N) values obtained from the flight records were simple averages of the maximum and minimum values noted over the sample time interval.

Time-history comparisons of simulation predictions and flight-test results for the stall and initial departure region of flight are given in figures 9 and 10. Figure 9 shows about a 30-sec time-history record, and figure 10 shows about a 20-sec record. For both comparisons, control surface deflections were obtained from the flight records and programed in tabular form every quarter of a second into the simulation so that identical control inputs would apply for both time histories. Thus, when compared, the δ_e, δ_a, and δ_r traces for simulation and flight appear identical. For the power-off case in figure 9, the pilot attempted to maintain altitude by applying up-elevator until the stall and then held the elevator fixed. The aircraft departed by rolling and yawing to the left. The oscillations appearing in the p and β traces suggest the possibility of a wing-rock situ-

ation. Although some differences exist in comparing traces for the different parameters, it was felt that part of the difficulty might be in achieving comparable initial conditions in the simulation. For example, since the throttle is already closed at $t = 0$, a deceleration condition exists for the airplane that requires six initial acceleration inputs in the simulation that are not all zero.

For the comparison in figure 10 the initial conditions were selected for straight and level trimmed flight. Thus a throttle chop is included, as well as a region of full-up elevator deflection and a large rudder kick in each direction. Since throttle information was omitted in the flight records, a 2-sec time interval was arbitrarily chosen for throttle closure in the simulation. This choice seems reasonable from the similar N traces shown. One trace of particular interest was the angle of attack in which the double peak appears in both flight and simulation traces. Pilot comments during the flight indicated that the aircraft was unresponsive to rudder deflections at very high angles of attack, and he demonstrated this fact by large rudder inputs. The altitude angles ψ, θ, and ϕ in figure 10(b) show the aircraft departed by rolling and yawing to the left along with pitching down.

From an examination and comparison of the various time-history traces in both figures 9 and 10, the impression is one of overall agreement between simulation and flight. Note that the radio interference indicated on some time-history traces in figure 9 resulted from the pilot activating the mike to record a brief comment.

To explore the range of validity of the simulation further, attempts were made to model the initial spin entry motion. Several time-history comparisons of simulation and flight results were made for vehicle configurations both with and without the wing leading-edge modification. These time-history comparisons involved a throttle chop early in the run, followed later by full-up elevator deflection and full rudder deflection. Maximum elevator and rudder deflections were applied before the angle of attack exceeded 20°. Fairly good agreement between simulation and flight time-history traces were evident only for about one-half to three-quarters of the first turn of the entry motion. The angular rates then began to build up, the airplane speed in the simulation dropped below the corresponding flight values, and the simulation angle of attack rapidly increased and exceeded 40° which was the upper limit of the tabular data. At this time, large sideslip angles were encountered in the simulation that were not evident in the flight records. Of course, once the limits of the tabulated data had been encountered, the remaining portion of the simulation time-history traces were invalid.

From various comparisons of simulation and flight-test results that have been made, it appears that the math-model formulation has a major influence on the range of validity of the simulation. Fairly good agreement with aircraft flight motions can be expected for time intervals of 40 sec and beyond when the angular rates remain fairly small and only partial control deflections are employed. Application of full control deflections and/or the presence of large angular rates, except for short time intervals, can lead to large discrepancies between simulation and flight-test data. Although all comparisons made herein were for the flaps-up condition, deflection of the flaps was not considered a complicating factor because of the small value of the ratio of flap area to wing area for this aircraft.

References

1. Burk, Sanger M., Jr.; Bowman, James S., Jr.; and White, William L.: *Spin-Tunnel Investigation of the Spinning Characteristics of Typical Single-Engine General Aviation Airplane Designs. I—Low-Wing Model A: Effects of Tail Configurations.* NASA TP-1009, 1977.
2. Bihrle, William, Jr.; Barnhart, Billy; and Pantason, Paul: *Static Aerodynamic Characteristics of a Typical Single-Engine Low-Wing General Aviation Design for an Angle-of-Attack Range of* -8° *to* 90°. NASA CR-2971, 1978.
3. Bihrle, William, Jr.; Hultberg, Randy S.; and Mulcay, William: *Rotary Balance Data for a Typical Single-Engine Low-Wing General Aviation Design for an Angle-of-Attack Range of* 30° *to* 90°. NASA CR-2972, 1978.
4. Bowman, James S., Jr.; Stough, Harry P.; Burk, Sanger M., Jr.; and Patton, James M., Jr.: Correlation of Model and Airplane Spin Characteristics for a Low-Wing General Aviation Research Airplane. AIAA Paper 78-1477, Aug. 1978.
5. Stough, H. P., III; and Patton, J. M., Jr.: The Effects of Configuration Changes on Spin and Recovery Characteristics of a Low-Wing General Aviation Research Airplane. AIAA Paper 79-1786, Aug. 1979.
6. Sliwa, Steven M.: Some Flight Data Extraction Techniques Used on a General Aviation Spin Research Aircraft. AIAA Paper 79-1802, Aug. 1979.
7. Staff of Langley Research Center: *Exploratory Study of the Effects of Wing-Leading-Edge Modifications on the Stall/Spin Behavior of a Light General Aviation Airplane.* NASA TP-1589, 1979.
8. Sliwa, Steven Mark: A Study of Data Extraction Techniques for Use in General Aviation Aircraft Spin Research. M.S. Thesis, George Washington Univ., Sept. 1978.
9. O'Bryan, Thomas C.; Edwards, Thomas E.; and Glover, Kenneth E.: Some Results From the Use of a Control Augmentation System To Study the Developed Spin of a Light Plane. AIAA Paper 79-1790, Aug. 1979.
10. DiCarlo, Daniel J.; Stough, Harry P., III; and Patton, James M., Jr.: Effects of Discontinuous Drooped Wing Leading-Edge Modification on the Spinning Characteristics of a Low-Wing General Aviation Airplane. AIAA-80-1843, Aug. 1980, and *J. Aircr.*, vol. 18, no. 9, Sept. 1981, pp. 786–792.
11. Moul, Thomas M.; and Taylor, Lawrence W., Jr.: Determination of an Angle of Attack Sensor Correction for a General Aviation Airplane at Large Angles of Attack as Determined From Wind Tunnel and Flight Tests. AIAA-80-1845, Aug. 1980, and *J. Aircr.*, vol. 18, no. 10, Oct. 1981, pp. 838–843.
12. Satran, Dale R.: *Wind-Tunnel Investigation of the Tail-Spoiler Concept for Stall Prevention on General Aviation Airplanes.* NASA TM-8208, 1981.
13. Stewart, Eric C.; Suit, William T.; Moul, Thomas M.; and Brown, Philip W.: *Spin Tests of a Single-Engine High-Wing Light Airplane.* NASA TP-1927, 1981.
14. Newsom, William A., Jr.; Satran, Dale R.; and Johnson, Joseph L., Jr.: *Effects of Wing-Leading-Edge Modifications on a Full-Scale, Low-Wing General Aviation Airplane—Wind-Tunnel Investigation of High-Angle-of-Attack Aerodynamic Characteristics.* NASA TP-2011, 1982.
15. Abbasy, Imran: *Determination of Stability and Control Parameters of a General Aviation Airplane From Flight Data.* NASA TM-84635, 1983.
16. Wykes, John H.; Casteel, Gilbert R.; and Collins, Richard A.: *An Analytical Study of the Dynamics of Spinning Aircraft. Part I—Flight Test Data Analyses and Spin Calculations.* WADC Tech. Rep. 58-381, Pt. I, U.S. Air Force, Dec. 1958. (Available from DTIC as AD 203 788.)
17. Etkin, Bernard: *Dynamics of Atmospheric Flight.* John Wiley & Sons, Inc., c.1972.
18. Dieudonne, James E.: *Description of a Computer Program and Numerical Technique for Developing Linear Perturbation Models From Nonlinear Systems Simulations.* NASA TM-78710, 1978.
19. Hemke, Paul E.: *Elementary Applied Aerodynamics.* Prentice-Hall, Inc., 1946.

TABLE I. PHYSICAL CHARACTERISTICS OF AIRPLANE

Engine:	
Type	Four cylinders horizontally opposed
Rated continuous power, hp	108
Rated continuous speed, rpm	2600
Propeller:	
Type	Two blades, fixed pitch
Diameter, in.	71
Pitch, in.	46
Overall dimensions:	
Span, ft	24.46
Length to rear of fuselage, ft	18.95
Height, ft	6.73
Wing:	
Span, ft	26.46
Area, ft^2	98.11
Root chord, ft	4.00
Tip chord, ft	4.00
Mean aerodynamic chord, ft	4.00
Aspect ratio	6.10
Dihedral, deg	5.0
Incidence:	
At root, deg	3.5
At tip, deg	3.5
Airfoil section	Modified NACA 64_2-415
Aileron (each):	
Area, ft^2	2.60
Span, ft	3.82
Chord, ft	0.68
Flap (each):	
Area, ft^2	2.72
Span, ft	3.76
Chord, ft	0.68
Horizontal tail:	
Span, ft	7.69
Incidence, deg	−3.0
Root chord, ft	3.60
Tip chord, ft	1.67
Mean aerodynamic chord, ft	2.75
Airfoil section	NACA 65_1-012
Tail length (distance $0.25\bar{c}_w$ to 0.25 mean aerodynamic chord of tail), ft	11.62
Elevator:	
Area (total), ft^2	7.22
Root chord, ft	1.13
Tip chord, ft	0.70
Span, ft	7.69
Area (forward of hinge line at tip), ft^2	0.92

TABLE I. Concluded

Vertical tail:	
Span, ft	4.09
Root chord, ft	3.60
Tip chord, ft	1.67
Airfoil section	NACA 65_1-012
Rudder:	
Area (total), ft^2	3.61
Root chord, ft	1.13
Tip chord, ft	0.70
Span, ft	4.09
Area (forward of hinge line at tip), ft^2	0.46
Control surface deflections:	
Elevator, deg	25 up, 15 down
Aileron, deg	25 up, 20 down
Rudder, deg	25 left, 25 right
Flap, deg	0 to 30 down
Nominal test weight, lb	1577
Center-of-gravity location	$0.25\bar{c}_w$
Moments of inertia:	
I_X, slug-ft^2	596
I_Y, slug-ft^2	738
I_Z, slug-ft^2	1268
I_{XZ}, slug-ft^2	0
I_p, slug-ft^2	1.15

TABLE II. COORDINATES OF AIRFOIL SECTIONS

[Stations and ordinates given in percent of airfoil chord]

(a) Coordinates of modified NACA 64_2-415 airfoil (basic wing)

Upper surface		Lower surface	
Station	Ordinates	Station	Ordinates
0	0	0	0
.299	1.291	.701	−1.091
.526	1.579	.974	−1.299
.996	2.038	1.504	−1.610
2.207	2.883	2.793	−2.139
4.673	4.121	5.327	−2.857
7.162	5.075	7.838	−3.379
9.662	5.864	10.338	−3.796
14.681	7.122	15.319	−4.430
19.714	8.066	20.286	−4.882
24.756	8.771	25.224	−5.191
29.803	9.260	30.197	−5.372
34.853	9.541	35.147	−5.421
39.904	9.614	40.096	−5.330
44.954	9.414	45.046	−5.034
50.000	9.016	50.000	−4.604
55.040	8.456	54.960	−4.076
60.072	7.762	60.000	−3.698
65.096	6.954	65.000	−3.281
70.111	6.055	70.000	−2.865
75.115	5.084	75.000	−2.343
80.109	4.062	80.000	−1.875
85.092	3.020	85.000	−1.458
90.066	1.982	90.000	−.990
95.032	.976	95.000	−.573
100.000	0	100.000	0

(b) Coordinates of leading-edge-droop-airfoil

Upper surface		Lower surface	
Station	Ordinates	Station	Ordinates
−2.769	−3.833	−2.769	−3.833
−2.658	−2.885	−2.658	−4.631
−2.217	−1.633	−2.217	−5.540
−1.773	−.817	−1.773	−5.983
−1.329	−.190	−1.329	−6.160
−.885	.350	−.885	−6.210
−.444	.875	−.700	−6.225
.000	1.254	.000	−6.210
.444	1.604	.444	−6.201
.885	1.983	.885	−6.191
1.329	2.319	1.329	−6.182
2.206	2.883	2.206	−6.164
4.673	4.121	4.673	−6.111
7.163	5.075	7.163	−6.059
9.662	5.865	9.662	−6.006
14.681	7.123	14.681	−5.900
19.715	8.065	19.715	−5.793
24.756	8.771	24.756	−5.687
29.802	9.258	29.802	−5.580
34.852	9.542	38.585	−5.394
39.904	9.615	40.096	−5.330
44.952	9.415	45.046	−5.034
50.000	9.017	50.000	−4.604
55.040	8.456	54.960	−4.076
60.071	7.763	60.000	−3.698
65.096	6.954	65.000	−3.281
70.110	6.056	70.000	−2.865
75.115	5.085	75.000	−2.343
80.108	4.063	80.000	−1.875
85.092	3.021	85.000	−1.458
90.065	1.983	90.000	−.990
95.031	.977	95.000	−.573
100.000	.000	100.000	.000

TABLE III. AERODYNAMIC COEFFICIENTS FOR BASELINE CONFIGURATION

(a) Lift-coefficient data

$C_{L,o}$

ALPHA	CT=0.0	CT=0.5
-10.00	-.4100	-.6700
-5.00	-.0100	-.1400
0.00	.4100	.4100
5.00	.8400	.9700
10.00	1.1600	1.4200
12.00	1.2300	1.5400
14.00	1.2600	1.6200
16.00	1.2600	1.6700
18.00	1.2600	1.7200
20.00	1.2500	1.7600
25.00	1.2200	1.8500
30.00	1.1700	1.9200
35.00	1.1300	1.9900
40.00	1.0800	2.0500

$C_{L_{\delta e}}$

ALPHA	CT=0.0	CT=0.5
-10.00	.0062	.0139
-5.00	.0063	.0134
0.00	.0062	.0131
5.00	.0058	.0123
10.00	.0053	.0109
12.00	.0051	.0104
14.00	.0050	.0101
16.00	.0049	.0098
18.00	.0048	.0094
20.00	.0047	.0090
25.00	.0044	.0080
30.00	.0042	.0073
35.00	.0039	.0061
40.00	.0037	.0055

$C_{L_{\delta_f}}$

ALPHA	CT=0.0	CT=0.5
-10.00	.0066	.0066
-5.00	.0075	.0075
0.00	.0077	.0077
5.00	.0078	.0078
10.00	.0068	.0068
12.00	.0060	.0060
14.00	.0053	.0053
16.00	.0047	.0047
18.00	.0041	.0041
20.00	.0035	.0035
25.00	.0030	.0030
30.00	.0025	.0025
35.00	.0020	.0020
40.00	.0015	.0015

$\Delta C_{L,\beta}$

ALPHA	BETA=±10.0	BETA=±20.0
-10.00	0.0000	0.0000
-5.00	0.0000	0.0000
0.00	0.0000	0.0000
5.00	-.0120	-.0500
10.00	-.0220	-.0870
12.00	-.0150	-.0600
14.00	-.0100	-.0390
16.00	-.0050	-.0210
18.00	-.0020	-.0090
20.00	0.0000	0.0000
25.00	0.0000	0.0000
30.00	0.0000	0.0000
35.00	.0090	.0360
40.00	.0180	.0710

C_{L_q}

ALPHA	CT=0.0	CT=0.5
-10.00	2.4100	3.0120
-5.00	2.4100	3.0120
0.00	2.4200	3.0290
5.00	2.4600	3.2220
10.00	2.5900	3.5940
12.00	2.9600	4.3510
14.00	3.7200	6.0720
16.00	4.7300	6.3820
18.00	5.2900	6.9880
20.00	5.1600	6.8330
25.00	5.0500	6.5610
30.00	5.0600	6.1270
35.00	5.0800	5.9660
40.00	5.0800	5.8110

$C_{L_{\dot{\alpha}}}$

ALPHA	CT=0.0	CT=0.5
-10.00	.6890	.8610
-5.00	.6890	.8610
0.00	.6750	.8430
5.00	.6370	.8330
10.00	.5100	.7030
12.00	.1310	.1930
14.00	-.6200	-1.0120
16.00	-.5960	-.8060
18.00	-.1310	-.1720
20.00	0.0000	0.0000
25.00	.1170	.1510
30.00	.1000	.1210
35.00	.0790	.0930
40.00	.0790	.0930

Table III. Continued

(b) Drag-coefficient data

$C_{D,o}$

ALPHA	CT=0.0	CT=0.5
-10.00	.0666	-.3273
-5.00	.0486	-.3499
0.00	.0526	-.3474
5.00	.0846	-.3139
10.00	.1456	-.2483
12.00	.1856	-.2057
14.00	.2446	-.1435
16.00	.3136	-.0709
18.00	.3786	-.0018
20.00	.4486	.0727
25.00	.6186	.2561
30.00	.7786	.4322
35.00	.9255	.5979
40.00	1.0636	.7572

$C_{D_{\delta_e}}$

ALPHA	CT=0.0	CT=0.5
-10.00	-.00138	-.00258
-5.00	-.00088	-.00148
0.00	-.00038	-.00038
5.00	.00012	.00072
10.00	.00062	.00182
12.00	.00082	.00226
14.00	.00102	.00270
16.00	.00122	.00314
18.00	.00142	.00358
20.00	.00162	.00402
25.00	.00212	.00512
30.00	.00262	.00622
35.00	.00312	.00732
40.00	.00362	.00842

$C_{D_{(\delta_e)^2}}$

ALPHA	CT=0.0	CT=0.5
-10.00	.0030 $\times 10^{-2}$	0.0000 $\times 10^{-2}$
-5.00	.0030	.0030
0.00	.0030	.0060
5.00	.0030	.0085
10.00	.0030	.0105
12.00	.0030	.0111
14.00	.0030	.0115
16.00	.0030	.0119
18.00	.0030	.0120
20.00	.0030	.0119
25.00	.0030	.0101
30.00	.0030	.0073
35.00	.0030	.0037
40.00	.0030	0.0000

$\Delta C_{D,\beta}$

ALPHA	EETA=±10.0	BETA=±20.0
-10.00	-.0053	-.0213
-5.00	-.0053	-.0213
0.00	-.0053	-.0213
5.00	-.0044	-.0178
10.00	-.0036	-.0142
12.00	-.0036	-.0142
14.00	-.0036	-.0142
16.00	-.0036	-.0142
18.00	-.0036	-.0142
20.00	-.0036	-.0142
25.00	-.0036	-.0142
30.00	-.0036	-.0142
35.00	-.0036	-.0142
40.00	-.0047	-.0187

$C_{D_{\delta_f}}$

ALPHA	CT=0.0	CT=0.5
-10.00	.00010	.00010
-5.00	.00030	.00030
0.00	.00050	.00050
5.00	.00090	.00090
10.00	.00140	.00140
12.00	.00160	.00160
14.00	.00180	.00180
16.00	.00200	.00200
18.00	.00200	.00200
20.00	.00200	.00200
25.00	.00200	.00200
30.00	.00200	.00200
35.00	.00200	.00200
40.00	.00200	.00200

$C_{D_{(\delta_r)^3}}$

ALPHA	CT=0.0	CT=0.5
-10.00	.0009 $\times 10^{-3}$	.0024 $\times 10^{-3}$
-5.00	.0009	.0024
0.00	.0009	.0024
5.00	.0009	.0024
10.00	.0009	.0024
12.00	.0009	.0024
14.00	.0007	.0018
16.00	.0005	.0012
18.00	.0002	.0006
20.00	0.0000	0.0000
25.00	0.0000	0.0000
30.00	0.0000	0.0000
35.00	0.0000	0.0000
40.00	0.0000	0.0000

TABLE III. Continued

(c) Pitching-moment-coefficient data

$C_{m,o}$

ALPHA	CT=0.0	CT=0.5
-10.00	.2700	.2700
-5.00	.1580	.1580
0.00	.0760	.0760
5.00	.0020	.0020
10.00	-.0800	-.0800
12.00	-.1180	-.1180
14.00	-.1670	-.1670
16.00	-.2250	-.2250
18.00	-.2770	-.2770
20.00	-.3160	-.3160
25.00	-.4080	-.4080
30.00	-.4800	-.4800
35.00	-.5560	-.5560
40.00	-.6060	-.6060

$C_{m_{\delta_e}}$

ALPHA	CT=0.0	CT=0.5
-10.00	-.0193	-.0374
-5.00	-.0193	-.0393
0.00	-.0193	-.0394
5.00	-.0180	-.0395
10.00	-.0165	-.0384
12.00	-.0164	-.0360
14.00	-.0163	-.0334
16.00	-.0162	-.0311
18.00	-.0162	-.0288
20.00	-.0162	-.0269
25.00	-.0162	-.0226
30.00	-.0150	-.0213
35.00	-.0130	-.0190
40.00	-.0100	-.0153

$C_{m_{\delta_f}}$

ALPHA	CT=0.0	CT=0.5
-10.00	-.0010	-.0010
-5.00	-.0010	-.0010
0.00	-.0010	-.0010
5.00	-.0010	-.0010
10.00	-.0018	-.0018
12.00	-.0016	-.0016
14.00	-.0014	-.0014
16.00	-.0012	-.0012
18.00	-.0010	-.0010
20.00	-.0008	-.0008
25.00	-.0009	-.0009
30.00	-.0010	-.0010
35.00	-.0011	-.0011
40.00	-.0012	-.0012

$\Delta C_{m,\beta}$

ALPHA	BETA=±10.0	BETA=±20.0
-10.00	-.0200	-.0800
-5.00	-.0200	-.0800
0.00	-.0200	-.0800
5.00	-.0140	-.0550
10.00	-.0070	-.0280
12.00	-.0040	-.0180
14.00	-.0020	-.0070
16.00	.0010	.0050
18.00	.0030	.0120
20.00	.0060	.0230
25.00	.0120	.0480
30.00	.0180	.0730
35.00	.0240	.0980
40.00	.0310	.1240

C_{m_q}

ALPHA	CT=0.0	CT=0.5
-10.00	-7.0000	-8.7500
-5.00	-7.0000	-8.7500
0.00	-7.0400	-8.8000
5.00	-7.1500	-9.3600
10.00	-7.5200	-10.4400
12.00	-8.6200	-12.6400
14.00	-10.8000	-17.6400
16.00	-13.7300	-18.5400
18.00	-15.3800	-20.3000
20.00	-15.0000	-19.8500
25.00	-14.6600	-19.0600
30.00	-14.7100	-17.8000
35.00	-14.7700	-17.3300
40.00	-14.7700	-16.8800

$C_{m_{\dot{\alpha}}}$

ALPHA	CT=0.0	CT=0.5
-10.00	0.0000	-2.5000
-5.00	0.0000	-2.5000
0.00	-1.9600	-2.4500
5.00	-1.8500	-2.4200
10.00	-1.4800	-2.0600
12.00	-.3800	-.5600
14.00	1.8000	2.9400
16.00	1.7300	2.3400
18.00	.3800	.5000
20.00	0.0000	0.0000
25.00	-.3400	-.4400
30.00	-.2900	-.3500
35.00	-.2300	-.2700
40.00	-.2300	-.2700

TABLE III. Continued

(d) Side-force-coefficient data

$C_{Y,o}$

ALPHA	CT=0.0	CT=0.5
-10.00	0.0000	.0810
-5.00	0.0000	.0540
0.00	0.0000	.0270
5.00	0.0000	0.0000
10.00	0.0000	-.0270
12.00	0.0000	-.0378
14.00	0.0000	-.0486
16.00	0.0000	-.0540
18.00	0.0000	-.0540
20.00	0.0000	-.0540
25.00	0.0000	-.0540
30.00	0.0000	-.0540
35.00	0.0000	-.0540
40.00	0.0000	-.0540

C_{Y_β}

ALPHA	CT=0.0	CT=0.5
-10.00	-.01300	-.02260
-5.00	-.01250	-.02260
0.00	-.01180	-.02260
5.00	-.01100	-.02260
10.00	-.01090	-.02260
12.00	-.01080	-.02260
14.00	-.00980	-.02210
16.00	-.00880	-.02130
18.00	-.00820	-.02100
20.00	-.00780	-.02080
25.00	-.00670	-.02030
30.00	-.00600	-.02020
35.00	-.00620	-.02100
40.00	-.00680	-.02220

$C_{Y_{\delta_a}}$

ALPHA	
-10.00	-.000100
-5.00	-.000080
0.00	-.000090
5.00	-.000100
10.00	-.000140
12.00	-.000150
14.00	-.000160
16.00	-.000130
18.00	-.000110
20.00	-.000100
25.00	-.000080
30.00	-.000100
35.00	0.000000
40.00	0.000000

$C_{Y_{\delta_r}}$

ALPHA	CT=0.0	CT=0.5
-10.00	.00244	.00589
-5.00	.00263	.00629
0.00	.00282	.00674
5.00	.00295	.00722
10.00	.00307	.00773
12.00	.00295	.00775
14.00	.00282	.00777
16.00	.00267	.00777
18.00	.00255	.00779
20.00	.00242	.00779
25.00	.00189	.00665
30.00	.00137	.00558
35.00	.00093	.00425
40.00	.00053	.00295

C_{Y_r}

ALPHA	CT=0.0	CT=0.5
-10.00	.8000	1.0110
-5.00	.9000	1.1110
0.00	1.0000	1.2110
5.00	1.1000	1.3110
10.00	.8000	1.0010
12.00	.6000	.8020
14.00	.4000	.5290
16.00	.2000	.2490
18.00	0.0000	.0560
20.00	-.2500	-.1870
25.00	-.2500	-.1680
30.00	-.1200	-.0450
35.00	0.0000	.0610
40.00	0.0000	.0520

C_{Y_p}

ALPHA	CT=0.0	CT=0.5
-10.00	-.0140	-.0140
-5.00	-.0040	-.0040
0.00	.0060	.0060
5.00	.0160	.0160
10.00	.0260	.0260
12.00	.0300	.0300
14.00	.0340	.0340
16.00	.0380	.0380
18.00	.0420	.0420
20.00	.0460	.0460
25.00	.0560	.0560
30.00	.0660	.0660
35.00	.0330	.0330
40.00	0.0000	0.0000

TABLE III. Continued

(e) Yawing-moment-coefficient data

$C_{n,o}$

ALPHA	CT=0.0	CT=0.5
-10.00	0.0000	-.0166
-5.00	0.0000	-.0166
0.00	0.0000	-.0166
5.00	0.0000	-.0166
10.00	0.0000	-.0166
12.00	0.0000	-.0166
14.00	-.0010	-.0142
16.00	-.0010	-.0118
18.00	-.0010	-.0094
20.00	-.0010	-.0070
25.00	-.0010	-.0010
30.00	-.0010	-.0040
35.00	-.0010	-.0070
40.00	-.0010	-.0100

C_{n_β}

ALPHA	CT=0.0	CT=0.5
-10.00	.00250	.00327
-5.00	.00220	.00304
0.00	.00192	.00292
5.00	.00175	.00287
10.00	.00142	.00265
12.00	.00128	.00256
14.00	.00110	.00242
16.00	.00090	.00227
18.00	.00080	.00221
20.00	.00070	.00216
25.00	.00032	.00190
30.00	-.00002	.00167
35.00	-.00025	.00156
40.00	-.00038	.00154

$C_{n_{\delta_a}}$

ALPHA	
-10.00	.000090
-5.00	.000070
0.00	.000050
5.00	.000030
10.00	.000010
12.00	0.000000
14.00	-.000030
16.00	-.000060
18.00	-.000100
20.00	-.000150
25.00	-.000090
30.00	-.000040
35.00	0.000000
40.00	.000030

$C_{n_{\delta_r}}$

ALPHA	CT=0.0	CT=0.5
-10.00	-.00116	-.00280
-5.00	-.00125	-.00299
0.00	-.00134	-.00320
5.00	-.00140	-.00343
10.00	-.00146	-.00367
12.00	-.00140	-.00368
14.00	-.00134	-.00369
16.00	-.00127	-.00369
18.00	-.00121	-.00370
20.00	-.00115	-.00370
25.00	-.00090	-.00316
30.00	-.00065	-.00265
35.00	-.00044	-.00202
40.00	-.00025	-.00140

C_{n_r}

ALPHA	CT=0.0	CT=0.5
-10.00	-.2000	-.2900
-5.00	-.2000	-.2900
0.00	-.2000	-.2900
5.00	-.2000	-.2900
10.00	-.2000	-.2870
12.00	-.2000	-.2860
14.00	-.1300	-.1850
16.00	-.0500	-.0710
18.00	-.0600	-.0840
20.00	-.0700	-.0970
25.00	-.1000	-.1350
30.00	-.1000	-.1320
35.00	-.1000	-.1260
40.00	-.1000	-.1220

C_{n_p}

ALPHA	CT=0.0	CT=0.5
-10.00	-.0300	-.0480
-5.00	-.0400	-.0580
0.00	-.0500	-.0680
5.00	-.0600	-.0780
10.00	-.0700	-.0880
12.00	-.0600	-.0770
14.00	-.0300	-.0470
16.00	0.0000	-.0160
18.00	.0300	.0140
20.00	.0400	.0400
25.00	.0150	.0150
30.00	.0150	.0150
35.00	.0150	.0100
40.00	.0150	.0070

TABLE III. Concluded

(f) Rolling-moment-coefficient data

$C_{l,o}$

ALPHA	CT=0.0	CT=0.5
-10.00	0.0000	.0060
-5.00	0.0000	.0040
0.00	0.0000	.0020
5.00	0.0000	0.0000
10.00	0.0000	0.0000
12.00	0.0000	0.0000
14.00	-.0025	-.0025
16.00	-.0050	-.0050
18.00	-.0075	-.0075
20.00	-.0075	-.0075
25.00	-.0075	-.0075
30.00	-.0075	-.0095
35.00	-.0075	-.0115
40.00	-.0075	-.0135

C_{l_β}

ALPHA	CT=0.0	CT=0.5
-10.00	-.00140	-.00273
-5.00	-.00115	-.00215
0.00	-.00115	-.00182
5.00	-.00190	-.00190
10.00	-.00315	-.00239
12.00	-.00365	-.00265
14.00	-.00400	-.00267
16.00	-.00420	-.00237
18.00	-.00435	-.00212
20.00	-.00450	-.00183
25.00	-.00450	-.00217
30.00	-.00420	-.00353
35.00	-.00400	-.00467
40.00	-.00390	-.00523

$C_{l_{\delta_a}}$

ALPHA	
-10.00	-.001040
-5.00	-.001040
0.00	-.001040
5.00	-.001000
10.00	-.000920
12.00	-.000880
14.00	-.000840
16.00	-.000790
18.00	-.000740
20.00	-.000690
25.00	-.000600
30.00	-.000500
35.00	-.000400
40.00	-.000330

$C_{l_{\delta_r}}$

ALPHA	CT=0.0	CT=0.5
-10.00	.00025	.00025
-5.00	.00025	.00025
0.00	.00025	.00025
5.00	.00025	.00025
10.00	.00025	.00025
12.00	.00025	.00025
14.00	.00025	.00025
16.00	.00025	.00025
18.00	.00025	.00025
20.00	.00025	.00025
25.00	.00013	.00013
30.00	0.00000	0.00000
35.00	0.00000	0.00000
40.00	0.00000	0.00000

C_{l_r}

ALPHA	CT=0.0	CT=0.5
-10.00	.1000	.1150
-5.00	.1300	.1450
0.00	.1600	.1750
5.00	.1900	.2050
10.00	.1400	.1540
12.00	.1300	.1450
14.00	.1200	.1290
16.00	.1100	.1140
18.00	.1000	.1040
20.00	.0900	.0950
25.00	.0700	.0760
30.00	.0700	.0750
35.00	.0700	.0740
40.00	.1000	.1040

C_{l_p}

ALPHA	CT=0.0	CT=0.5
-10.00	-.5200	-.5200
-5.00	-.5200	-.5200
0.00	-.5200	-.5200
5.00	-.5200	-.5200
10.00	-.4000	-.4000
12.00	-.3100	-.3100
14.00	-.2200	-.2200
16.00	-.1300	-.1300
18.00	-.0400	-.0400
20.00	.0500	.0500
25.00	0.0000	0.0000
30.00	-.0500	-.0500
35.00	-.1000	-.1000
40.00	-.1500	-.1500

TABLE IV. AERODYNAMIC COEFFICIENTS FOR MODIFIED CONFIGURATION

(a) Lift-coefficient data

$C_{L,o}$

ALPHA	CT=0.0	CT=0.5
-10.00	-.4630	-.7230
-5.00	-.0479	-.1779
0.00	.3873	.3873
5.00	.8324	.9624
10.00	1.1600	1.4200
12.00	1.2300	1.5400
14.00	1.2600	1.6200
16.00	1.2764	1.6864
18.00	1.2880	1.7480
20.00	1.3050	1.8150
25.00	1.3350	1.9650
30.00	1.3450	2.0950
35.00	1.3500	2.2100
40.00	1.3470	2.3170

$C_{L_{\delta_e}}$

ALPHA	CT=0.0	CT=0.5
-10.00	.0062	.0139
-5.00	.0063	.0134
0.00	.0062	.0131
5.00	.0058	.0123
10.00	.0053	.0109
12.00	.0051	.0104
14.00	.0050	.0101
16.00	.0049	.0098
18.00	.0048	.0094
20.00	.0047	.0090
25.00	.0044	.0080
30.00	.0042	.0073
35.00	.0039	.0061
40.00	.0037	.0055

$C_{L_{\delta_f}}$

ALPHA	CT=0.0	CT=0.5
-10.00	.0066	.0066
-5.00	.0075	.0075
0.00	.0077	.0077
5.00	.0078	.0078
10.00	.0068	.0068
12.00	.0060	.0060
14.00	.0053	.0053
16.00	.0047	.0047
18.00	.0041	.0041
20.00	.0035	.0035
25.00	.0030	.0030
30.00	.0025	.0025
35.00	.0020	.0020
40.00	.0015	.0015

$\Delta C_{L,\beta}$

ALPHA	BETA=±10.0	BETA=±20.0
-10.00	0.0000	0.0000
-5.00	0.0000	0.0000
0.00	0.0000	0.0000
5.00	-.0120	-.0500
10.00	-.0220	-.0870
12.00	-.0150	-.0600
14.00	-.0100	-.0390
16.00	-.0050	-.0210
18.00	-.0020	-.0090
20.00	0.0000	0.0000
25.00	0.0000	0.0000
30.00	0.0000	0.0000
35.00	.0090	.0360
40.00	.0180	.0710

C_{L_q}

ALPHA	CT=0.0	CT=0.5
-10.00	2.4100	3.0120
-5.00	2.4100	3.0120
0.00	2.4200	3.0290
5.00	2.4600	3.2220
10.00	2.5900	3.5940
12.00	2.9600	4.3510
14.00	3.7200	6.0720
16.00	4.7300	6.3820
18.00	5.2900	6.9880
20.00	5.1600	6.8330
25.00	5.0500	6.5610
30.00	5.0600	6.1270
35.00	5.0800	5.9660
40.00	5.0800	5.8110

$C_{L_{\dot{\alpha}}}$

ALPHA	CT=0.0	CT=0.5
-10.00	.6890	.8610
-5.00	.6890	.8610
0.00	.6750	.8430
5.00	.6370	.8330
10.00	.5100	.7030
12.00	.1310	.1930
14.00	-.6200	-1.0120
16.00	-.5960	-.8060
18.00	-.1310	-.1720
20.00	0.0000	0.0000
25.00	.1170	.1510
30.00	.1000	.1210
35.00	.0790	.0930
40.00	.0790	.0930

TABLE IV. Continued

(b) Drag-coefficient data

$C_{D,o}$

ALPHA	CT=0.0	CT=0.5
-10.00	.0786	-.3153
-5.00	.0546	-.3433
0.00	.0526	-.3474
5.00	.0846	-.3139
10.00	.1456	-.2483
12.00	.1856	-.2047
14.00	.2460	-.1421
16.00	.3164	-.0681
18.00	.3828	.0024
20.00	.4542	.0783
25.00	.6277	.2652
30.00	.7912	.4448
35.00	.9416	.6140
40.00	1.0832	.7768

$C_{D_{\delta_e}}$

ALPHA	CT=0.0	CT=0.5
-10.00	-.00138	-.00258
-5.00	-.00088	-.00148
0.00	-.00038	-.00038
5.00	.00012	.00072
10.00	.00062	.00182
12.00	.00082	.00226
14.00	.00102	.00270
16.00	.00122	.00314
18.00	.00142	.00358
20.00	.00162	.00402
25.00	.00212	.00512
30.00	.00262	.00622
35.00	.00312	.00732
40.00	.00362	.00842

$C_{D_{(\delta_e)^2}}$

ALPHA	CT=0.0	CT=0.5
-10.00	.0030 $\times 10^{-2}$	0.0000 $\times 10^{-2}$
-5.00	.0030	.0030
0.00	.0030	.0060
5.00	.0030	.0085
10.00	.0030	.0105
12.00	.0030	.0111
14.00	.0030	.0115
16.00	.0030	.0119
18.00	.0030	.0120
20.00	.0030	.0119
25.00	.0030	.0101
30.00	.0030	.0073
35.00	.0030	.0037
40.00	.0030	0.0000

$\Delta C_{D,\beta}$

ALPHA	BETA=±10.0	BETA=±20.0
-10.00	-.0053	-.0213
-5.00	-.0053	-.0213
0.00	-.0053	-.0213
5.00	-.0044	-.0178
10.00	-.0036	-.0142
12.00	-.0036	-.0142
14.00	-.0036	-.0142
16.00	-.0036	-.0142
18.00	-.0036	-.0142
20.00	-.0036	-.0142
25.00	-.0036	-.0142
30.00	-.0036	-.0142
35.00	-.0036	-.0142
40.00	-.0047	-.0187

$C_{D_{\delta_f}}$

ALPHA	CT=0.0	CT=0.5
-10.00	.00010	.00010
-5.00	.00030	.00030
0.00	.00050	.00050
5.00	.00090	.00090
10.00	.00140	.00140
12.00	.00160	.00160
14.00	.00180	.00180
16.00	.00200	.00200
18.00	.00200	.00200
20.00	.00200	.00200
25.00	.00200	.00200
30.00	.00200	.00200
35.00	.00200	.00200
40.00	.00200	.00200

$C_{D_{(\delta_r)^3}}$

ALPHA	CT=0.0	CT=0.5
-10.00	.0009 $\times 10^{-3}$	.0024 $\times 10^{-3}$
-5.00	.0009	.0024
0.00	.0009	.0024
5.00	.0009	.0024
10.00	.0009	.0024
12.00	.0009	.0024
14.00	.0007	.0018
16.00	.0005	.0012
18.00	.0002	.0006
20.00	0.0000	0.0000
25.00	0.0000	0.0000
30.00	0.0000	0.0000
35.00	0.0000	0.0000
40.00	0.0000	0.0000

TABLE IV. Continued

(c) Pitching-moment-coefficient data

$C_{m,o}$

ALPHA	CT=0.0	CT=0.5
-10.00	.2650	.2650
-5.00	.1650	.1650
0.00	.0910	.0910
5.00	.0200	.0200
10.00	-.0600	-.0600
12.00	-.0980	-.0980
14.00	-.1470	-.1470
16.00	-.2060	-.2060
18.00	-.2600	-.2600
20.00	-.3020	-.3020
25.00	-.4010	-.4010
30.00	-.4860	-.4860
35.00	-.5670	-.5670
40.00	-.6140	-.6140

$C_{m_{\delta_e}}$

ALPHA	CT=0.0	CT=0.5
-10.00	-.0193	-.0374
-5.00	-.0193	-.0393
0.00	-.0193	-.0394
5.00	-.0180	-.0395
10.00	-.0165	-.0384
12.00	-.0164	-.0360
14.00	-.0163	-.0334
16.00	-.0162	-.0311
18.00	-.0162	-.0288
20.00	-.0162	-.0269
25.00	-.0162	-.0226
30.00	-.0150	-.0213
35.00	-.0130	-.0190
40.00	-.0100	-.0153

$C_{m_{\delta_f}}$

ALPHA	CT=0.0	CT=0.5
-10.00	-.0010	-.0010
-5.00	-.0010	-.0010
0.00	-.0010	-.0010
5.00	-.0010	-.0010
10.00	-.0018	-.0018
12.00	-.0016	-.0016
14.00	-.0014	-.0014
16.00	-.0012	-.0012
18.00	-.0010	-.0010
20.00	-.0008	-.0008
25.00	-.0009	-.0009
30.00	-.0010	-.0010
35.00	-.0011	-.0011
40.00	-.0012	-.0012

$\Delta C_{m,\beta}$

ALPHA	BETA=±10.0	BETA=±20.0
-10.00	-.0200	-.0800
-5.00	-.0200	-.0800
0.00	-.0200	-.0800
5.00	-.0140	-.0550
10.00	-.0070	-.0280
12.00	-.0040	-.0180
14.00	-.0020	-.0070
16.00	.0010	.0050
18.00	.0030	.0120
20.00	.0060	.0230
25.00	.0120	.0480
30.00	.0180	.0730
35.00	.0240	.0980
40.00	.0310	.1240

C_{m_q}

ALPHA	CT=0.0	CT=0.5
-10.00	-7.0000	-8.7500
-5.00	-7.0000	-8.7500
0.00	-7.0400	-8.8000
5.00	-7.1500	-9.3600
10.00	-7.5200	-10.4400
12.00	-8.6200	-12.6400
14.00	-10.8000	-17.6400
16.00	-13.7300	-18.5400
18.00	-15.3800	-20.3000
20.00	-15.0000	-19.8500
25.00	-14.6600	-19.0600
30.00	-14.7100	-17.8000
35.00	-14.7700	-17.3300
40.00	-14.7700	-16.8800

$C_{m_{\dot{\alpha}}}$

ALPHA	CT=0.0	CT=0.5
-10.00	0.0000	-2.5000
-5.00	0.0000	-2.5000
0.00	-1.9600	-2.4500
5.00	-1.8500	-2.4200
10.00	-1.4800	-2.0600
12.00	-.3800	-.5600
14.00	1.8000	2.9400
16.00	1.7300	2.3400
18.00	.3800	.5000
20.00	0.0000	0.0000
25.00	-.3400	-.4400
30.00	-.2900	-.3500
35.00	-.2300	-.2700
40.00	-.2300	-.2700

TABLE IV. Continued

(d) Side-force-coefficient data

$C_{Y,o}$

ALPHA	CT=0.0	CT=0.5
-10.00	0.0000	.0810
-5.00	0.0000	.0540
0.00	0.0000	.0270
5.00	0.0000	0.0000
10.00	0.0000	-.0270
12.00	0.0000	-.0378
14.00	0.0000	-.0486
16.00	0.0000	-.0540
18.00	0.0000	-.0540
20.00	0.0000	-.0540
25.00	0.0000	-.0540
30.00	0.0000	-.0540
35.00	.0250	-.0290
40.00	.0400	-.0140

C_{Y_β}

ALPHA	CT=0.0	CT=0.5
-10.00	-.01550	-.02510
-5.00	-.01500	-.02510
0.00	-.01430	-.02510
5.00	-.01350	-.02510
10.00	-.01350	-.02520
12.00	-.01350	-.02530
14.00	-.01350	-.02580
16.00	-.01350	-.02600
18.00	-.01350	-.02630
20.00	-.01350	-.02650
25.00	-.01350	-.02660
30.00	-.01350	-.02670
35.00	-.01350	-.02830
40.00	-.01350	-.02890

$C_{Y_{\delta_a}}$

ALPHA	
-10.00	-.000100
-5.00	-.000100
0.00	-.000100
5.00	-.000100
10.00	-.000100
12.00	-.000100
14.00	-.000100
16.00	-.000100
18.00	-.000100
20.00	-.000100
25.00	-.000100
30.00	-.000100
35.00	-.000100
40.00	-.000100

$C_{Y_{\delta_r}}$

ALPHA	CT=0.0	CT=0.5
-10.00	.00244	.00589
-5.00	.00263	.00629
0.00	.00282	.00674
5.00	.00295	.00722
10.00	.00307	.00773
12.00	.00295	.00775
14.00	.00282	.00777
16.00	.00267	.00777
18.00	.00255	.00779
20.00	.00242	.00779
25.00	.00189	.00665
30.00	.00137	.00558
35.00	.00093	.00425
40.00	.00053	.00295

C_{Y_r}

ALPHA	CT=0.0	CT=0.5
-10.00	.8000	1.0110
-5.00	.9000	1.1110
0.00	1.0000	1.2110
5.00	1.1000	1.3110
10.00	.8000	1.0010
12.00	.6000	.8020
14.00	.4000	.5290
16.00	.2000	.2490
18.00	0.0000	.0560
20.00	-.2500	-.1870
25.00	-.2500	-.1680
30.00	-.1200	-.0450
35.00	0.0000	.0610
40.00	0.0000	.0520

C_{Y_p}

ALPHA	CT=0.0	CT=0.5
-10.00	-.0140	-.0140
-5.00	-.0040	-.0040
0.00	.0060	.0060
5.00	.0160	.0160
10.00	.0260	.0260
12.00	.0350	.0350
14.00	.0450	.0450
16.00	.0550	.0550
18.00	.0650	.0650
20.00	.0750	.0750
25.00	.0750	.0750
30.00	.0750	.0750
35.00	.0750	.0750
40.00	0.0000	0.0000

TABLE IV. Continued

(e) Yawing-moment-coefficient data

$C_{n,o}$

ALPHA	CT=0.0	CT=0.5
-10.00	0.0000	-.0166
-5.00	0.0000	-.0166
0.00	0.0000	-.0166
5.00	0.0000	-.0166
10.00	0.0000	-.0166
12.00	0.0000	-.0166
14.00	0.0000	-.0132
16.00	0.0000	-.0108
18.00	0.0000	-.0084
20.00	0.0000	-.0060
25.00	0.0000	0.0000
30.00	0.0000	-.0030
35.00	-.0015	-.0075
40.00	-.0035	-.0125

C_{n_β}

ALPHA	CT=0.0	CT=0.5
-10.00	.00290	.00367
-5.00	.00270	.00354
0.00	.00250	.00350
5.00	.00230	.00342
10.00	.00210	.00333
12.00	.00200	.00328
14.00	.00180	.00311
16.00	.00160	.00297
18.00	.00140	.00281
20.00	.00110	.00266
25.00	.00030	.00188
30.00	-.00060	.00109
35.00	-.00150	.00031
40.00	-.00200	-.00008

$C_{n_{\delta_a}}$

ALPHA	
-10.00	.000090
-5.00	.000080
0.00	.000070
5.00	.000060
10.00	.000050
12.00	.000030
14.00	.000010
16.00	0.000000
18.00	-.000030
20.00	-.000060
25.00	-.000100
30.00	-.000100
35.00	-.000090
40.00	-.000040

$C_{n_{\delta_r}}$

ALPHA	CT=0.0	CT=0.5
-10.00	-.00116	-.00280
-5.00	-.00125	-.00299
0.00	-.00134	-.00320
5.00	-.00140	-.00343
10.00	-.00146	-.00367
12.00	-.00140	-.00368
14.00	-.00134	-.00369
16.00	-.00127	-.00369
18.00	-.00121	-.00370
20.00	-.00115	-.00370
25.00	-.00090	-.00316
30.00	-.00065	-.00265
35.00	-.00044	-.00202
40.00	-.00025	-.00140

C_{n_r}

ALPHA	CT=0.0	CT=0.5
-10.00	-.2000	-.2900
-5.00	-.2000	-.2900
0.00	-.2000	-.2900
5.00	-.2000	-.2900
10.00	-.2000	-.2870
12.00	-.2000	-.2860
14.00	-.2200	-.2750
16.00	-.1600	-.1810
18.00	-.1000	-.1240
20.00	-.1000	-.1270
25.00	-.1000	-.1350
30.00	-.1000	-.1320
35.00	0.0000	-.0260
40.00	.2000	.1780

C_{n_p}

ALPHA	CT=0.0	CT=0.5
-10.00	-.0100	-.0280
-5.00	-.0300	-.0480
0.00	-.0500	-.0680
5.00	-.1100	-.1280
10.00	-.1300	-.1480
12.00	-.1300	-.1480
14.00	-.1300	-.1470
16.00	-.1300	-.1460
18.00	-.1300	-.1460
20.00	-.1400	-.1400
25.00	-.1350	-.1350
30.00	-.1000	-.1000
35.00	-.1000	-.0950
40.00	-.1000	-.0920

TABLE IV. Concluded

(f) Rolling-moment-coefficient data

$C_{l,o}$

ALPHA	CT=0.0	CT=0.5
-10.00	0.0000	.0060
-5.00	C.0000	.0040
0.00	0.0000	.0020
5.00	0.0000	0.0000
10.00	0.0000	0.0000
12.00	0.0000	0.0000
14.00	0.0000	0.0000
16.00	0.0000	0.0000
18.00	0.0000	0.0000
20.00	0.0000	0.0000
25.00	0.0000	0.0000
30.00	0.0000	-.0020
35.00	-.0085	-.0130
40.00	-.0145	-.0205

C_{l_β}

ALPHA	CT=0.0	CT=0.5
-10.00	-.00100	-.00233
-5.00	-.00120	-.00220
0.00	-.00150	-.00217
5.00	-.00250	-.00250
10.00	-.00390	-.00314
12.00	-.00440	-.00340
14.00	-.00470	-.00337
16.00	-.00500	-.00317
18.00	-.00530	-.00307
20.00	-.00560	-.00293
25.00	-.00640	-.00407
30.00	-.00710	-.00643
35.00	-.00760	-.00827
40.00	-.00790	-.00933

$C_{l_{\delta_a}}$

ALPHA	
-10.00	-.001040
-5.00	-.001040
0.00	-.001040
5.00	-.001040
10.00	-.001040
12.00	-.001000
14.00	-.000920
16.00	-.000880
18.00	-.000840
20.00	-.000790
25.00	-.000740
30.00	-.000690
35.00	-.000600
40.00	-.000500

$C_{l_{\delta_r}}$

ALPHA	CT=0.0	CT=0.5
-10.00	.00025	.00025
-5.00	.00025	.00025
0.00	.00025	.00025
5.00	.00025	.00025
10.00	.00025	.00025
12.00	.00025	.00025
14.00	.00025	.00025
16.00	.00025	.00025
18.00	.00025	.00025
20.00	.00025	.00025
25.00	.00013	.00013
30.00	0.00000	0.00000
35.00	0.00000	0.00000
40.00	0.00000	0.00000

C_{l_r}

ALPHA	CT=0.0	CT=0.5
-10.00	.1000	.1150
-5.00	.1300	.1450
0.00	.1600	.1750
5.00	.1900	.2050
10.00	.1400	.1540
12.00	.1300	.1450
14.00	.1200	.1290
16.00	.1100	.1140
18.00	.1000	.1040
20.00	.0900	.0950
25.00	.0700	.0760
30.00	.0700	.0740
35.00	.3500	.3540
40.00	.6000	.6040

C_{l_p}

ALPHA	CT=0.0	CT=0.5
-10.00	-.5200	-.5200
-5.00	-.5200	-.5200
0.00	-.5200	-.5200
5.00	-.5200	-.5200
10.00	-.4800	-.4800
12.00	-.4000	-.4000
14.00	-.3200	-.3200
16.00	-.2600	-.2600
18.00	-.2000	-.2000
20.00	-.2600	-.2600
25.00	-.2900	-.2900
30.00	-.3100	-.3100
35.00	-.3300	-.3300
40.00	-.3500	-.3500

TABLE V. NUMERICAL VALUES OF HINGE-MOMENT COEFFICIENTS

$C_{H_{e_o}}$

ALPHA	CT=0.0	CT=0.5
-10.00	.0030	.0253
-5.00	.0015	.0178
0.00	0.0000	.0103
5.00	0.0000	.0043
10.00	0.0000	-.0025
12.00	.0020	-.0025
14.00	.0040	-.0015
16.00	.0050	.0015
18.00	0.0000	0.0000
20.00	-.0080	-.0042
25.00	-.0350	-.0175
30.00	-.0720	-.0405
35.00	-.1200	-.0745
40.00	-.1680	-.1080

$C_{H_{e_{\delta_e}}}$

ALPHA	CT=0.0	CT=0.5
-10.00	-.0070	-.0130
-5.00	-.0070	-.0143
0.00	-.0066	-.0166
5.00	-.0064	-.0174
10.00	-.0059	-.0159
12.00	-.0055	-.0148
14.00	-.0052	-.0122
16.00	-.0051	-.0106
18.00	-.0050	-.0093
20.00	-.0050	-.0085
25.00	-.0053	-.0086
30.00	-.0059	-.0074
35.00	-.0059	-.0065
40.00	-.0059	-.0059

TABLE VI. FLIGHT-TEST AND SIMULATION SPEED COMPARISONS FOR BASELINE CONFIGURATION

Variable	Maximum speed		High speed	
	Flight test	Simulation	Flight test	Simulation
W, lb	1558	1556	1556	1556
h, ft	6090	6100	6087	6100
V, ft/sec . . .	165	165	161.9	162
N, rpm . . .	2673	2675	2683	2681
MP, psi . . .	9.69	10.20	9.93	10.41
δ_t		0.856		0.884
α, deg	2.81	1.84	2.96	2.09
δ_e, deg	1.33	2.17	1.44	1.98

TABLE VII. DYNAMIC-STABILITY COMPARISONS

	Longitudinal				Lateral	
	Phugoid mode		Short-period mode		Dutch roll mode	
Variable	Flight test	Simulation	Flight test	Simulation	Flight test	Simulation
W, lb	1500	1500		1500	1550	1550
h, ft	5450	5450		5450	3200	3200
V, ft/sec	135	135		140	175	175
N, rpm	2330	2332		2330	2650	2650
Period, sec:						
Leading-edge modification off	([a])	20.60	([a])	2.20	([a])	2.25
Leading-edge modification on	21.67	20.37	([b])	3.27	2.74	1.98
Damping ratio:						
Leading-edge modification off	([a])	0.065	([a])	0.457	([a])	0.205
Leading-edge modification on	0.063	0.065	([b])	0.476	0.17	0.18

[a]Not tested.
[b]Data not obtainable from flight records.

TABLE VIII. POWER-OFF SUMMARY OF TURN/SPIN BEHAVIOR FOR BASELINE AND MODIFIED CONFIGURATIONS

[$\delta_{t,c} = 0$; $W = 1577$ lb; $V = 120$ ft/sec; $h = 5000$ ft at trim]

Elevator-ramp amplitude, $\Delta\delta_e$, deg	Maneuver[a] initiated at β_{trim} of—						
	−12.5	−10	−5	0	5	10	12.5
Baseline configuration							
−9		TR	TR	TL	TL	SL	
−12	SR	SR	TR	TL	SL	SL	SL
−15			TR then TL	TL			
Modified configuration							
−9		TR				TL	
−12	TR	TR	TR	M	TL	TL	TL
−15							

[a]Maneuver type: M, mush; T, turn; S, spin. Maneuver direction: L, left; R, right.

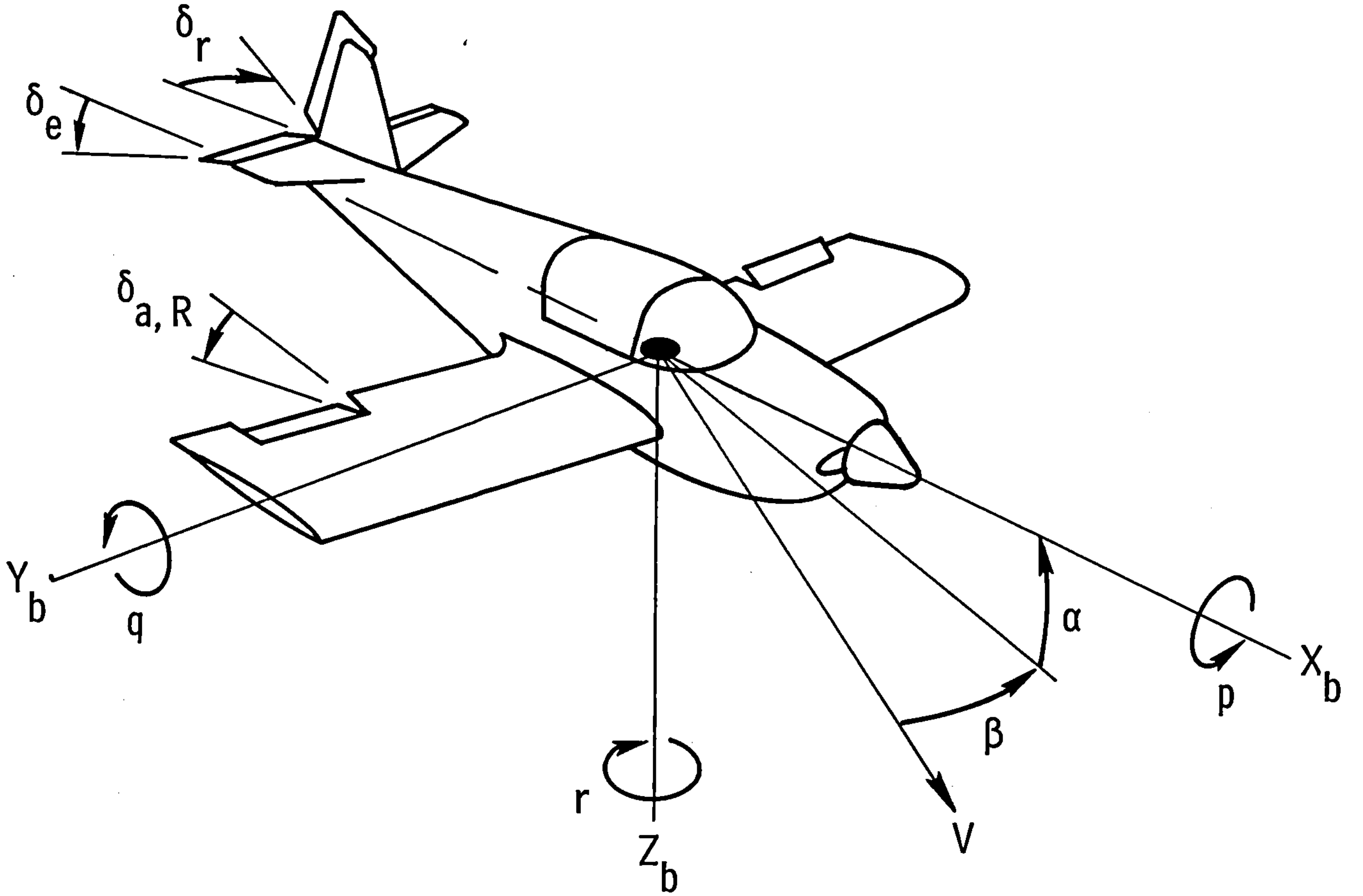

Figure 1. Body-axis system. Arrows indicate positive directions.

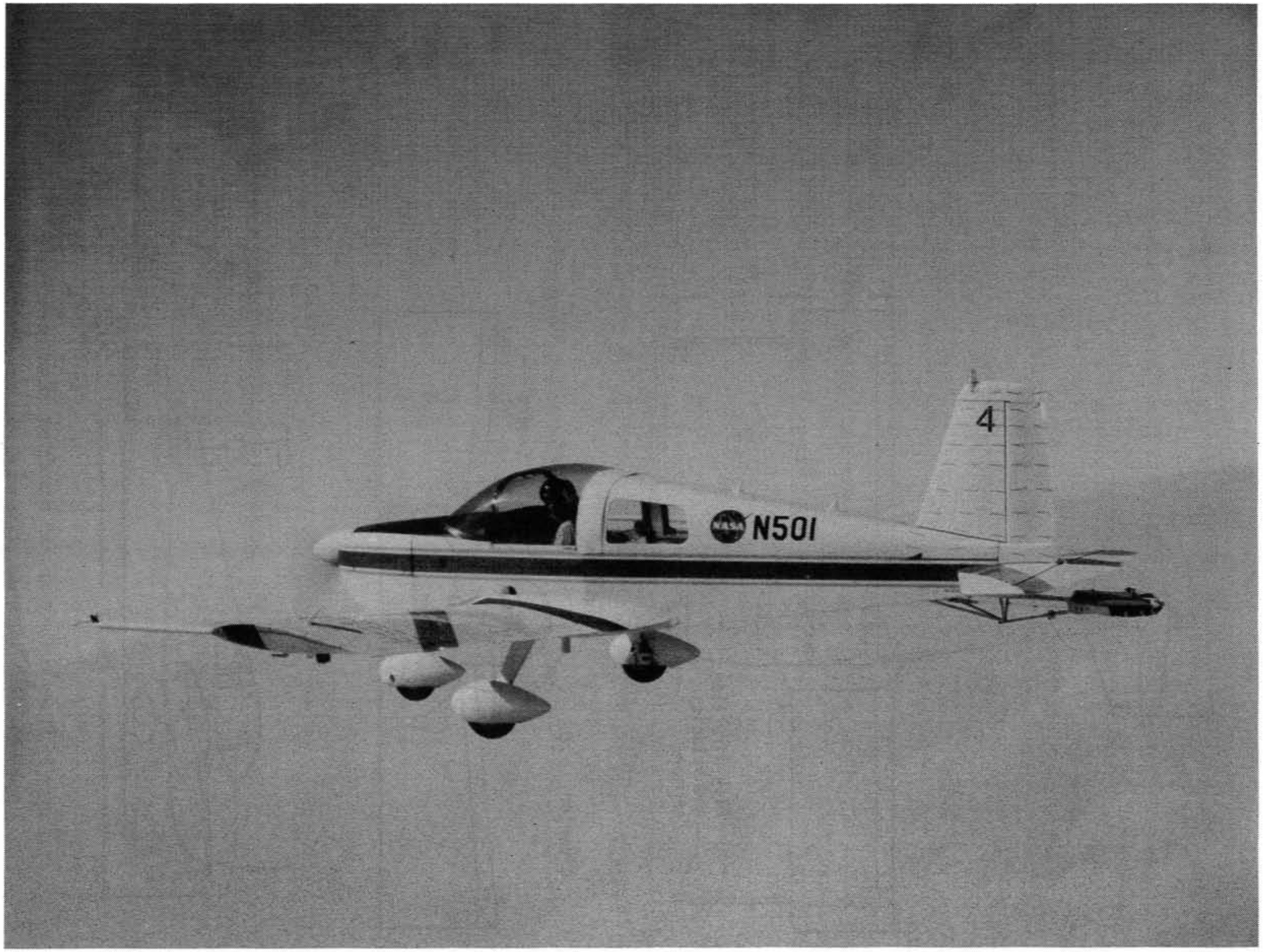

L-85-28

Figure 2. Photograph of aircraft simulated.

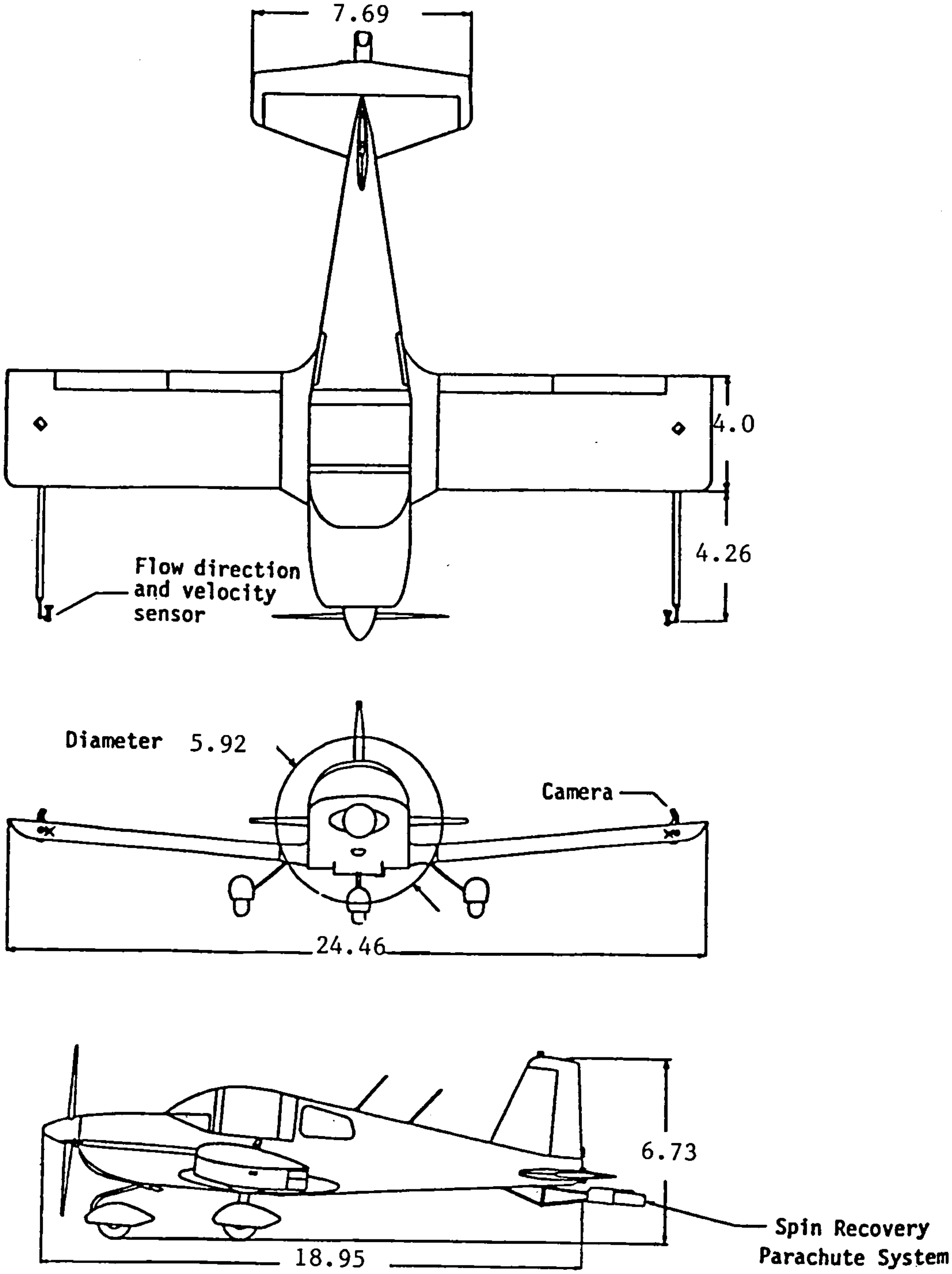

Figure 3. Three views of aircraft simulated. Dimensions are in feet.

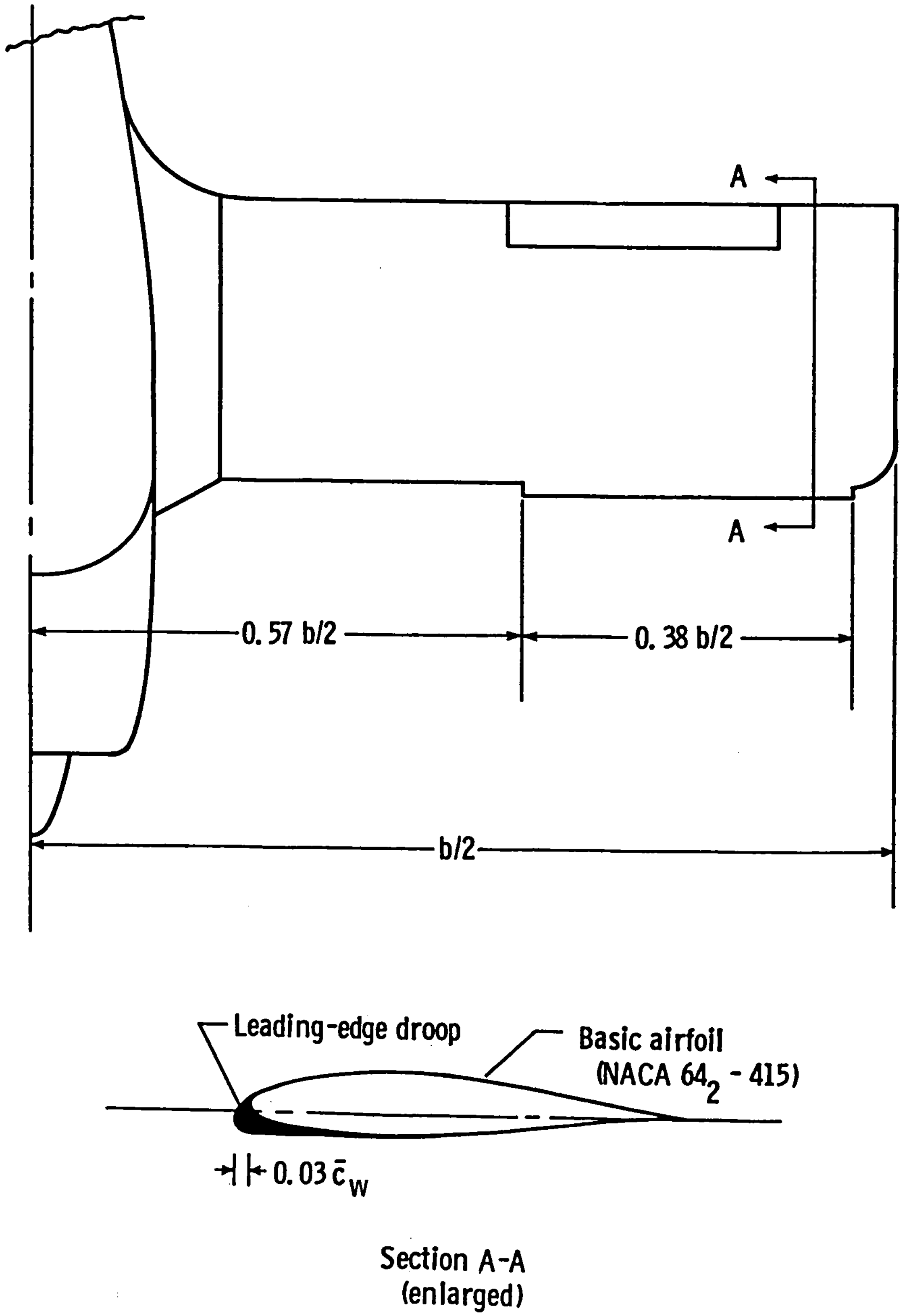

Figure 4. Wing-leading-edge droop modification.

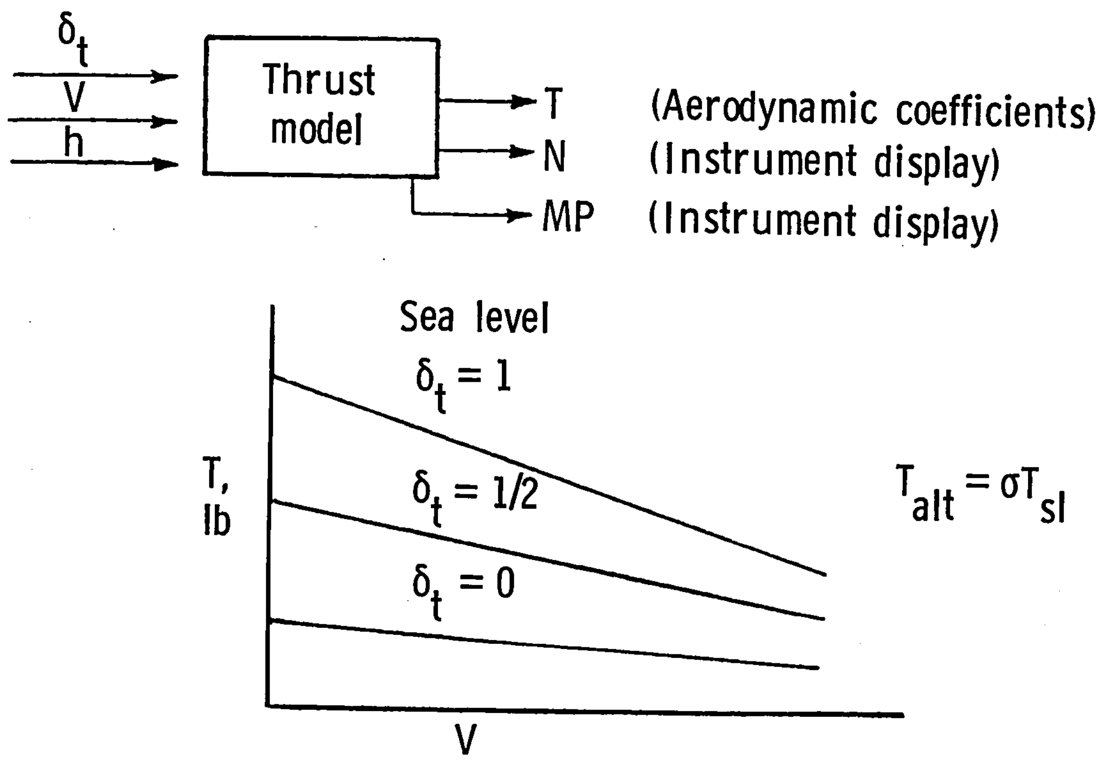

Figure 5. Diagram of steady-state thrust model.

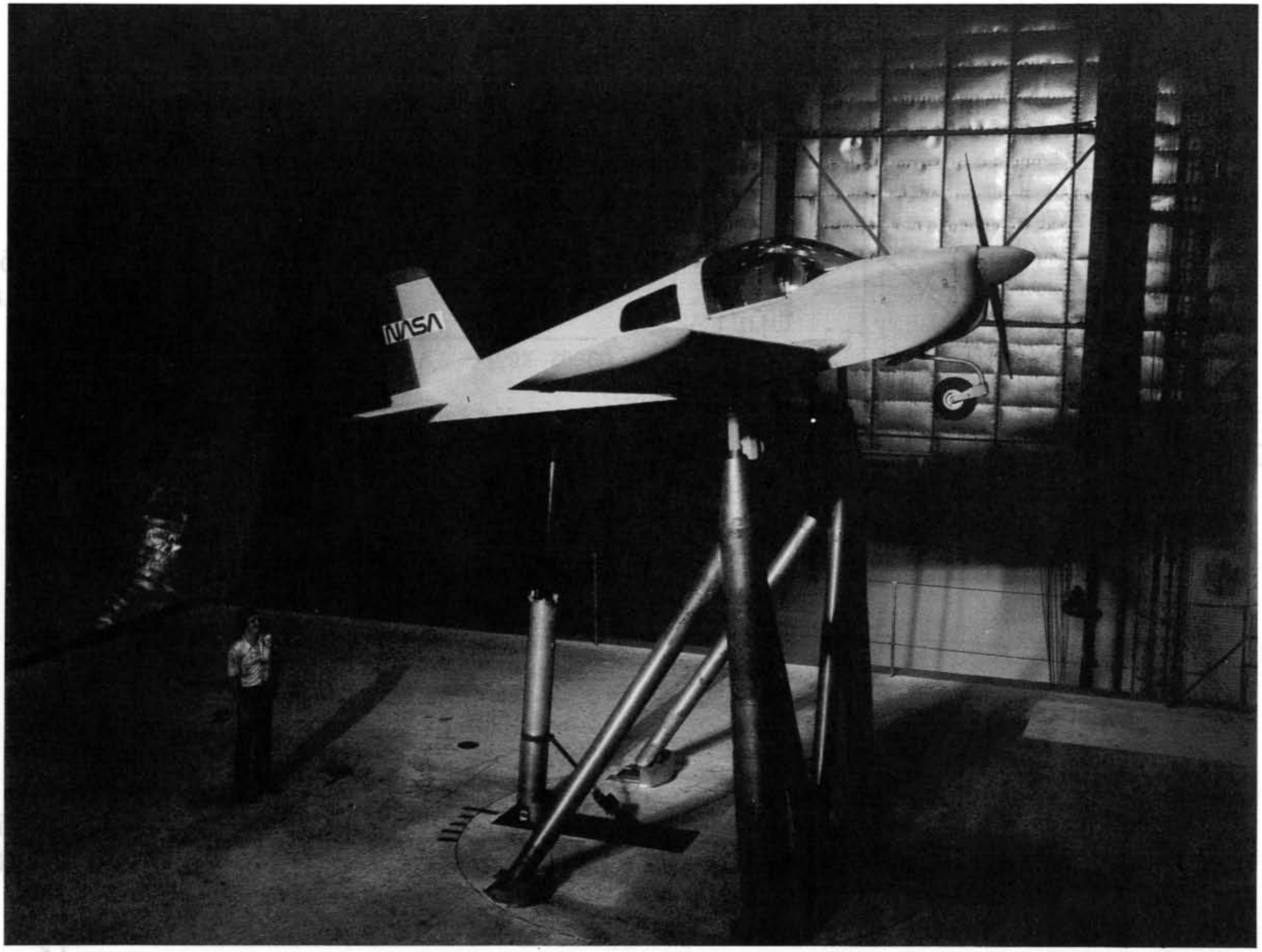

L-79-7117

Figure 6. Airplane in Langley 30- by 60-Foot Tunnel.

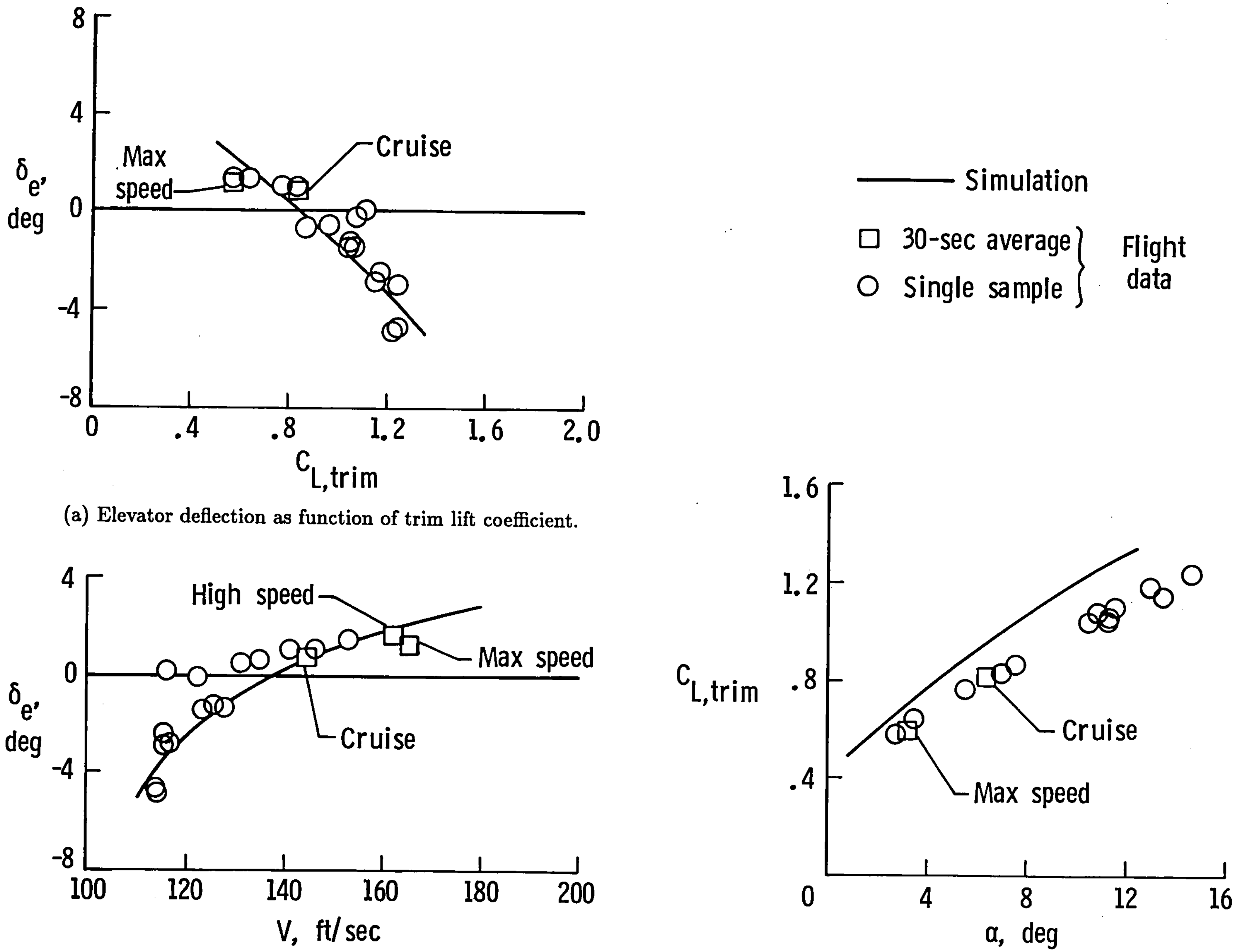

(a) Elevator deflection as function of trim lift coefficient.

(b) Elevator deflection as function of true airspeed.

(c) Trim lift coefficient as function of angle of attack.

Figure 7. Comparison of simulation and flight-test data for constant-altitude straight and level flight conditions for baseline configuration.

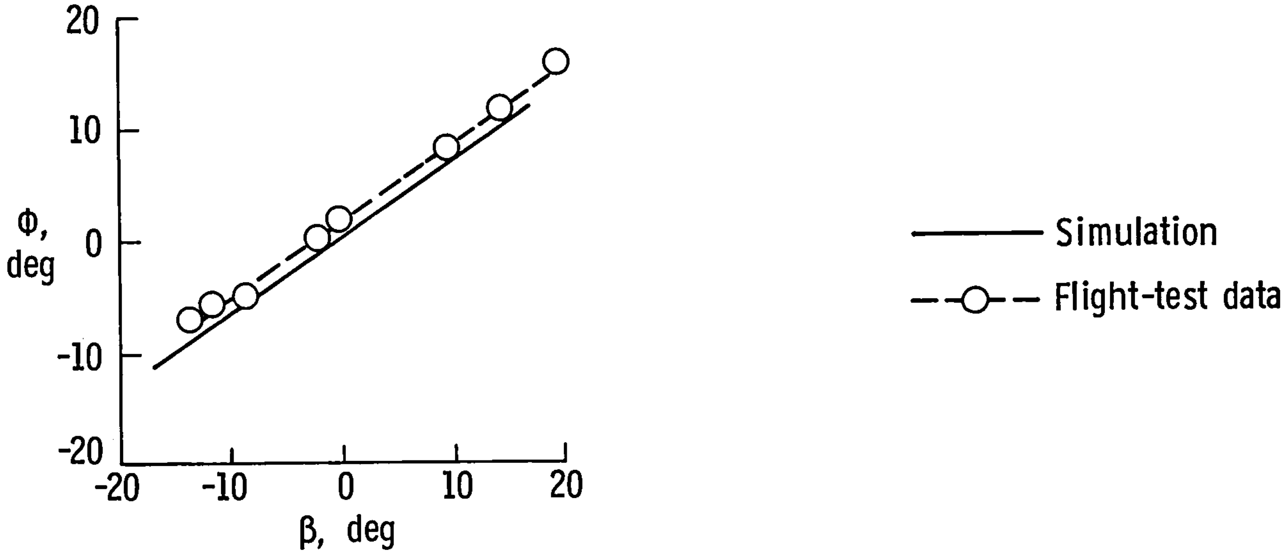

(a) Roll angle as function of sideslip angle.

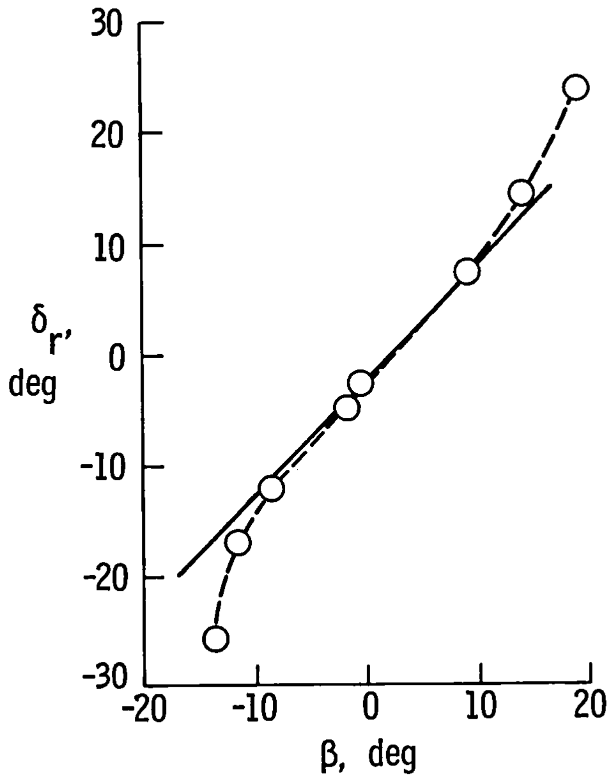

(b) Rudder deflection as function of sideslip angle.

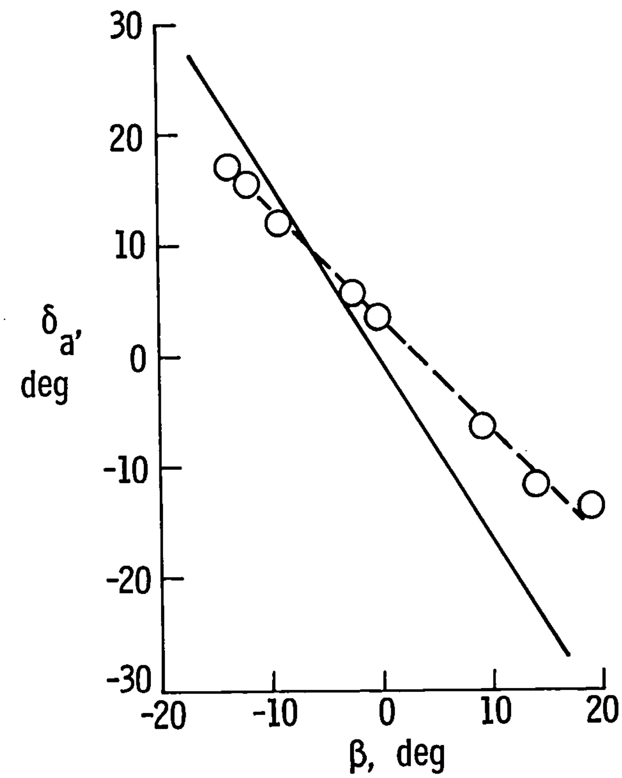

(c) Aileron deflection as function of sideslip angle.

Figure 8. Comparison of simulation and flight-test data for power-on steady-heading sideslips for baseline configuration.

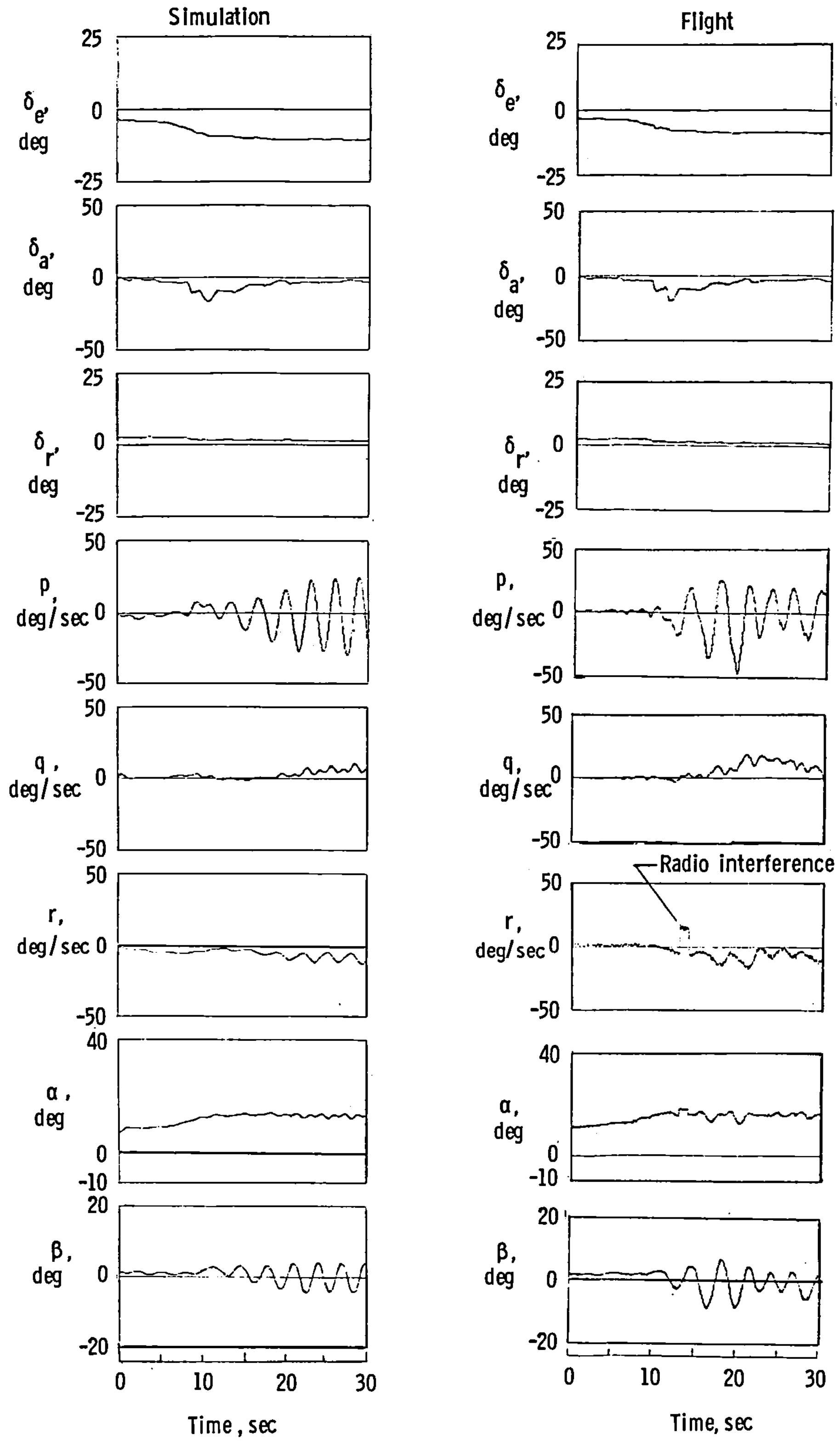

Figure 9. Stall-departure time-history comparisons of simulation and flight results when elevator is held fixed at the stall for baseline configuration with power off ($\delta_{t,c} = 0$).

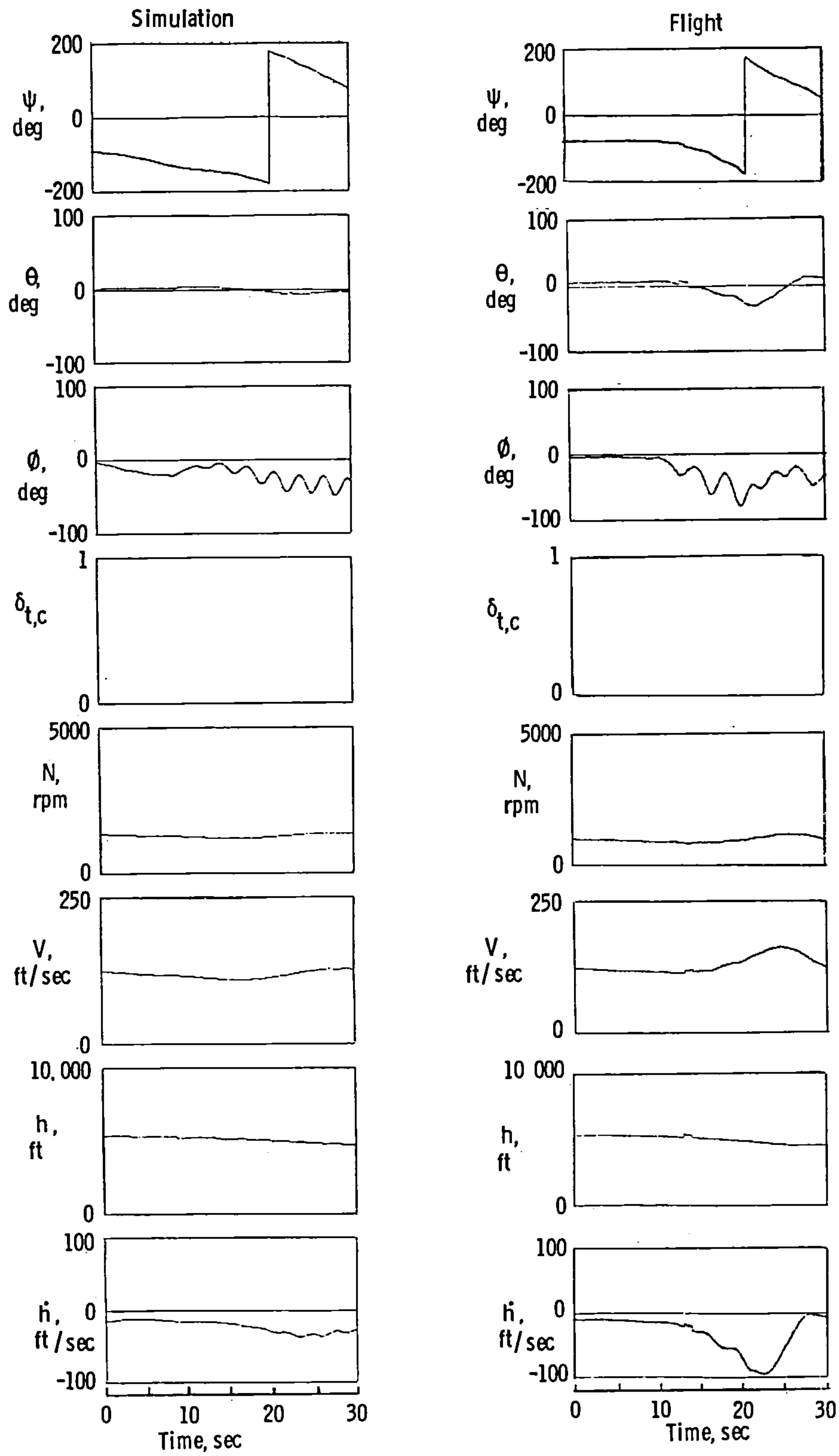

Figure 9. Continued.

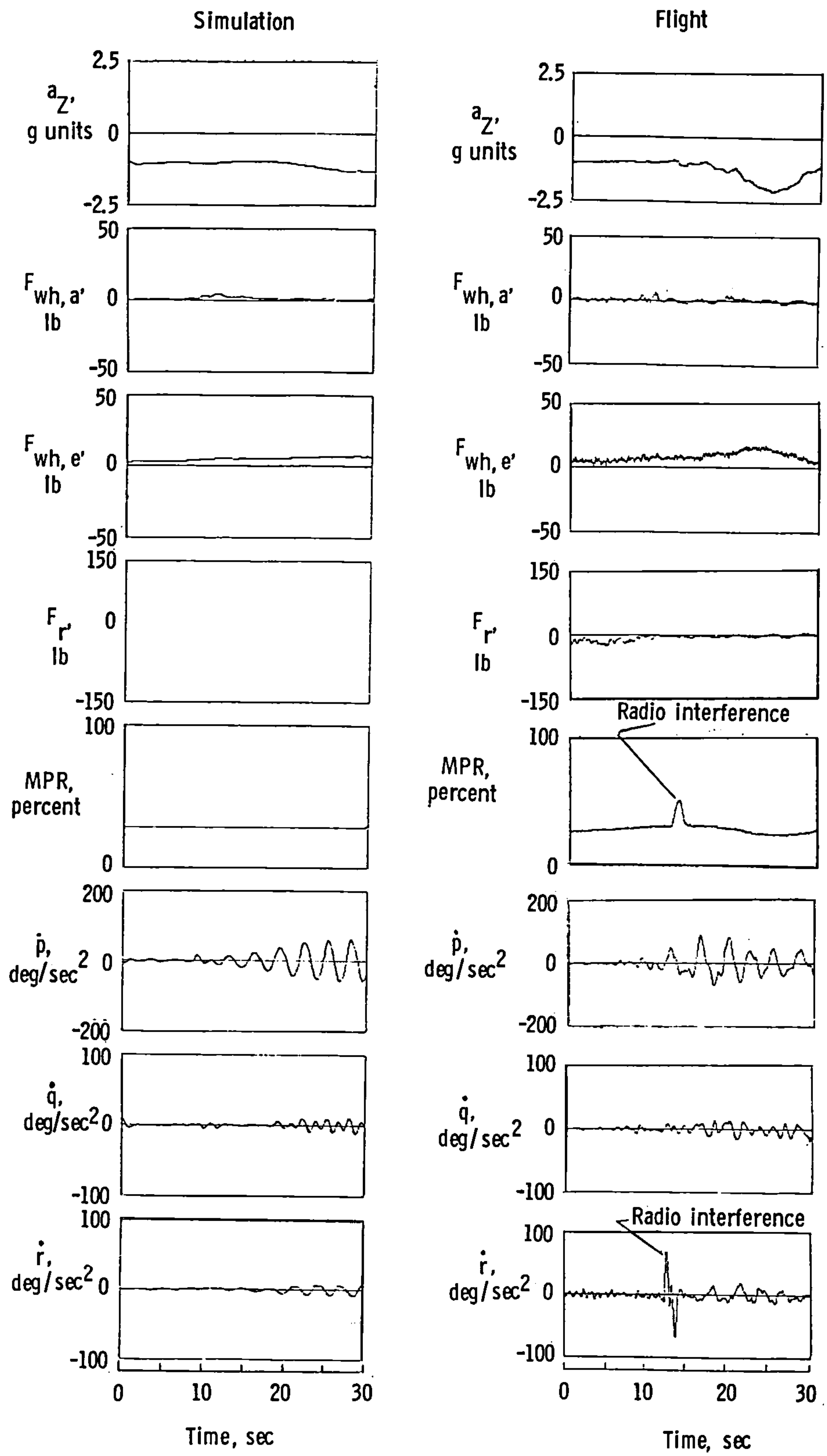

Figure 9. Concluded.

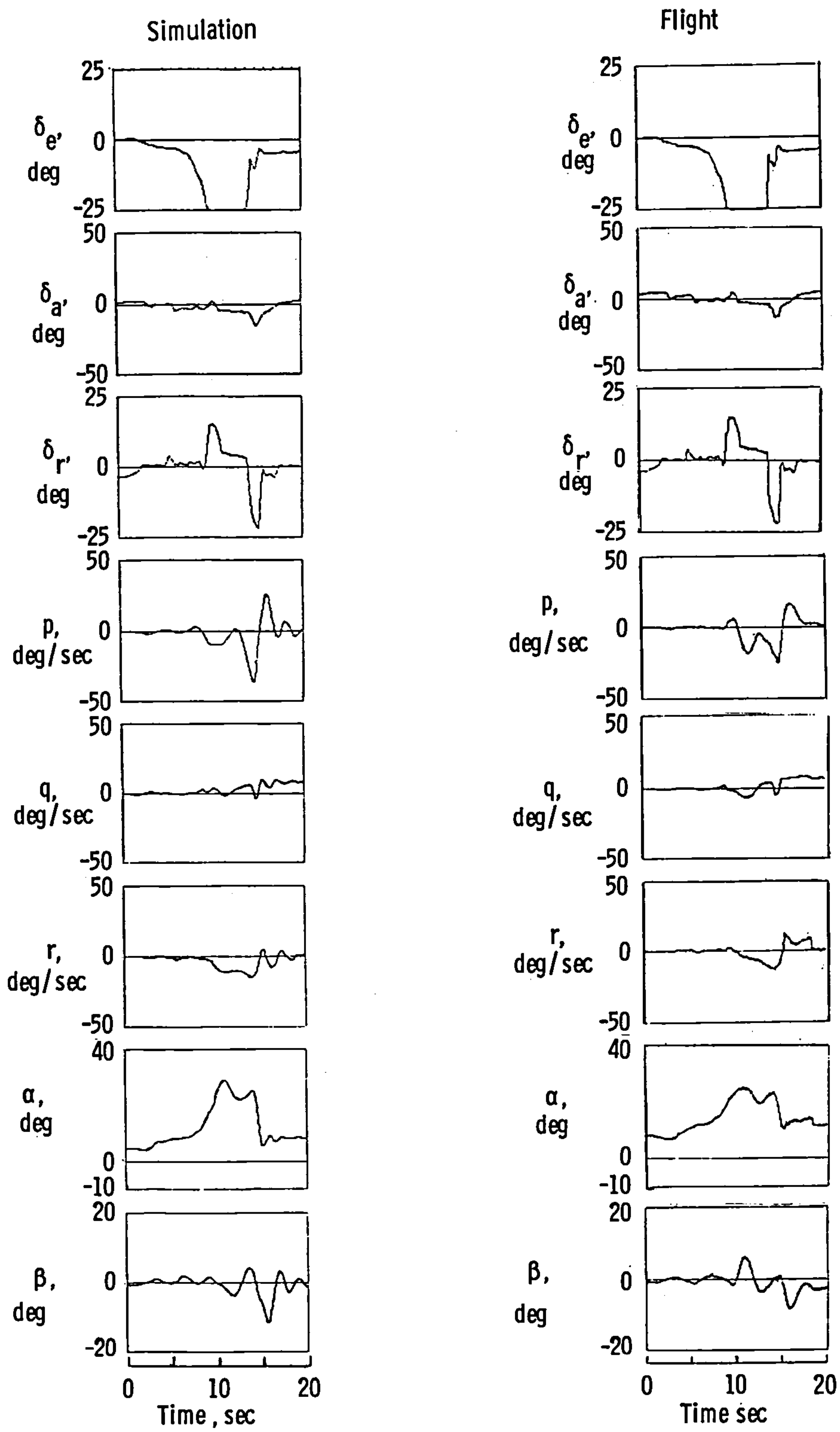

Figure 10. Stall-departure time-history comparisons of simulation and flight results including a throttle chop and full-up-elevator deflection for baseline configuration.

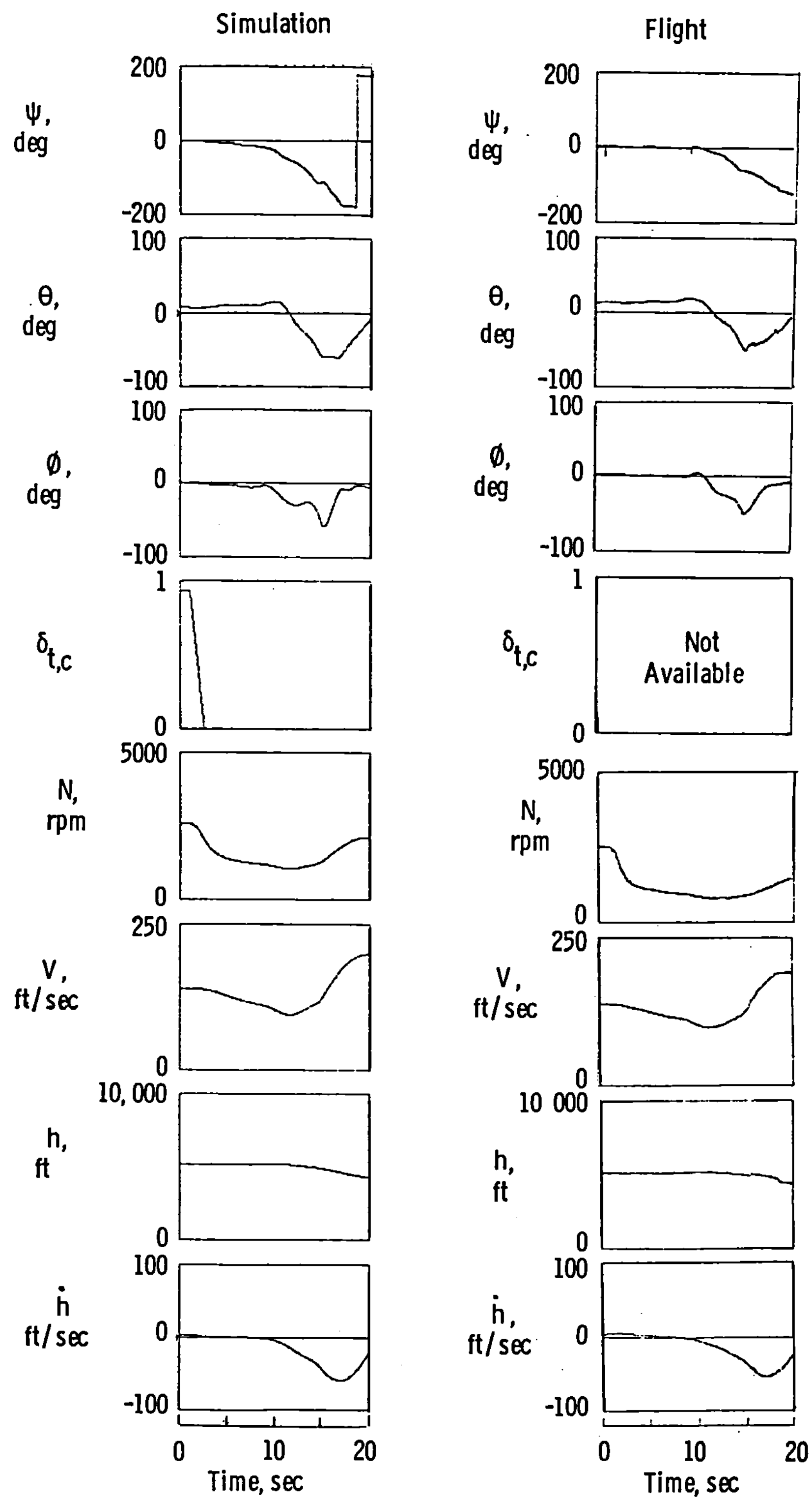

Figure 10. Continued.

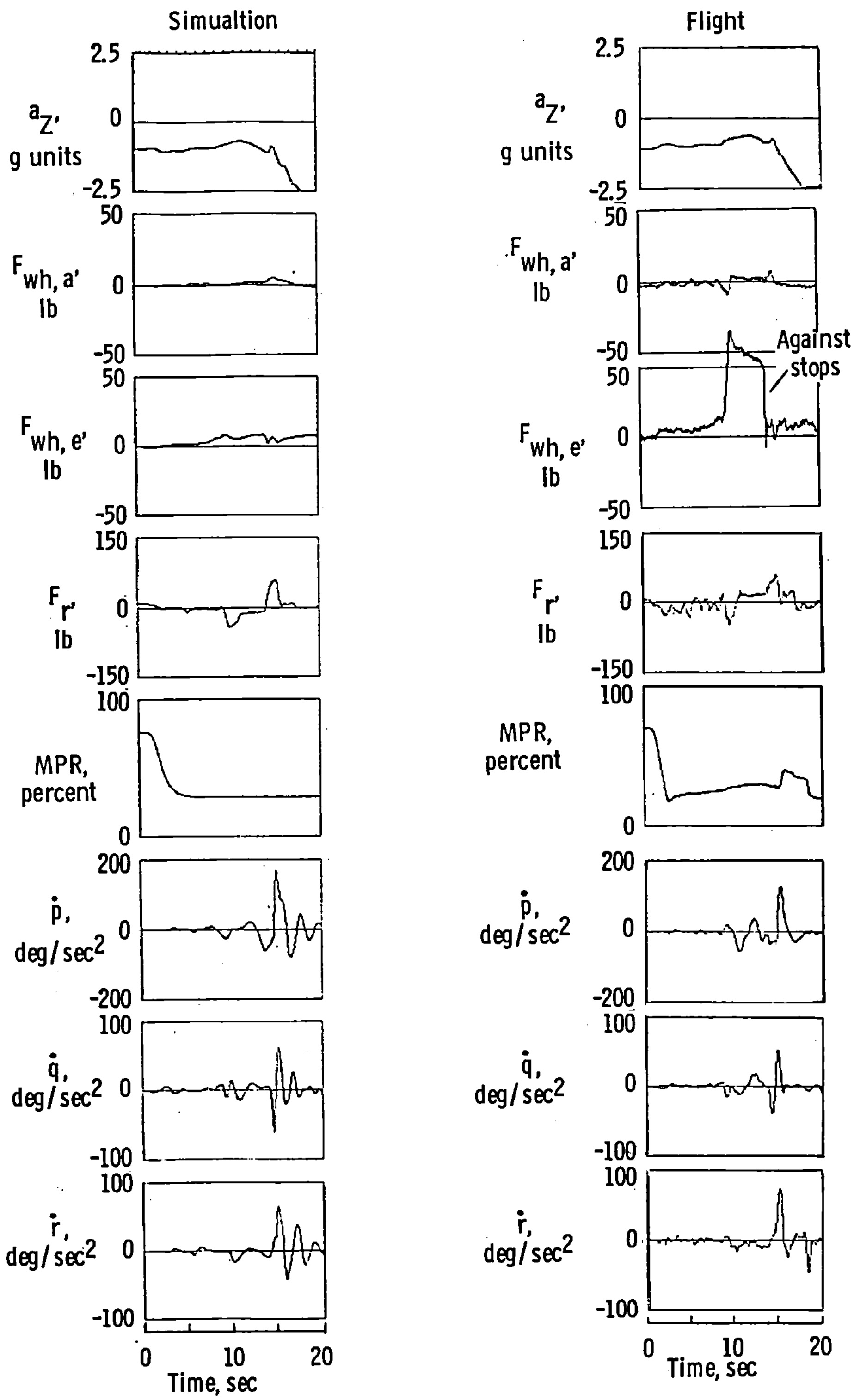

Figure 10. Concluded.

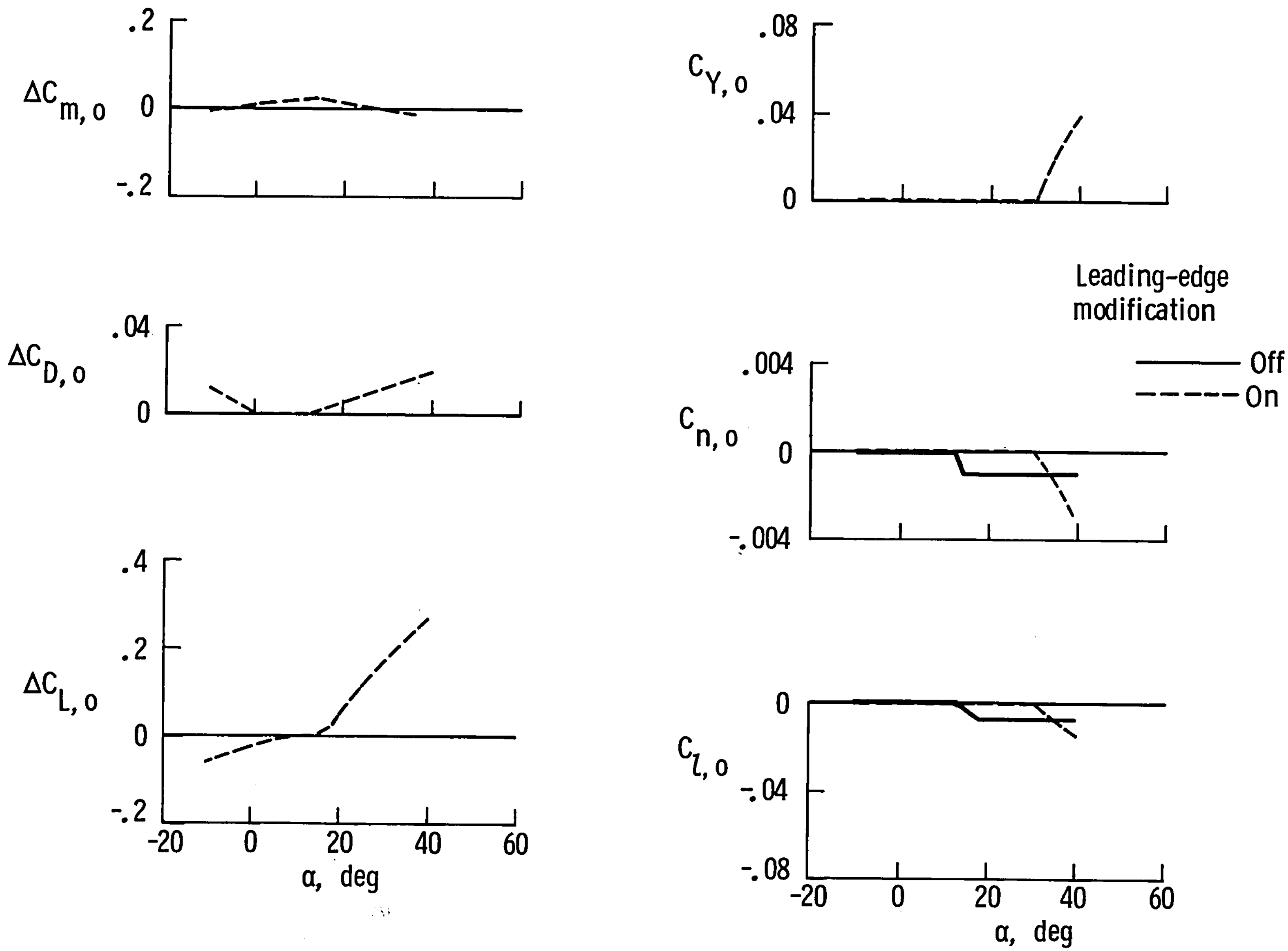

(a) Increments due to modification on longitudinal characteristics.

(b) Lateral characteristics at $\beta = 0$.

Figure 11. Comparisons of baseline and modified configurations from tabulated coefficient data for power-off condition ($C_T = 0$).

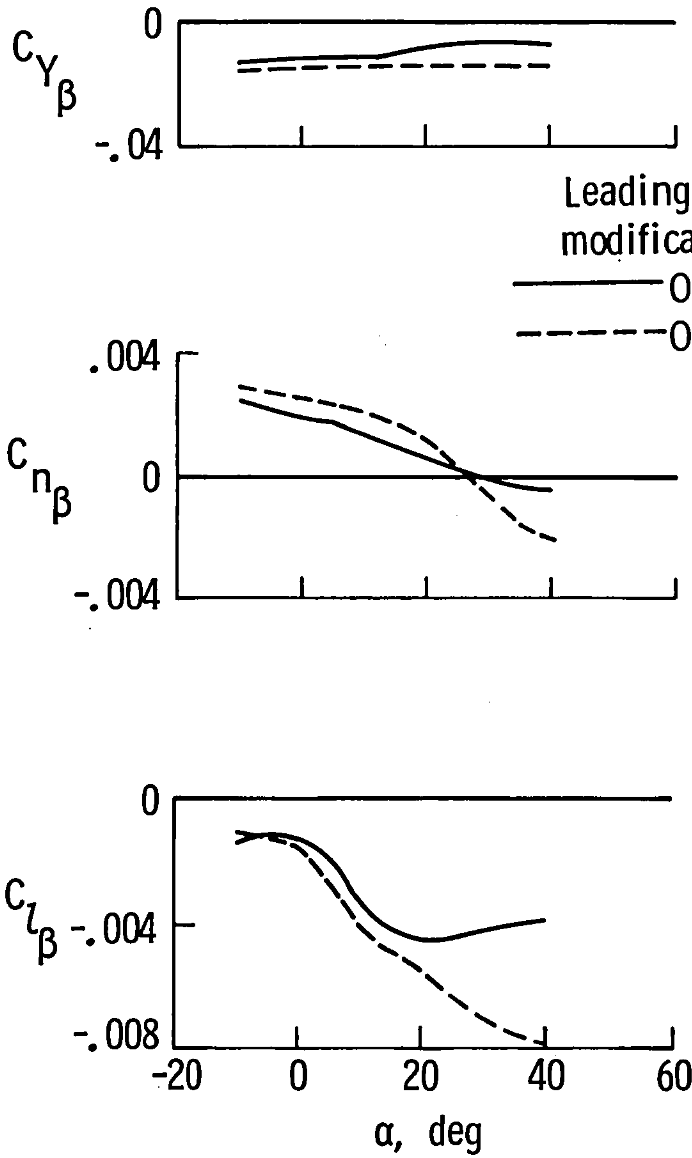

(c) Sideslip derivatives.

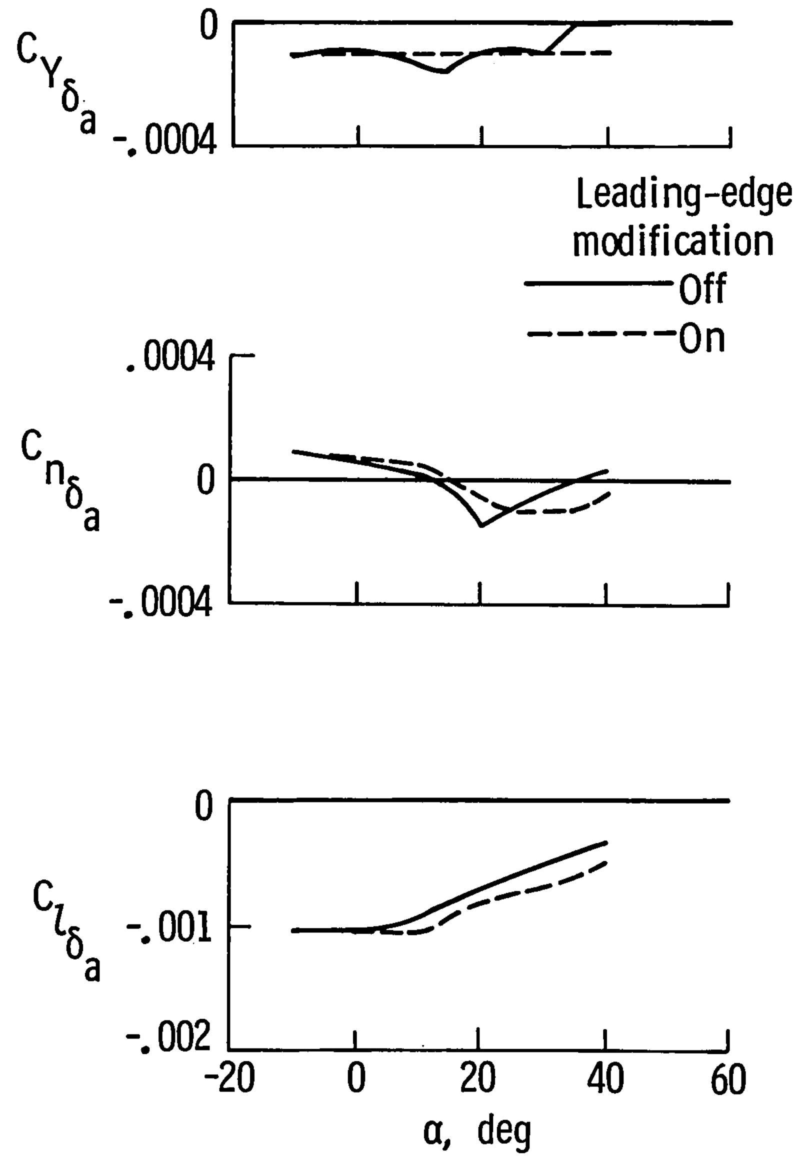

(d) Aileron-control derivatives.

Figure 11. Continued.

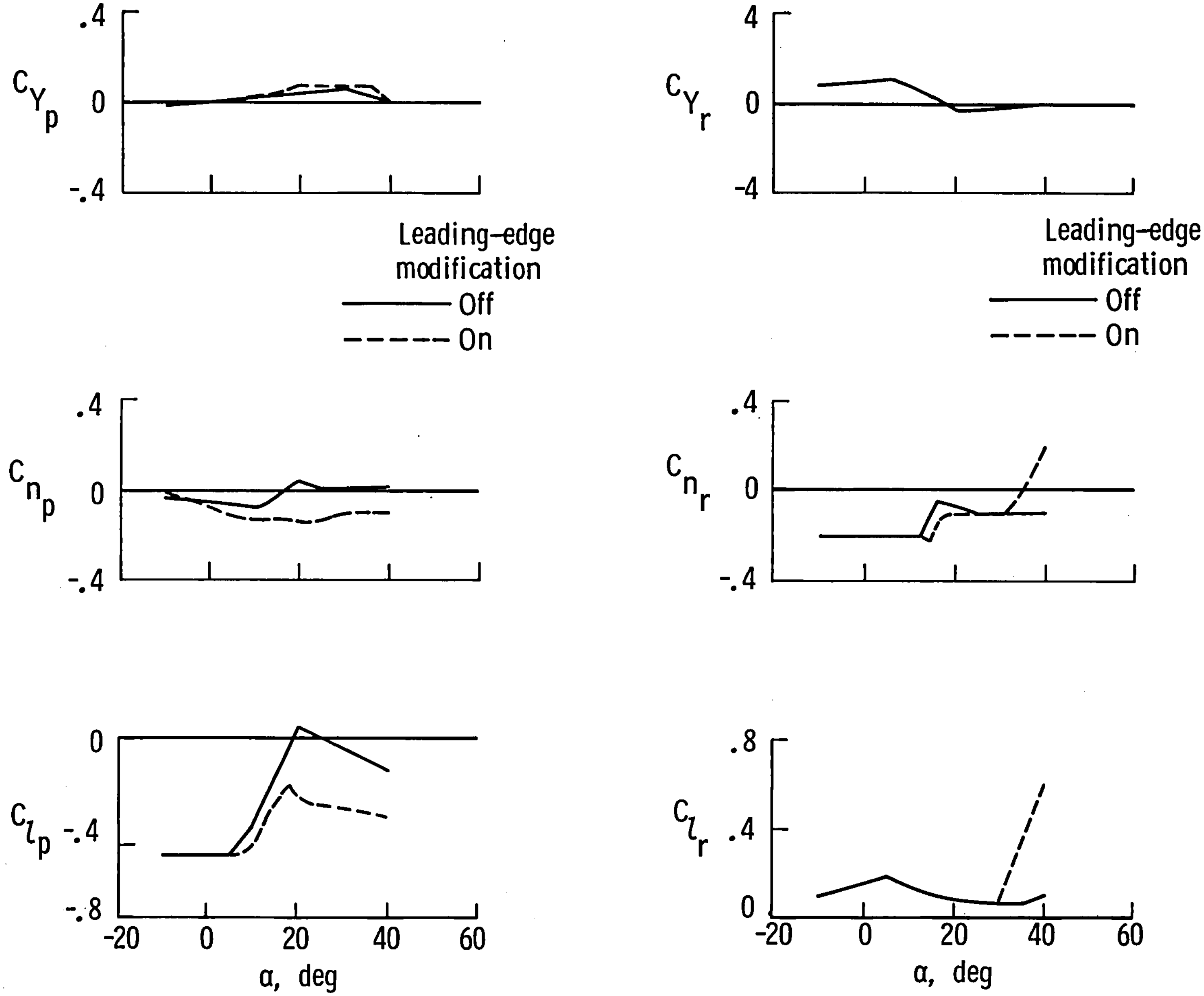

(e) Steady-rolling derivatives.

(f) Steady-yawing derivatives.

Figure 11. Concluded.

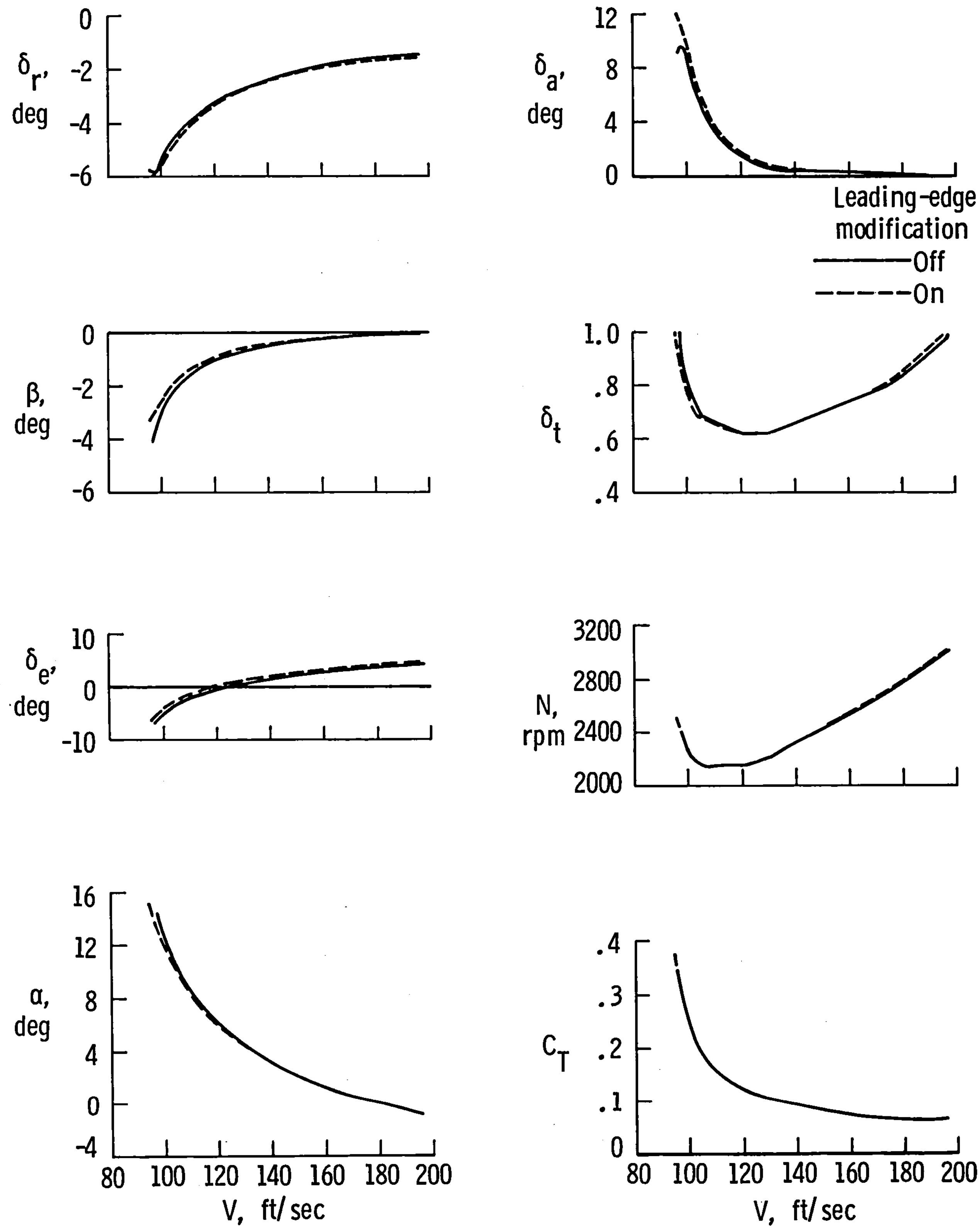

Figure 12. Comparison of straight and level trim conditions at sea level for baseline and modified configurations with $\delta_f = 0$ and $W = 1577$ lb.

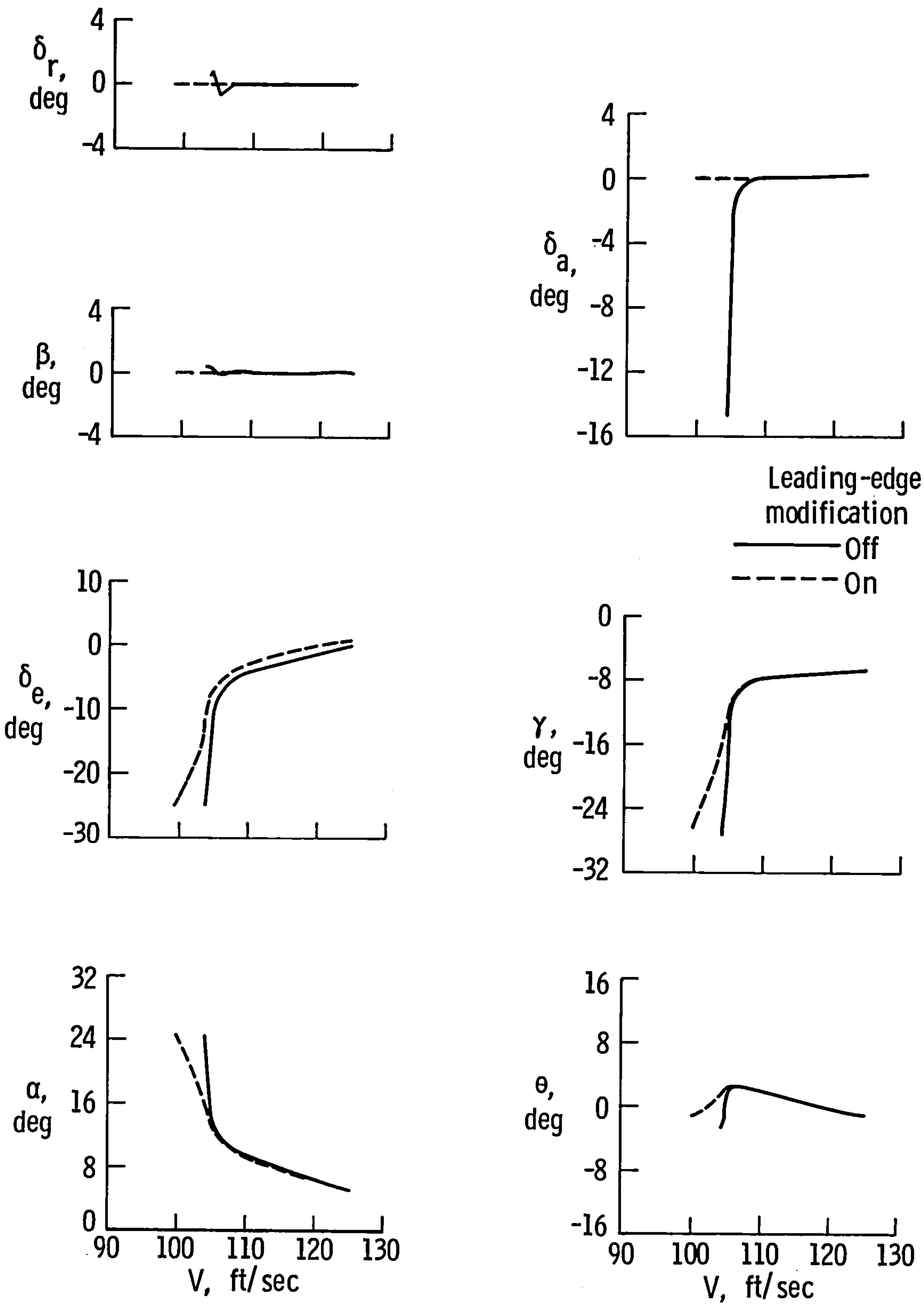

Figure 13. Comparison of throttle-closed trim curves for baseline and modified configurations at sea level with $\delta_t = 0$, $\delta_f = 0$, and $W = 1577$ lb.

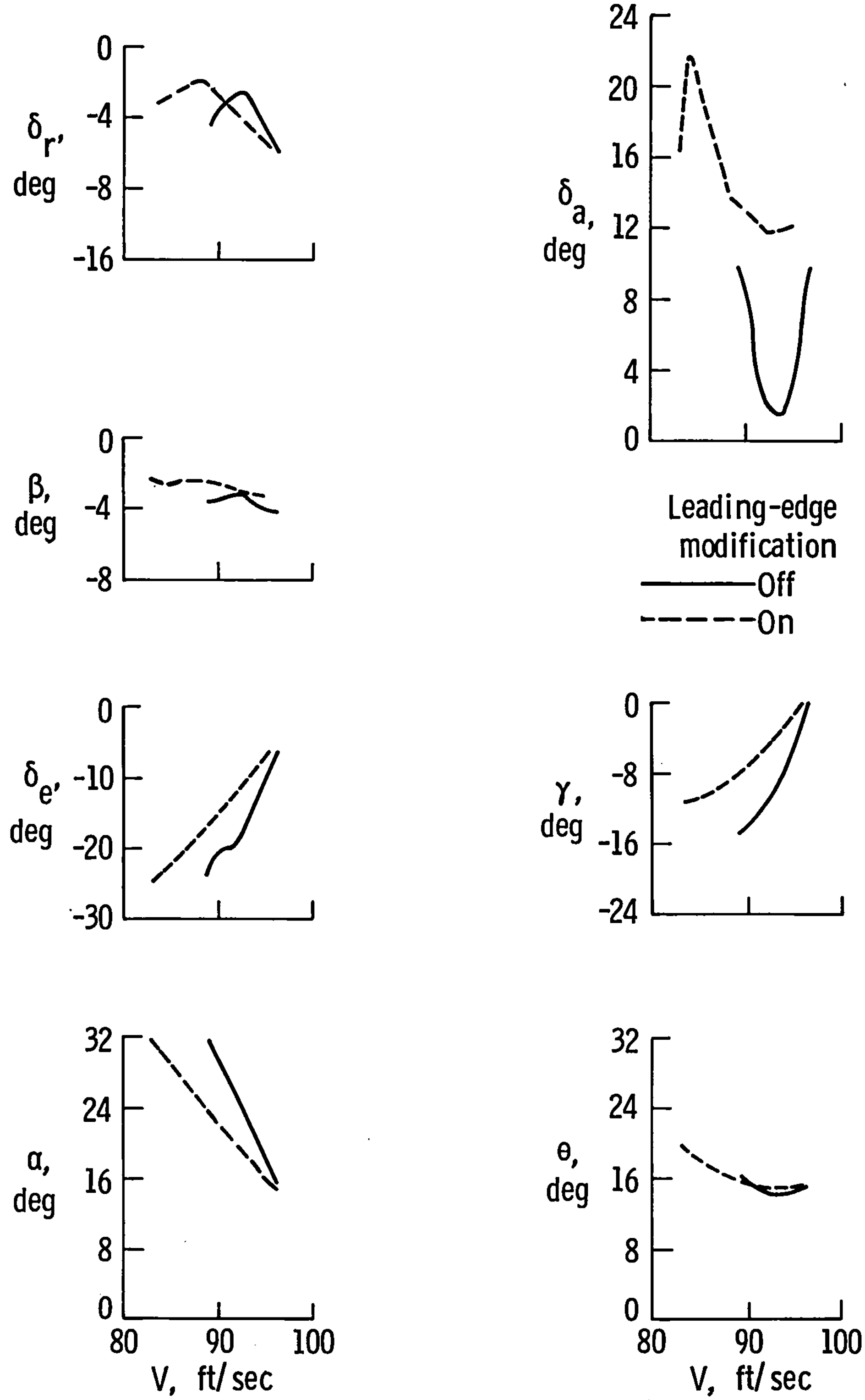

Figure 14. Comparison of full-throttle trim curves for baseline and modified configurations for speeds less than straight and level flight at sea level with $\delta_t = 1.0$, $\delta_f = 0$, and $W = 1577$ lb.

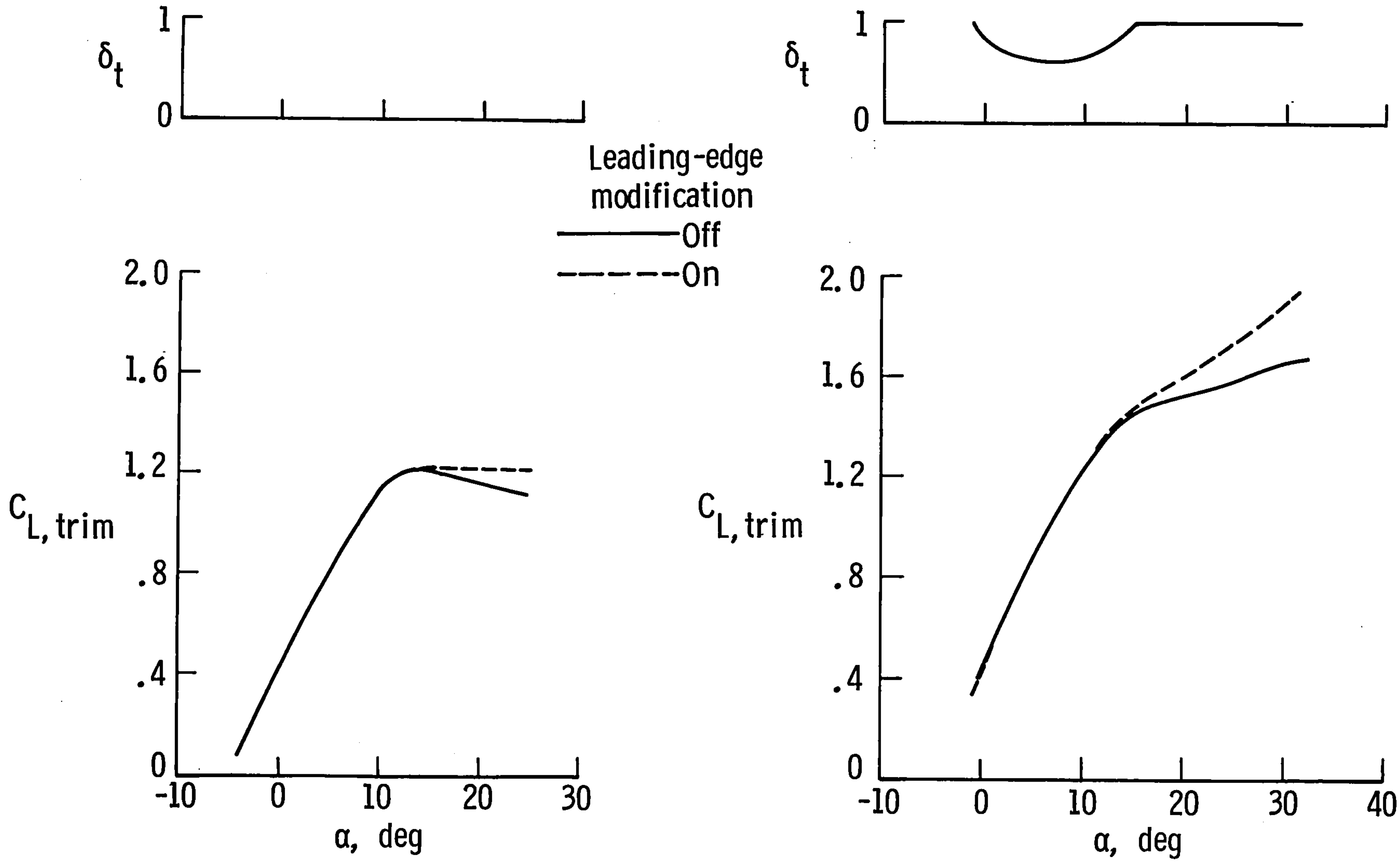

(a) Throttle closed ($\delta_t = 0$).

(b) Power on.

Figure 15. Comparisons of trimmed lift coefficients for baseline and modified configurations.

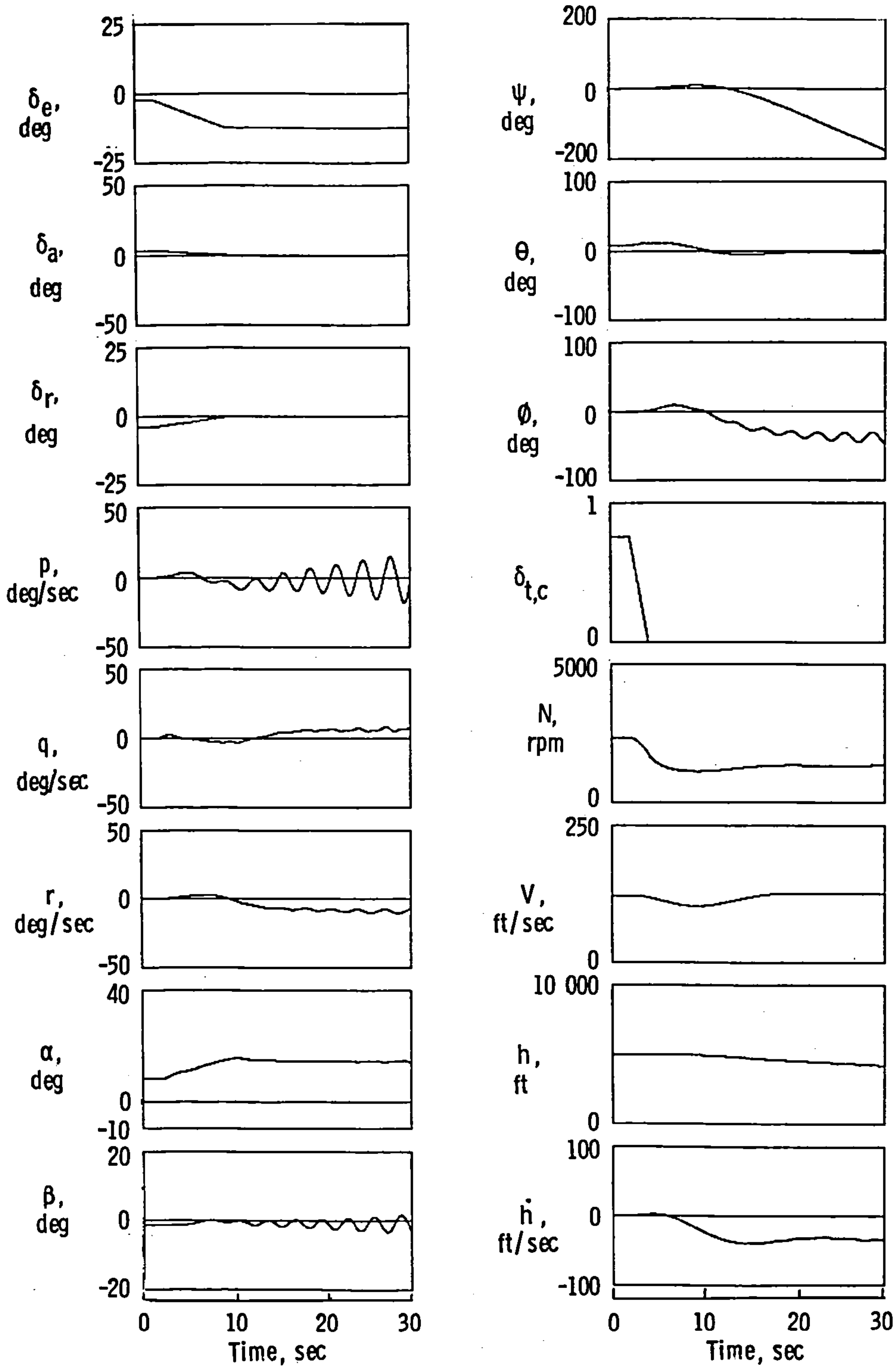

(a) Baseline configuration.

Figure 16. Simulation time histories for baseline and modified configurations for an elevator-ramp input and throttle chop from a straight and level trim flight condition. Initial conditions of h = 5000 ft, V = 120 ft/sec, and W = 1577 lb.

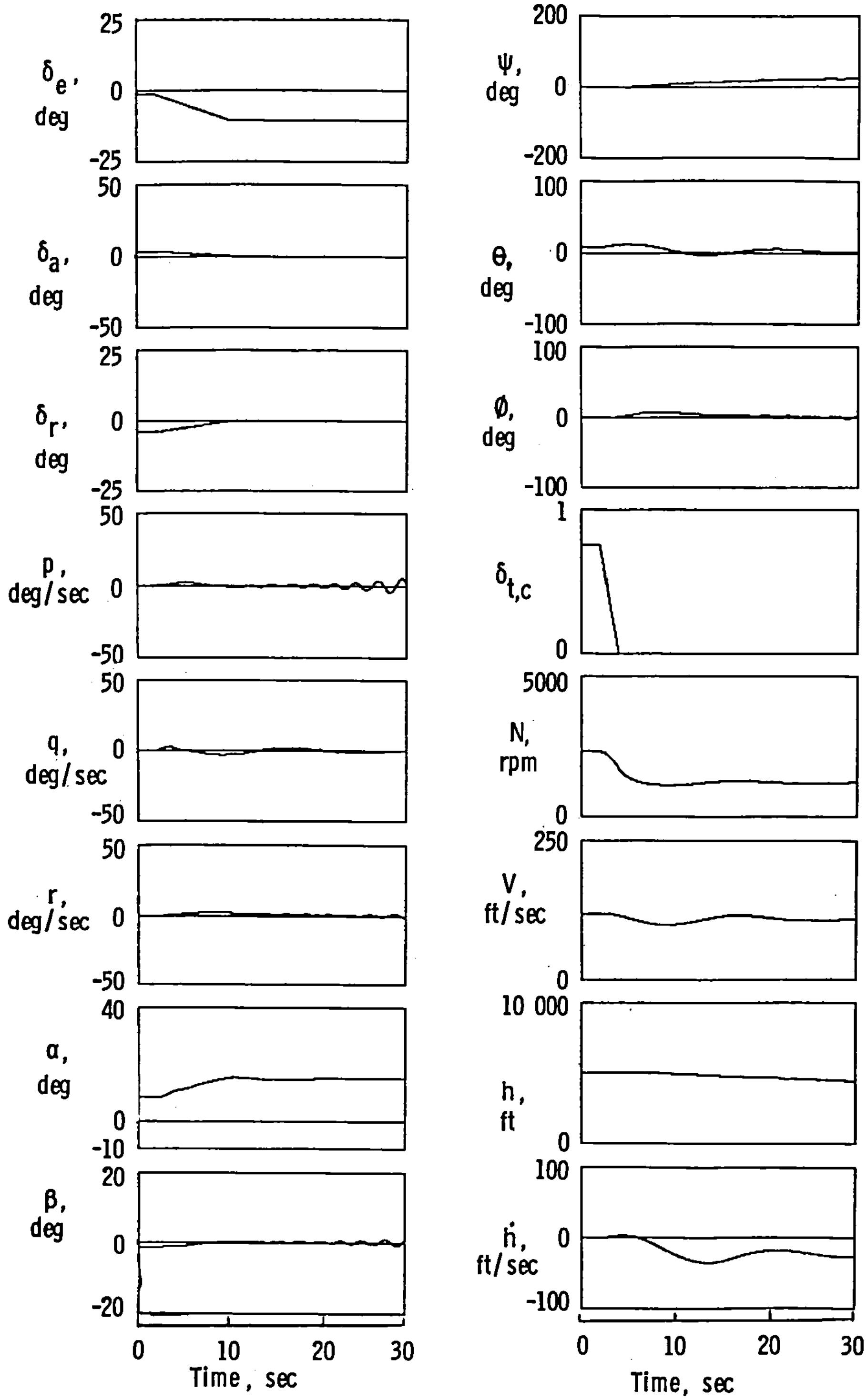

(b) Modified configuration.

Figure 16. Concluded.

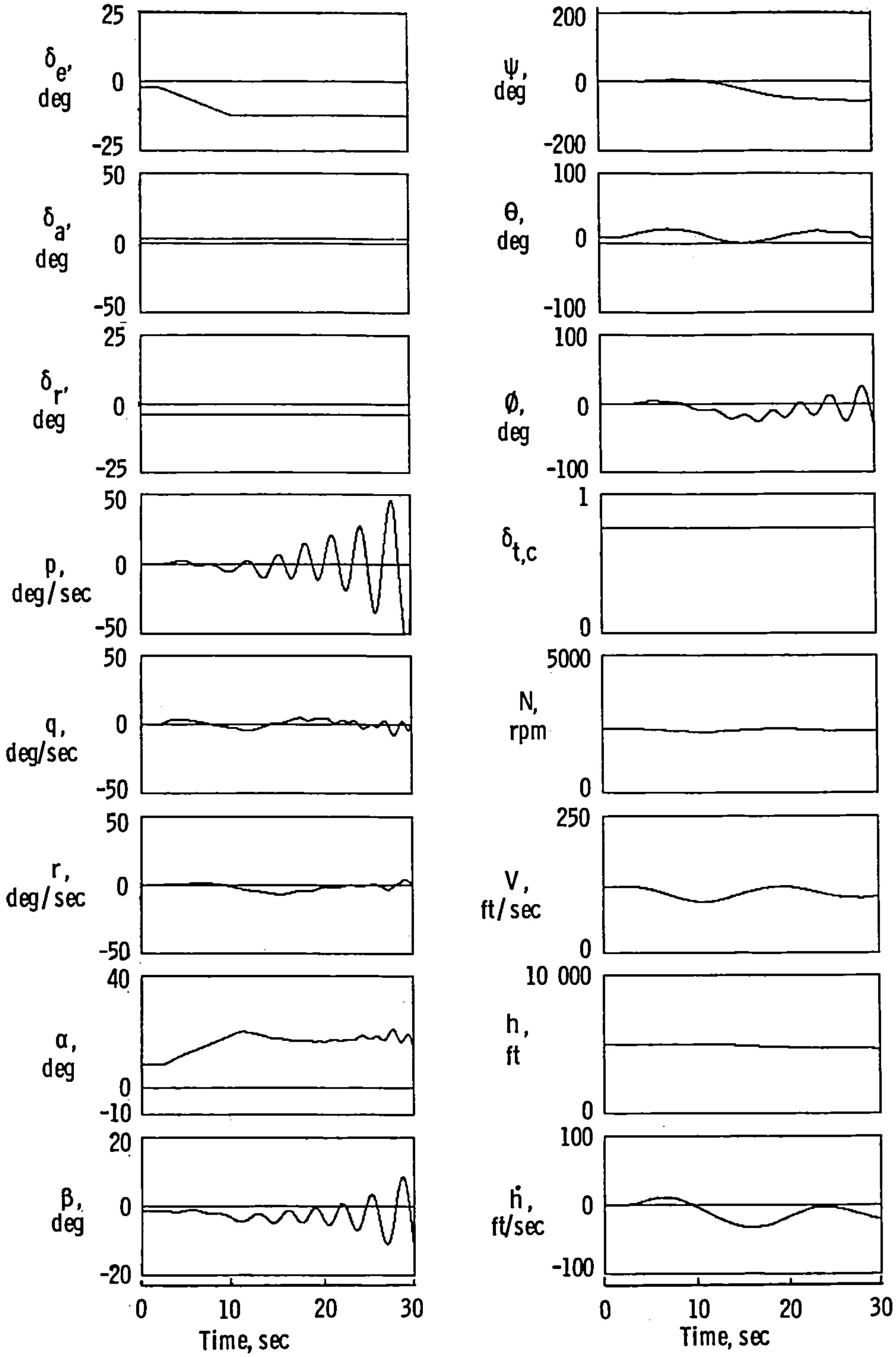

(a) Baseline configuration.

Figure 17. Simulation time histories for baseline and modified configurations for an elevator-ramp input from a straight and level trim flight condition. Initial conditions of h = 5000 ft, V = 120 ft/sec, and $W = 1577$ lb.

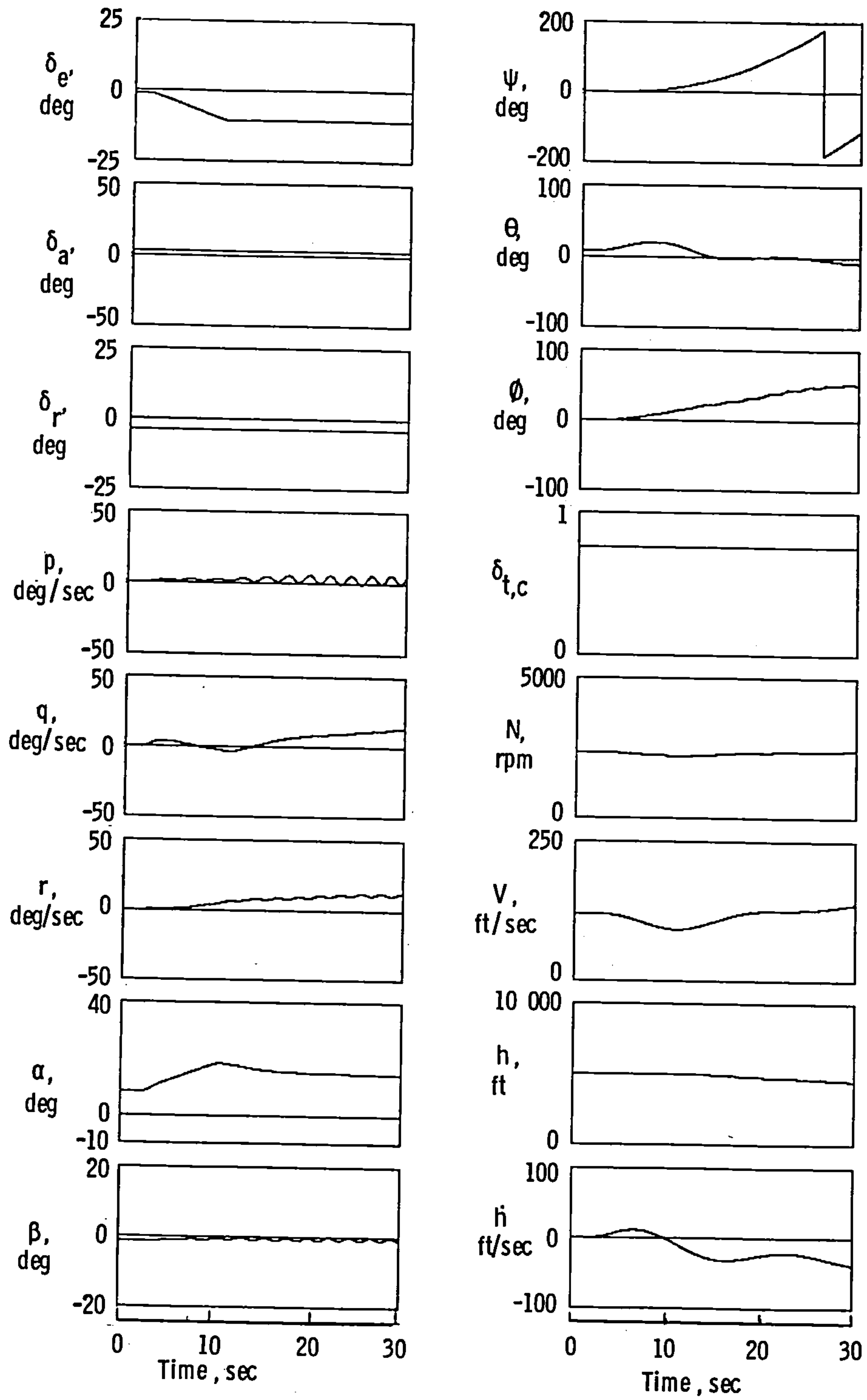

(b) Modified configuration.

Figure 17. Concluded.

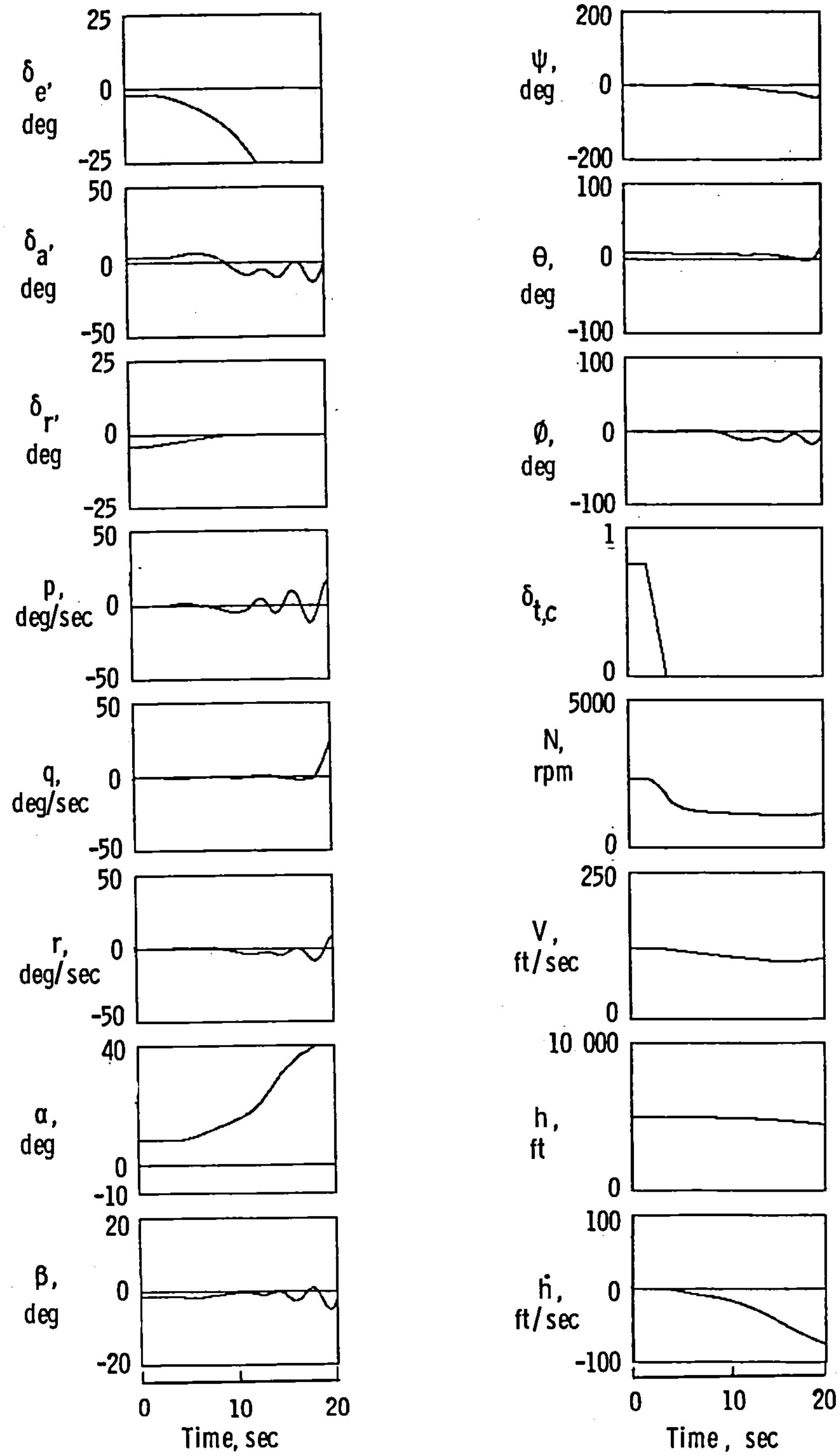

(a) Baseline configuration.

Figure 18. Simulation time histories for baseline and modified configurations for continuous elevator and aileron control inputs and throttle chop from a straight and level trim flight condition. Initial conditions of $h = 5000$ ft, $V = 120$ ft/sec, and $W = 1577$ lb.

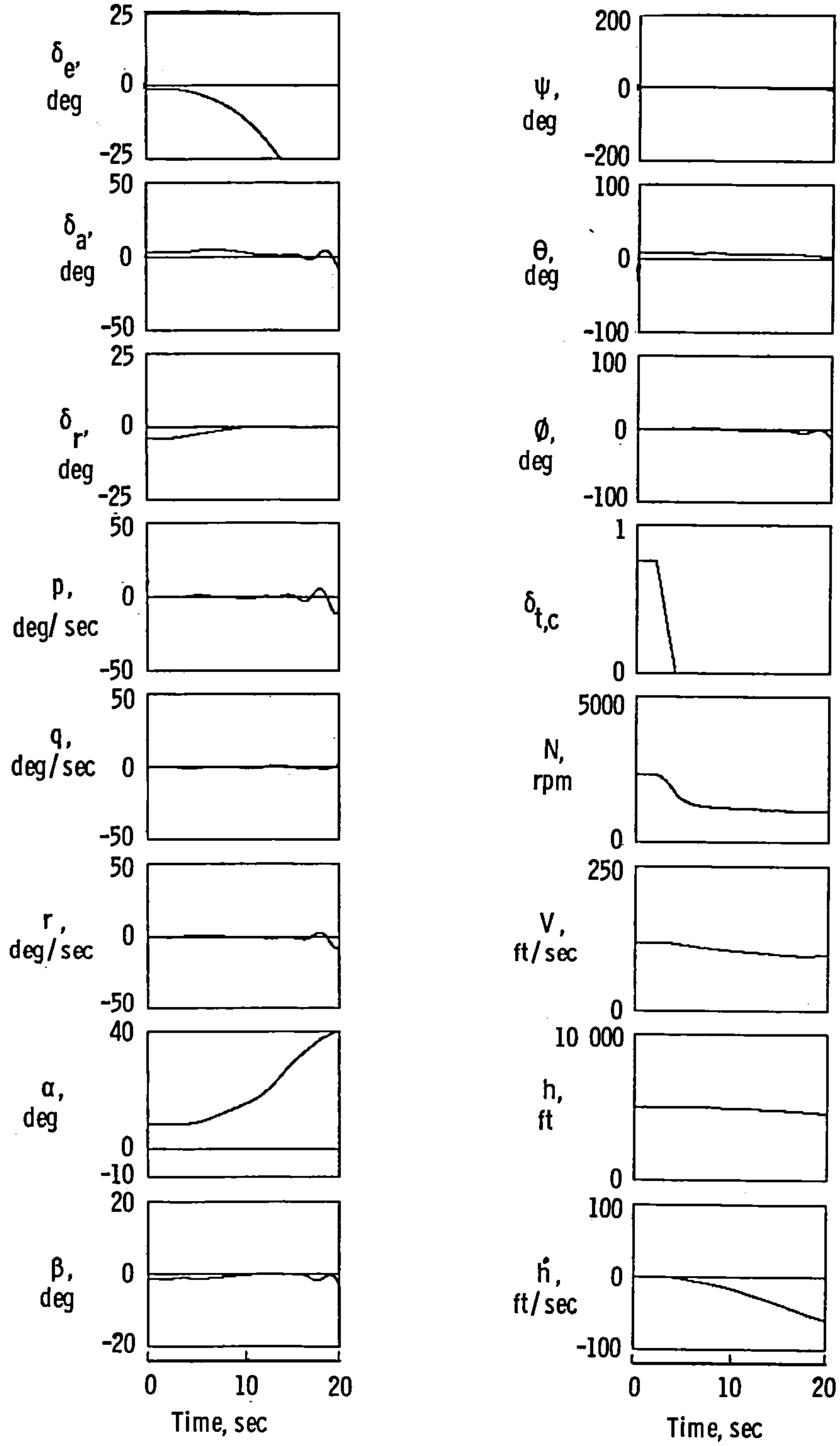

(b) Modified configuration.

Figure 18. Concluded.

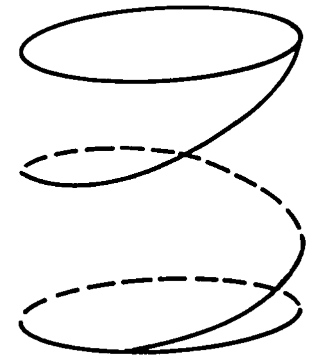

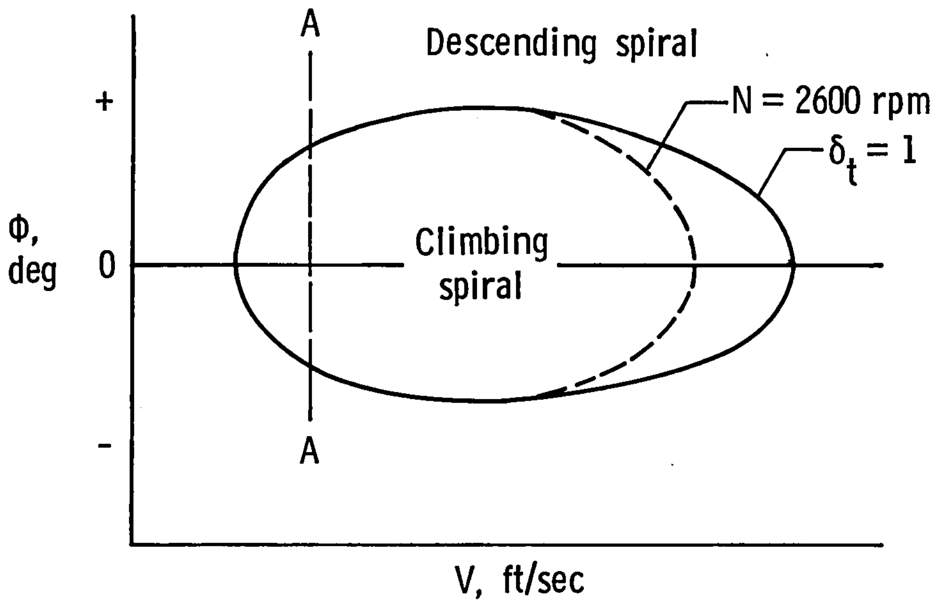

(a) Boundary for circular flight at constant altitude.

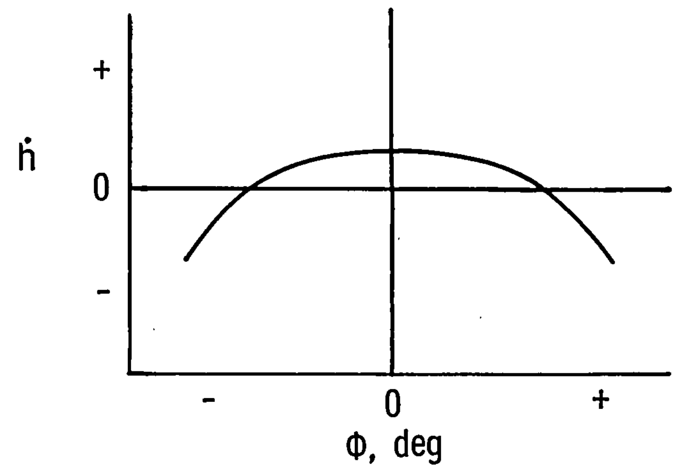

(c) Section A-A for full throttle.

Figure 19. Sketches of typical simulation trim results for turning flight.

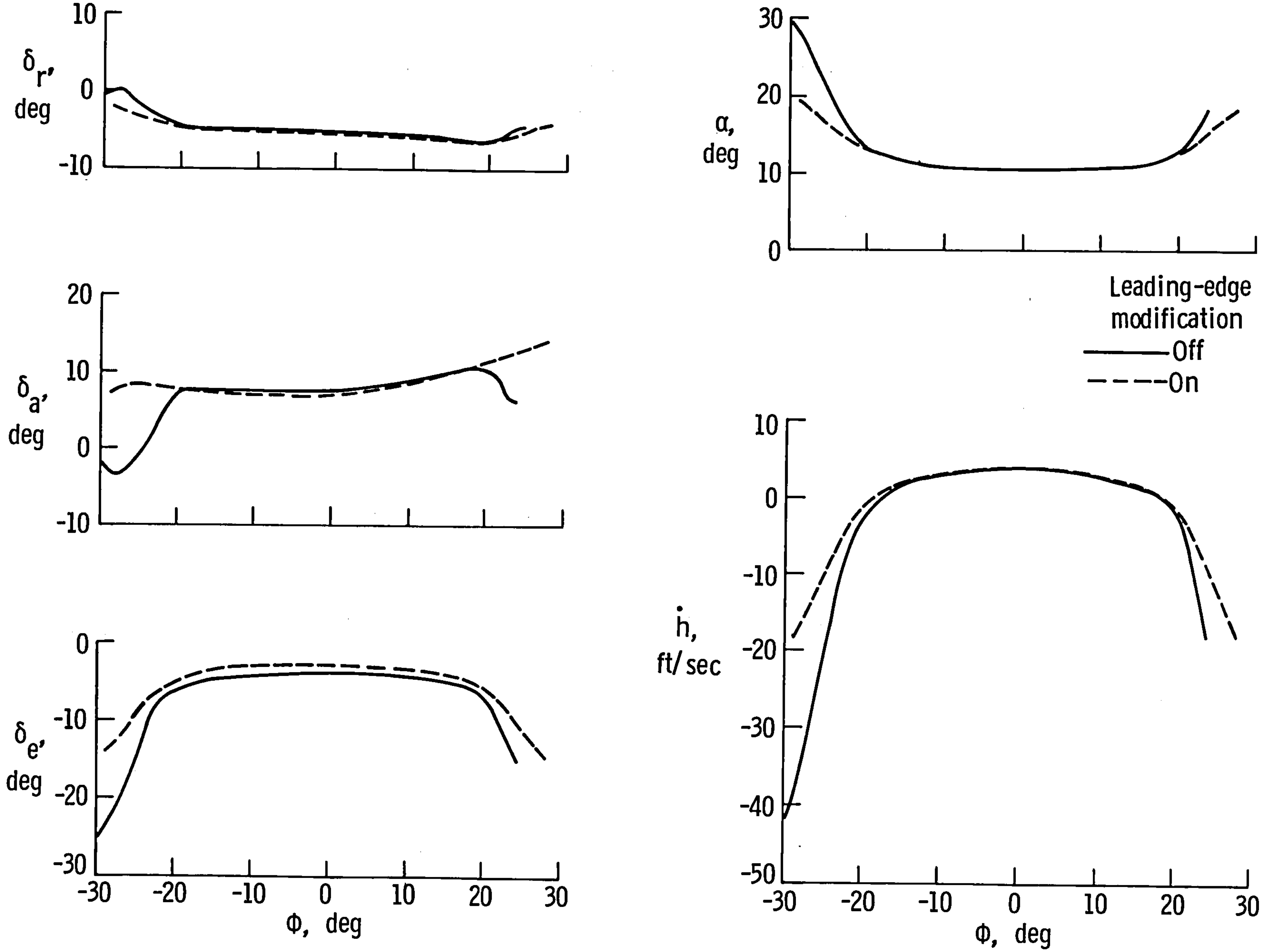

Figure 20. Comparison of simulation full-throttle trim results for turning flight for baseline and modified configurations at $h = 5000$ ft.

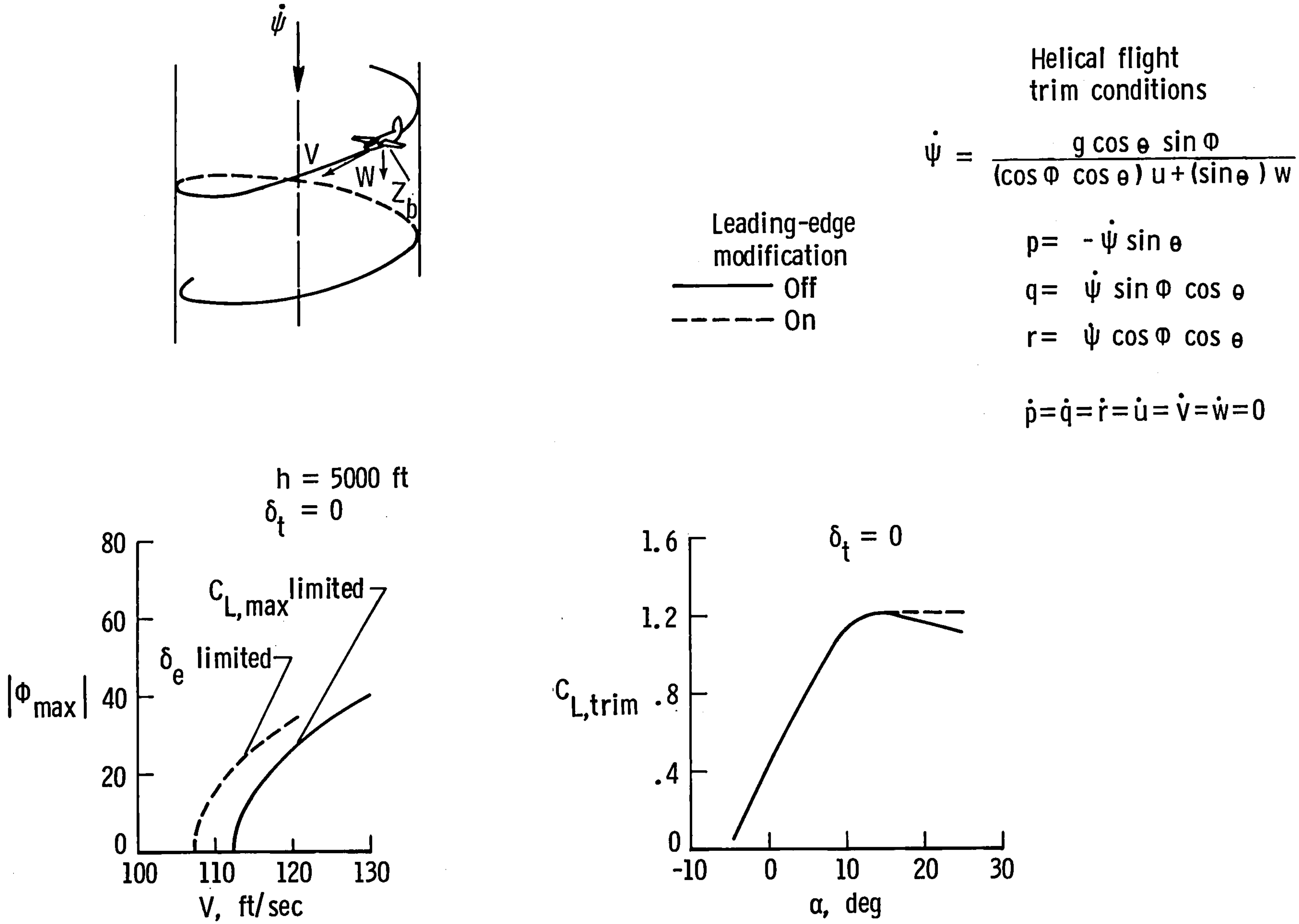

Figure 21. Trim conditions for power-off turning flight ($\delta_f = 0$).

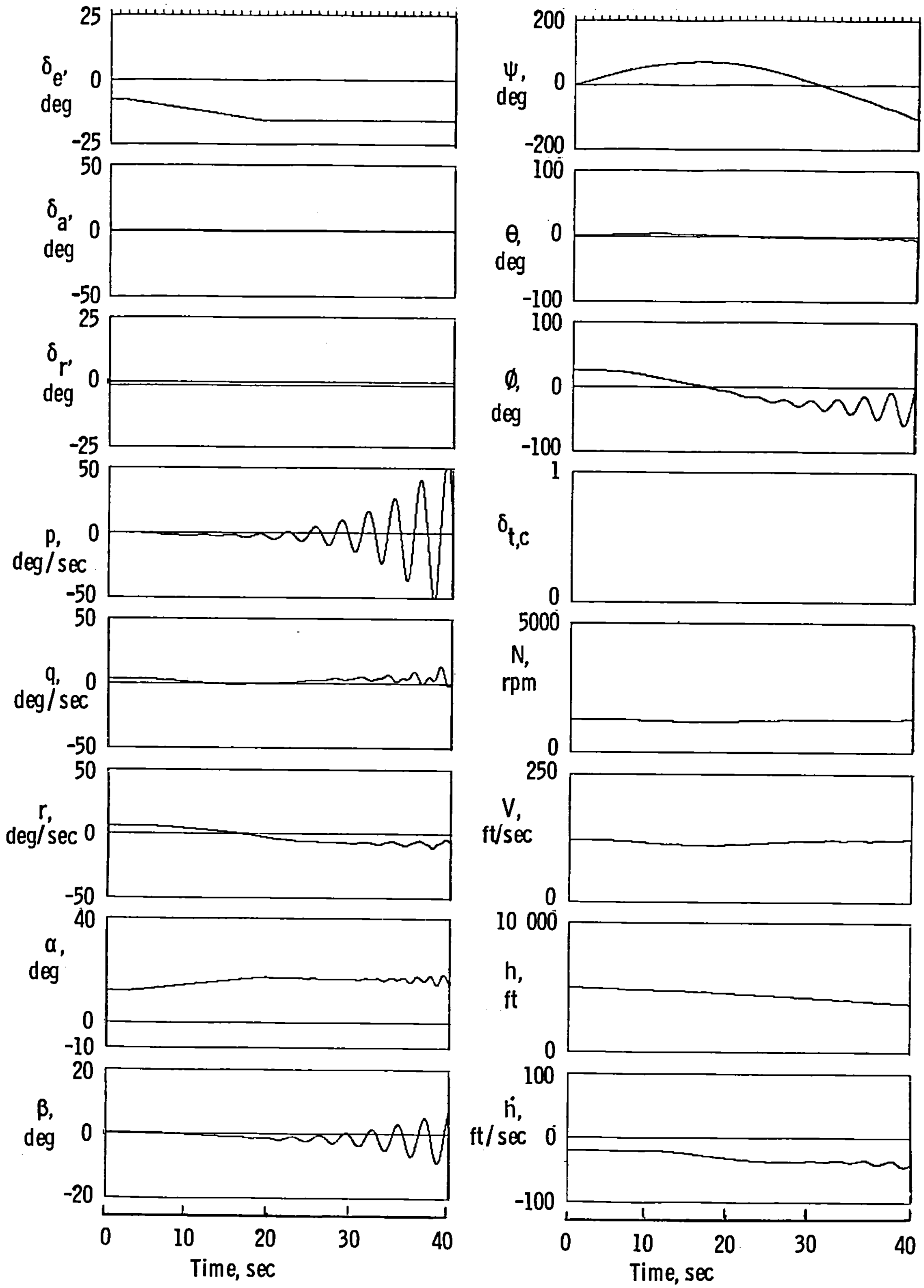

Figure 22. Time histories of a departure in turning flight due to an elevator-ramp input for baseline configuration with power off ($\delta_t = 0$).

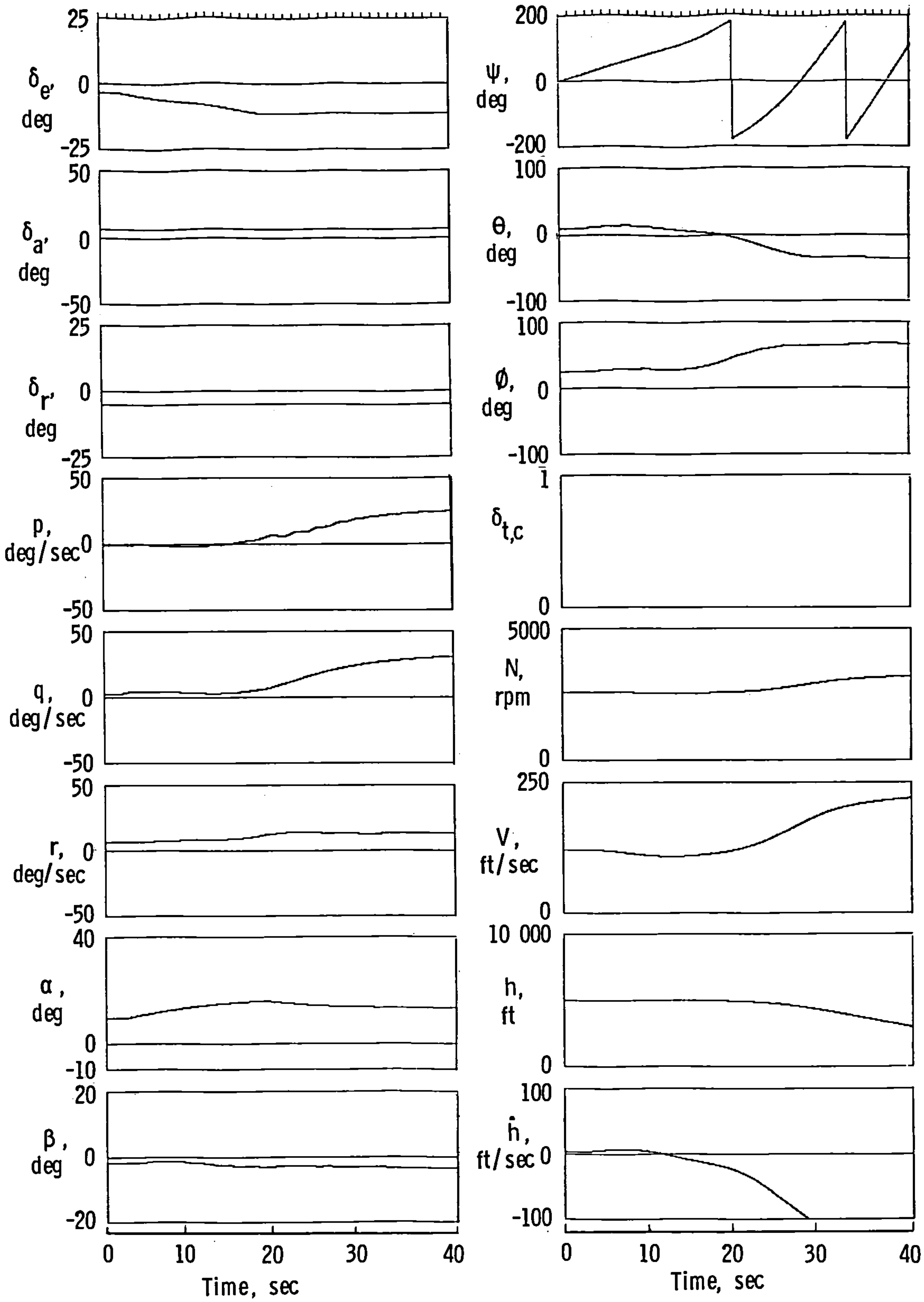

Figure 23. Time histories of a departure in turning flight due to an elevator-ramp input for baseline configuration with power on ($\delta_t = 1.0$).

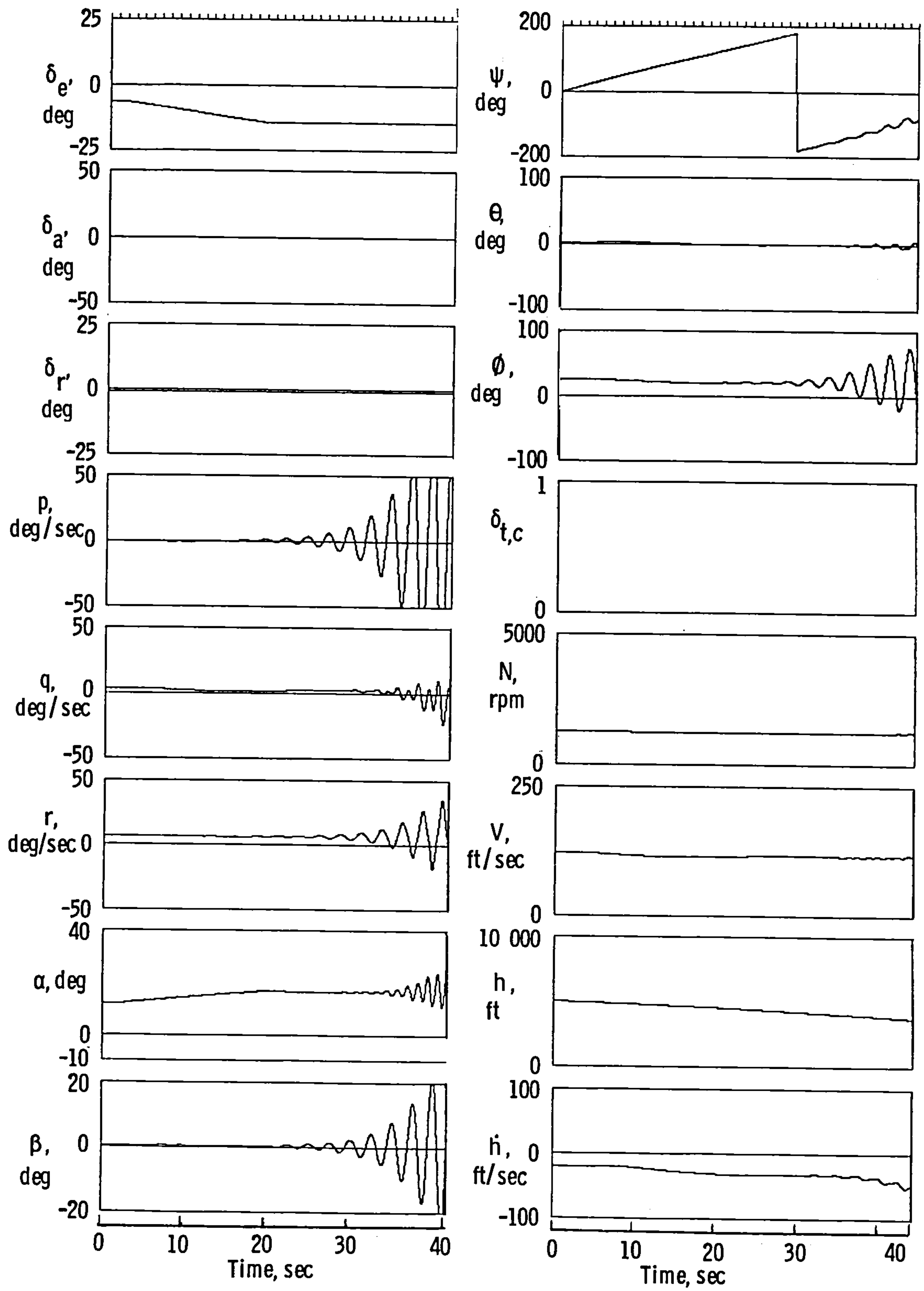

Figure 24. Time histories of a departure in turning flight due to an elevator-ramp input for modified configuration with power off ($\delta_t = 0$).

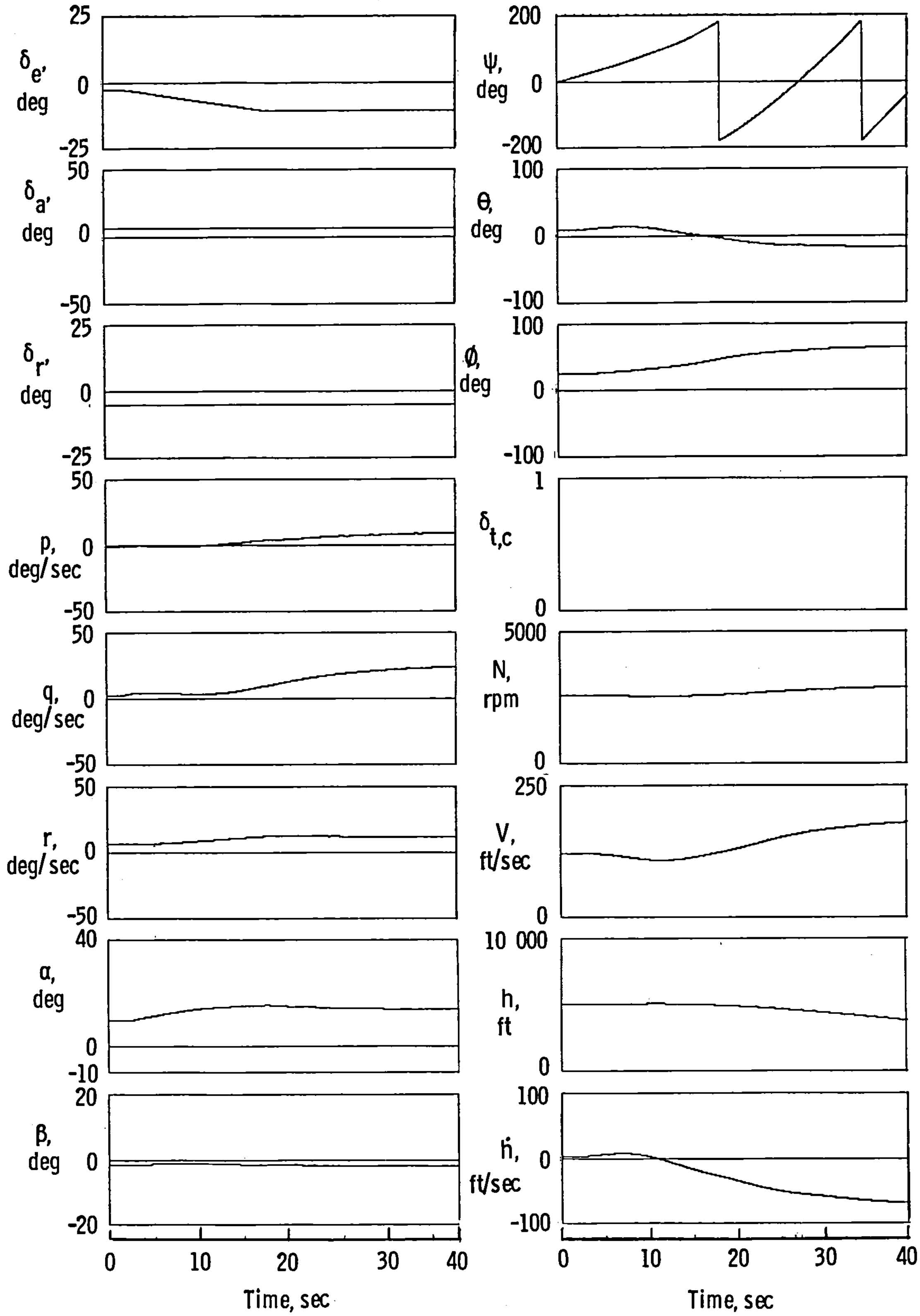

Figure 25. Time histories of a departure in turning flight due to an elevator-ramp input for modified configuration with power on ($\delta_t = 1.0$).

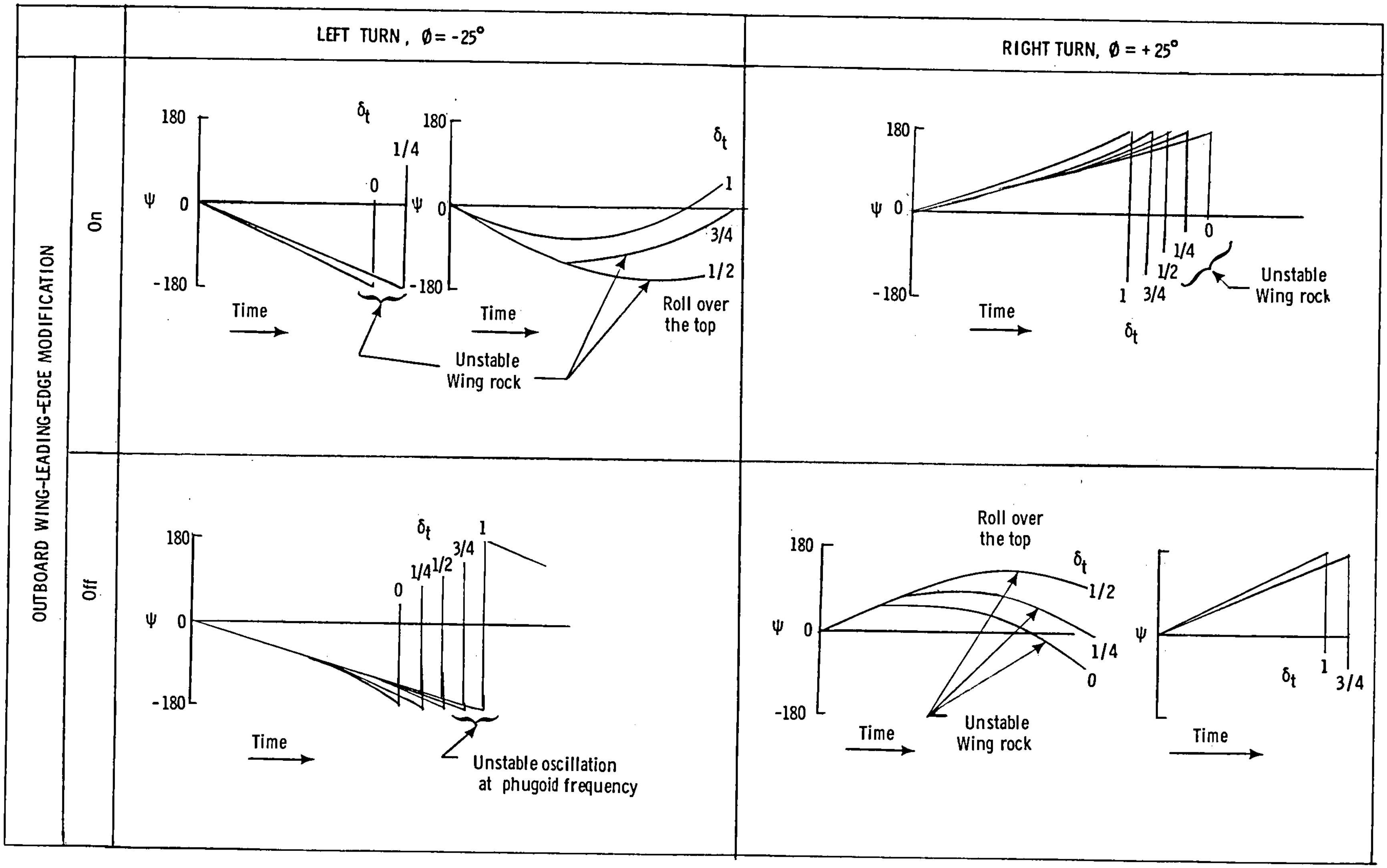

Figure 26. Time-history sketches of initial directional response from trimmed turning flight with application of an elevator ramp of −0.5 deg/sec for 16 sec. Initial conditions of h = 5000 ft, V = 120 ft/sec, and W = 1577 lb.

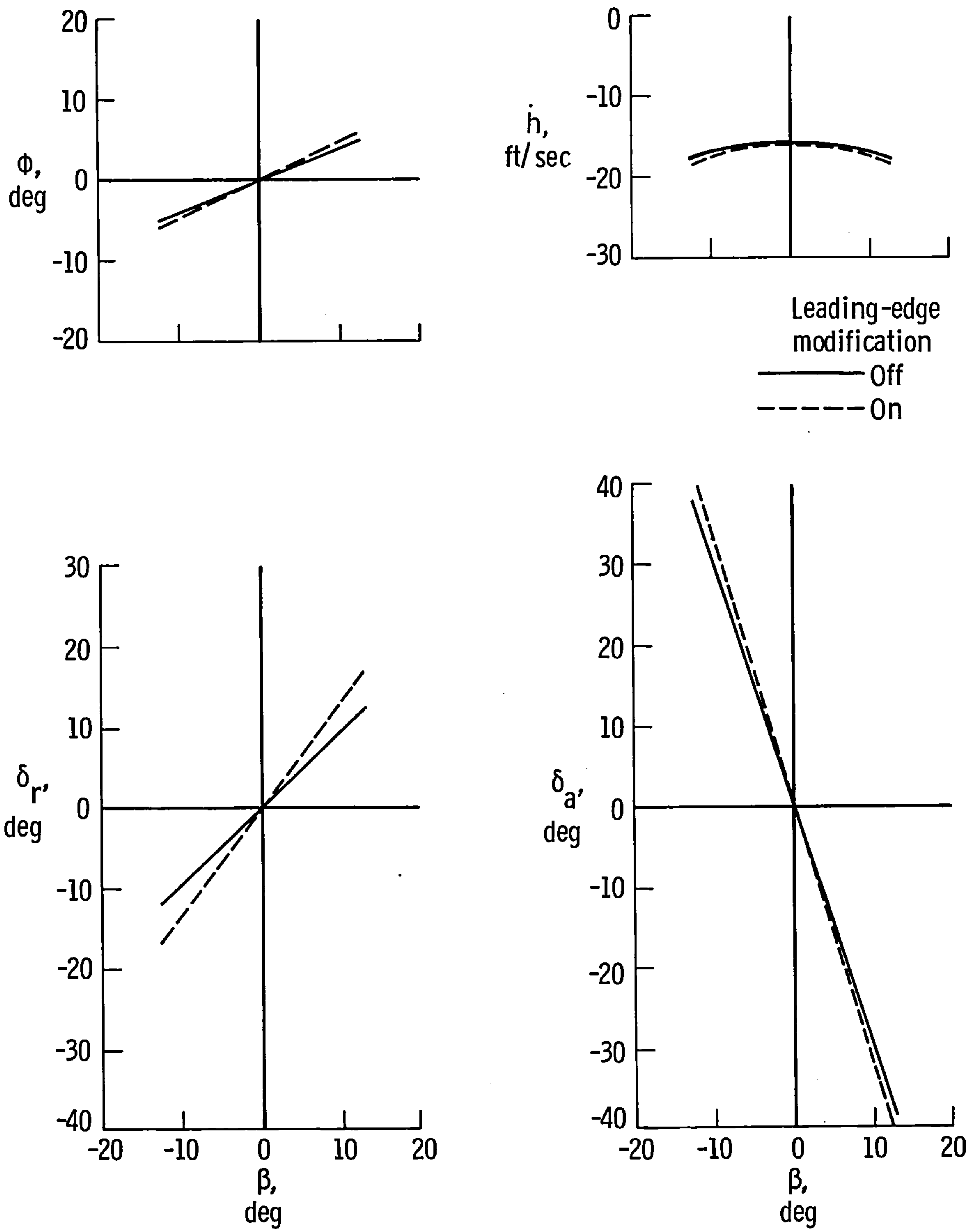

Figure 27. Comparison of throttle-closed trim curves for baseline and modified configurations with $V = 120$ ft/sec, $h = 5000$ ft, $W = 1577$ lb, $\delta_f = 0$, and $\delta_t = 0$.

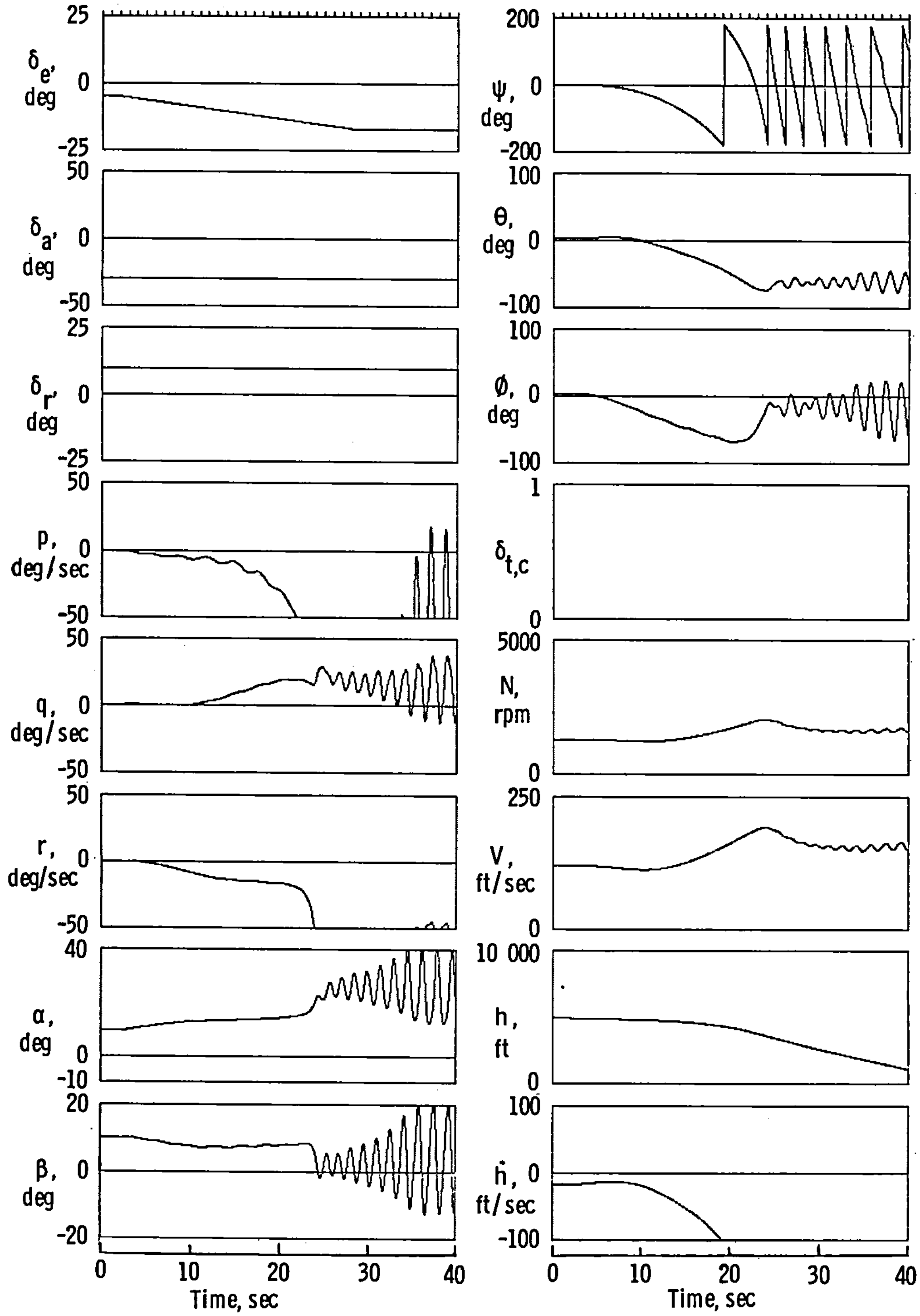

(a) Baseline configuration.

Figure 28. Departure time histories for baseline and modified configurations due to an elevator-ramp input for power-off condition ($\delta_t = 0$). Initial conditions of $\beta_{trim} = 10°$, $h = 5000$ ft, $V = 120$ ft/sec, and $W = 1577$ lb.

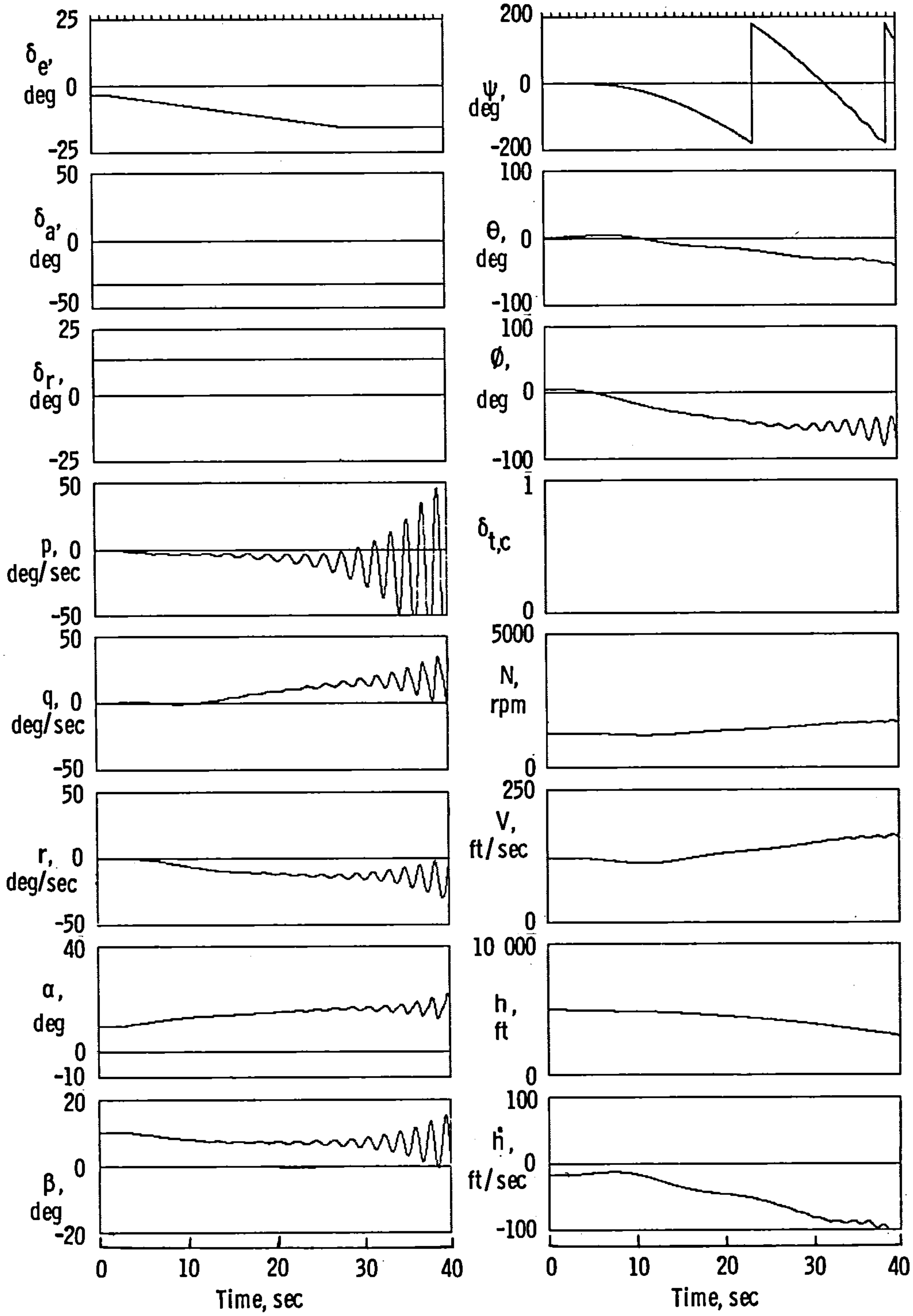

(b) Modified configuration.

Figure 28. Concluded.

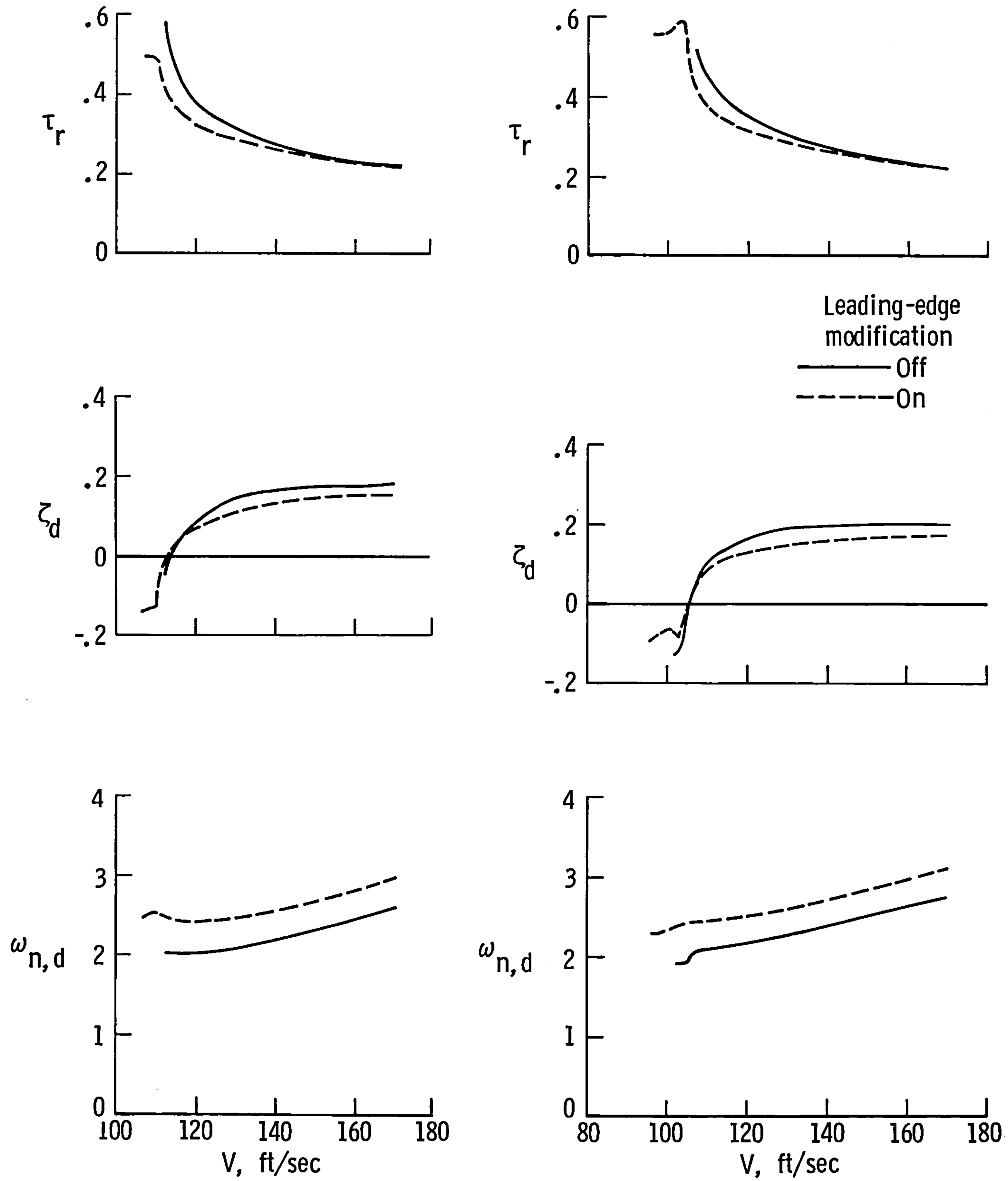

(a) $\delta_t = 0$.

(b) $\delta_t = 1.0$.

Figure 29. Comparison of Dutch roll characteristics and roll-mode time constant for baseline and modified configurations trimmed for straight flight condition at $h = 5000$ ft.

δ_t	α, deg	$C_{L,s}$	$\dot{h}$, ft/sec	C_T
0	11.6	1.19	-20.7	-0.014
.25	11.0	1.19	-14.7	.042
.50	10.3	1.20	-8.0	.099
.75	9.8	1.20	-2.3	.152
1.00	9.4	1.20	3.5	.210

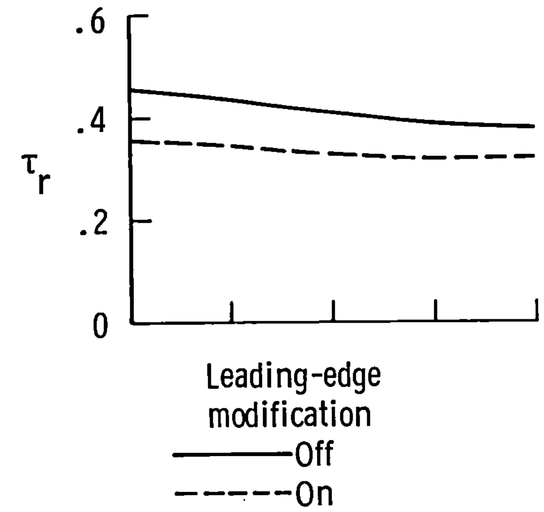

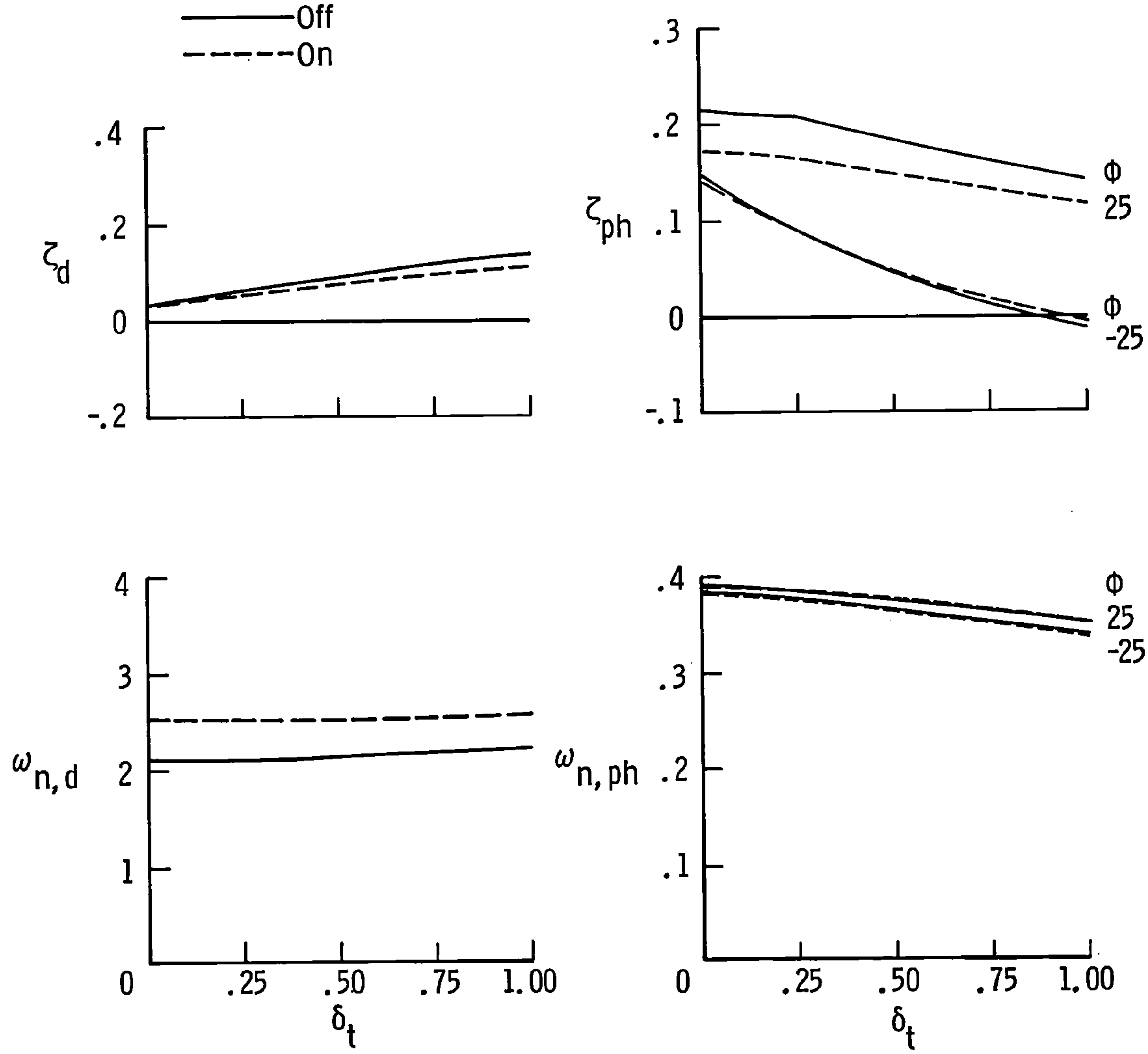

Figure 30. Dynamic-stability comparisons for baseline and modified configurations for left and right turning flight with $\phi = \pm 25°$, $h = 5000$ ft, $V = 120$ ft/sec, and $W = 1577$ lb.

1. Report No. NASA TM-86309	2. Government Accession No.	3. Recipient's Catalog No.
4. Title and Subtitle Simulator Study of the Stall Departure Characteristics of a Light General Aviation Airplane With and Without a Wing-Leading-Edge Modification		5. Report Date May 1985
		6. Performing Organization Code 505-45-43-01
7. Author(s) Donald R. Riley		8. Performing Organization Report No. L-15792
9. Performing Organization Name and Address NASA Langley Research Center Hampton, VA 23665		10. Work Unit No.
		11. Contract or Grant No.
12. Sponsoring Agency Name and Address National Aeronautics and Space Administration Washington, DC 20546		13. Type of Report and Period Covered Technical Memorandum
		14. Sponsoring Agency Code
15. Supplementary Notes		

16. Abstract

A six-degree-of-freedom nonlinear simulation was developed for a two-place, single-engine, low-wing general aviation airplane for the stall and initial departure regions of flight. Two configurations, one with and one without an outboard wing-leading-edge modification, were modeled. This paper presents the math models developed, compares simulation predictions and flight-test data for validation purposes, and compares simulation results for the two configurations for various maneuvers and power settings to show the beneficial influence of adding the wing-leading-edge modification.

17. Key Words (Suggested by Authors(s)) Stall departure, Stall resistance, Wing-leading-edge modification, General aviation, Simulation	18. Distribution Statement Unclassified—Unlimited. Subject Category 05

19. Security Classif.(of this report) Unclassified	20. Security Classif.(of this page) Unclassified	21. No. of Pages 84	22. Price A05

For sale by the National Technical Information Service, Springfield, Virginia 22161

National Aeronautics and
Space Administration

Washington, D.C.
20546

Official Business

Penalty for Private Use, $300

THIRD-CLASS BULK RATE

Postage and Fees Paid
National Aeronautics and
Space Administration
NASA-451

U.S.MAIL

NASA

POSTMASTER: If Undeliverable (Section 158 Postal Manual) Do Not Return